# PYROLYSIS AND COMBUSTION PROPERTIES OF SELECTED STRUCTURAL FUELS IN RESIDENTIAL BUILDINGS

by

Wenxu Yang

A thesis submitted to the faculty of
The University of North Carolina at Charlotte
in partial fulfillment of the requirements
for the degree of Master of Science in
Fire Protection and Administration

Charlotte

2016

Approved by:

_____
Dr. Aixi Zhou

_____
Dr. Stephen L. Quarles

_____
Prof. Jeffrey T. Kimble

# ABSTRACT

WENXU YANG. Pyrolysis and combustion properties of selected structural fuels in residential buildings (Under the direction of Dr. AIXI ZHOU)

Firebrands are a major ignition source in large scale wildland and Wildland-Urban Interface (WUI) fires. Limited studies have been reported regarding firebrand generation. It was hypothesized that firebrand production characteristics can be described by using thermal and combustion properties and geometry factors of the fuel, and the ember production characteristics will be functions of these controlling factors.

As a first step to test this hypothesis, this thesis measured the basic pyrolysis and combustion properties (at small scale) of selected structural fuels (construction materials) under a range of heating rates, radiant heat flux (HF) levels, and moisture content (MC) levels. The following seven commercially available structural fuels were selected for the study: one Southern Yellow Pine (SYP) framing lumber product, one Spruce-Pine-Fir (SPF) framing lumber product, three Oriented Strand Board (OSB) products [two sheathing types (OSB-PF and OSB-H) and one siding type (OSB-siding)], one Plywood sheathing product (CDX grade), and one Hardboard (HB) siding product.

The pyrolysis properties of the selected structural fuels were measured by using the Thermogravimetric Analysis (TGA) technique at various heating rates and different fuel MC levels. The combustion properties of the selected structural fuels were measured by using the Cone Calorimeter at various HF levels and different fuel MC levels.

The results showed strong effects of MC level on the material properties of the fuels. As the MC level increased, the density of SYP, OSB-Siding, OSB-H and CDX increased slightly, while SPF and OBS-sheathing decreased slightly. HB had the highest density at MC level 10%. The thermal conductivity of the selected fuels increased as the MC level increased. The pyrolysis properties were affected by both the MC levels and heating rate levels. The pre-exponential factor and activation energy values varied in the early stage of pyrolysis, but appeared to be more stable when the conversion factor $\alpha$ was 0.25 or higher. Both MC level and heating rate had strong effect on the pre-exponential factor but less effect on activation energy. The MC levels and HF levels had strong effect on the combustion properties of the selected structural fuels. Heat flux had significant effect on Time to Ignition (TTI), the higher the heat flux levels, the smaller the TTI values. MC levels had significant effect at low heat flux levels. As the MC level increased, the Critical Heat Flux (CHF) for ignition values increased for SYP and OSB-Siding, but decreased for CDX and HB. SPF, OSB-PF and OSB-H had highest CHF values at 10% MC level. The Peak Heat Release Rate (PHRR) of all selected structural materials increased as the heat flux level increased, and decreased as the MC level increased, although with a few exceptions. As the MC level increased, the Effective Heat of Combustion (EHC) of materials also increased. HF levels had less effect on the EHC values. The Mass Loss (ML) and Mass Los Rate (MRL) of materials increased as the HF level increased. MC levels showed less effect on ML and MLR. The Time to Flameout (TTF) of all materials increased as the MC level increased, but decreased as the heat flux increased.

# AKNOWLEDGEMENTS

This thesis was completed with the guidance and assistance from my advisor, Dr. Aixi Zhou. He provided a comprehensive and effective instruction to conduct the research. I, hereby, give him my greatest appreciation for being a knowledgeable advisor, who helped me learn how to solve academic problems and laboratory equipment troubles.

Besides, I would like to thank Dr. Stephen L. Quarles, my committee member and Senior Scientist-at the Insurance Institute for Business and Home Safety (IBHS) Research Center, for all his significant help, and access to the IBHS research facilities. I thank Professor Jeffrey T. Kimble for serving as a committee member, and for his insightful comments. I thank Dr. Katherine Weaver, manager for the Material Characterization Laboratory (MCL), for her valuable advices during the thermal analysis tests. I thank Mr. Parks Davidson, manager for the Material Flammability Laboratory, for his help in the equipment instruction and maintenance. I also thank Mr. Wes Maxwell, for his help to cut the experimental samples.

My sincere thanks go to my dear friend, Babak Bahrani, a doctoral student at UNC Charlotte, for all his help during this research.

Additionally, I thank the Joint Fire Science Program for providing the financial support for this research.

Last but not the least, I express the deepest gratitude to my family for being helpful and empathetic, and for giving their endless encouragement and financial support during my graduate study.

TABLE OF CONTENTS

# LIST OF FIGURES

# LIST OF TABLES

# LIST OF SYMBOLS

| | | |
|---|---|---|
| $A_s$ | Nominal specimen exposed surface area | $[m^2]$ |
| $\Delta h_{c,eff}$ | Effective heat of combustion | $[kJ/kg]$ |
| $\rho$ | Density | $[kg/m^3]$ |
| $\alpha$ | Thermal diffusivity | $[m^2/s]$ |
| $\varepsilon$ | Emissivity | |
| $I$ | Thermal inertia | $[k\rho c(J^2/m^4K^2s^1)]$ |
| $k$ | Thermal conductivity | $[W/mK]$ |
| $A$ | Pre-exponential factor | $[s^{-1}]$ |
| E | Activation energy | $[Jmol^{-1}]$ |
| $c$ | Specific heat | $[J/kgK]$ |
| $\dot{m}^{"}$ | Mass loss rate per unit area | $[kg/s \cdot m^2]$ |
| $\dot{q}_e^{"}$ | External irradiance or exposure | $[kW/m^2]$ |
| $\dot{q}_f^{"}$ | Heat flux from the flame | $[kW/m^2]$ |
| $\dot{q}_l^{"}$ | Heat losses from the surface | $[kW/m^2]$ |
| $\Delta h_g$ | Heat of gasification | $[kJ/kg]$ |
| $T$ | Temperature | $[K]$ |
| $t$ | Time | $[s]$ |
| $\dot{Q}_{(t)}$ | Rate of heat release | $[kJ/s]$ |
| C | Calibration constant for oxygen consumption | $[m^{\frac{1}{2}}kg^{\frac{1}{2}}K^{\frac{1}{2}}]$ |
| ΔP | Orifice meter pressure differential | $[Pa]$ |

| | | |
|---|---|---|
| $T_e$ | Gas temperature at the orifice plate | $[K]$ |
| $X_{O_2}$ | Measured mole fraction of $O_2$ in the exhaust air | |
| $t_{ig}$ | Time to sustained flaming | [s] |

# LIST OF ABBREVIATIONS

| | |
|---|---|
| ASTM | American society of testing and materials |
| EHC | effective heat of combustion |
| HRR | heat release rate |
| IBHS | insurance institute for business and home safety |
| NIST | national institute of standards and technology |
| TTI | time to ignition |
| WUI | wildland-urban interface |
| MC | moisture content |
| DTC | thermal conductivity meter |
| ML | mass loss |
| MLR | mass loss rate |
| HF | heat flux |
| PHRR | peak of heat release rate |
| MCL | materials characterization laboratory |
| MFL | materials flammability laboratory |
| DSC | differential scanning calorimetry |
| SDT | simultaneous DSC and TGA |
| TGA | thermogravimetric analysis |

# CHAPTER 1: INTRODUCTION

## 1.1 Problem Statement

The home destruction problem related to wildfires, identified as the wildland-urban interface (WUI) fire problem, has been nationally recognized in the U.S. since the 1980s (Cohen, 2008). The WUI is generally defined as the area where human-built structures and infrastructure abut or mix with naturally occurring vegetation types (Mell et al., 2010). According to the NFPA statistics, of the 25 largest-loss fires in the U.S., eight of the top 15 that have occurred since 1990 were WUI fire losses (NFPA 2016). The WUI fire problem has been recognized as a principal national issue, as shown in several federal and state wildland fire management policy documents (Stephens and Ruth, 2015). Around the world, WUI fire disasters have been increasing globally recently, such as in Australia (Haynes et al., 2010) and some European countries (Lampin- Maillet et al., 2010).

Spot fires caused by wind-blown burning firebrands (also called embers) are a significant mechanism of fire spread in the WUI (Koo et al., 2010; Mell et al., 2010; Maraghides and Mell, 2011; Manzello and Foote, 2014; Caton et al., 2016). The firebrand phenomenon can be understood in three major processes: firebrand production, firebrand transport, and firebrand ignition of the recipient fuel.

Considerable work on firebrand transport has been conducted, but much less work has been done to understand firebrand production and firebrand ignition of fuels (Caton et al., 2016). Firebrand production is the first step in the firebrand phenomenon and is the basis for understanding the subsequent transport and ignition processes.

Since 2015, the Joint Fire Science Program (JFSP) has sponsored a new multi-institutional study designed to reduce wildfires and mitigate WUI fire damages due to ignition or fire spread by wind-blown firebrands (JFSP, 2016; UNCC, 2015). The purpose of the project was to investigate firebrand production from selected burning wildland and structural (construction materials) fuels under a range of environmental conditions through full-, intermediate- and small-scale laboratory experiments. The resulting data will enable us to relate the fuel's basic thermal degradation, geometrical structure and combustion properties to its firebrand production characteristics and investigate link between some commonly used environmental indices and firebrand production. Specific project objectives included determining basic thermal decomposition (or pyrolysis) and combustion properties; determining production rate, mass, shape and dimensions of firebrands under a range of conditions; determining the travel distance of firebrands; and determining the burning duration; and evaluating the impact of these properties on ignition potential and fire spread.

As a first step of the JFSP firebrand production project, the purpose of this research was to determine basic pyrolysis and combustion properties of selected structural fuels in typical residential buildings in the U.S. This work was based on the hypothesis that the firebrand production characteristics are related to pyrolysis and

combustion properties and geometry factors of the fuel and will be functions of these controlling factors. Specifically, the objective of this research was to determine the basic pyrolysis properties and combustion properties at a small scale of selected fuels under a range of heating rates, radiant heat flux levels, and moisture content (MC) levels.

## 1.2 Goal, Objectives and Tasks

The goal of this research was to measure the pyrolysis and combustion properties of selected structural fuels as a function of a few controlling factors, including material type (and thus the geometrical structure of the fuel), fuel MC levels, and heating conditions (such as heating rate and heat flux levels).

To achieve this goal, the following research objectives were developed:

(1) Measure the pyrolysis properties of selected structural fuels using the Thermogravimetric Analysis (TGA) technique at various heating rates and different fuel MC levels;

(2) Measure the combustion properties of selected structural fuels using the Cone Calorimeter at various heat flux levels and different fuel MC levels;

In order to accomplish the above objectives, the following tasks were planned:

(a) To select appropriate representative structural fuels in typical residential buildings in the U.S. as specimens for this study;

(b) To perform laboratory studies to measure and control the moisture content of the selected fuels at designed MC levels;

(c) To carry out TGA experiments and subsequent data analysis in order to obtain basic pyrolysis kinetics parameters of the selected structural fuels at three pre-

determined MC levels and three pre-determined heating rates;

(d)To conduct Cone Calorimeter experiments and subsequent data analysis in order to obtain basic combustion properties of the selected structural fuels at three pre-determined MC levels and three pre-determined heat flux levels.

In addition, the thermal conductivity of the selected structural fuels was also measured using a C-Therm TCi Thermal Property Analyzer.

## 1.3 Organization of Thesis

The thesis has five chapters. The first chapter presents the problem statement, goal, objectives and tasks of this research. Chapter Two serves as a literature review to explain the firebrand phenomenon, the pyrolysis properties of wood and wood-based composites, and the combustion properties of wood and wood-based composites. Chapter Three provides details about the experimental design and procedures, research questions about the experiments and experimental specimens, as well as explains the method and procedures for conditioning and controlling MC levels of the specimens. Chapter Four presents the obtained results and discussions for the experiments. Finally, Chapter Five summarizes major conclusions from this study and proposes future work.

# CHARPTER 2: LITERATURE REVIEW

## 2.1 Firebrand Phenomenon

Firebrands are a critical mechanism of fire spread in large outdoor fires, such as urban fires in Japan and WUI fires common in Australia, Southern Europe, and the USA (Brown et al., 20014). Firebrands are thought to be one of the primary sources of ignition in the WUI because they can either directly ignite components of vulnerable structures or can ignite nearby vegetation and other combustibles, which can subsequently ignite the structure via radiant heating or direct flame contact (Quarles, 2012). Fire spread and structure ignition by firebrands can be understood in three major processes or mechanisms: firebrand production, firebrand transport, and firebrand ignition of fuel.

Firebrands have been studied for some time, most of these studies have focused on spotting distance. Few studies have reported firebrand generation and the subsequent ignition of building materials or vegetative fuels. To develop scientifically based mitigation strategies for WUI fires, it is necessary to understand the firebrand generation process (Brown et al., 2014). In fact, firebrand generation is the first step of the firebrand phenomena and is the basis for understanding the subsequent transport and ignition processes. Understanding the firebrand production process will also help us improve fire spread modeling of large scale fires (wildland, WUI, or urban) and

develop appropriate mitigation strategies.

A limited number of experimental studies have been performed on firebrand production over the past several decades. Table 2.1 shows a summary of studies on firebrand production since the 1960s. Clearly, the existing ember production studies have been conducted on a limited number of wildland and structural fuels under limited fuel MC levels and environmental conditions. A systematic study (e.g., the JFSP project mentioned in Chapter 1) to quantify ember production by examining a range of fuels under various conditions is needed to improve our understanding of firebrand production characteristics.

Table 2.1. Summary of fire ember production experiments (Canton et al., 2016)

| Author | Fuel | Test Condition |
|---|---|---|
| Tarifa et al. (1967) | Wood (pine, oak, spruce, aspen, and balsa), charcoal, natural pine cones and pine brackets | Indoor; wind 0-90mph, MC 2%-25%, individual firebrand study |
| Vodvarka (1969) | Wood-frame structures (3 wood siding, 1 asphalt siding, and 1 brick veneer) | Outdoor; wind 1-7 mph, temp. 73-88°F, R.H. 50-70% |
| Waterman (1969) | Roofing (wood, asphalt, and cement-asbestos singles; roll and build-up roofing; and no covering) | Indoor; in a test chamber (internal pressure from an aircraft engine) |
| Muraszew et al. (1975-1976) | Wood (birch, white pine, and Ponderosa pine), and natural fuels (bark plates, pine cones, limb wood) | Indoor; wind 0- 25 mph, temp. 85-90°F, R.H. 10-55% |
| Clements (1977) | Broadleaf tree leaves, pine needles and cones, moss, bark and fronds | Outdoor; with a vertical wind tunnel |
| Ellis (2000) | Eucalypt bark in Australia | Indoor; wind 0-90mph, MC 7%-13% |
| Woycheese (2000) | Balsa, light balsa, western red cedar, Douglas fir, red oak, red wood, and walnut | Indoor; wind 0- 16 mph |
| Yoshioka et al. (2004) | Wood crib and wooden house (with outer wall siding and slate roofing) | In a large wind tunnel, 4.5-9.0 mph |
| Manzello et al. (2007-2014) | Douglas fir, Korean pine | Indoor; wind 0-16 mph, MC 10-50% for fir and 10-80% for pine, ember generator |
| Suzuki et al. (2012-2014) | Residential building components (wall and corner assemblies) and a full-scale structure | Indoor; wind 0-22 mph, MC about 10% |

Firebrand production is affected by many factors (Caton et al., 2016), such as the fuel material type, condition of the fuel (e.g., live or dead fuels, moisture content

levels, etc.), the thermal degradation properties of the fuel, the combustion properties of the fuel, and environmental conditions the fuel is subjected to (such as wind, relative humidity, temperature, and heating condition.). These controlling factors will affect the outcome variables such as the possibility of firebrand formation, firebrand production rate, the physical characteristics of firebrands (e.g., firebrand size, mass and shape, travel distance) and combustion properties of firebrands (e.g., burning duration, burning duration intensity, potential heat energy, potential heat flux and temperature). Particularly, there is a need for additional information relating basic structural (geometry and dimensions), pyrolysis and combustion properties of the fuel with the firebrand production process and the associated characteristics of the produced firebrands.

## 2.2 Pyrolysis Properties of Wood and Wood-Based Composites

Wood and wood-based composites are major construction materials in residential and no-residential buildings in the U.S., Canada, Japan and other countries (e.g., Australia, New Zealand, and some countries in Europe, etc.).

From the chemical point of view, wood is a composite material comprised of cellulose, hemicellulose and lignin, along with smaller quantities of extractives and inorganic matter. Wood is the most frequently used combustible material in one-dimensional modeling. They can be classified into hardwoods and softwoods, which have different percentages of cellulose, hemicelluloses, lignin and extractives etc. These three components have different thermal pyrolysis characteristics. Subsection 2.2.1 addresses the thermal decomposition of cellulose and lignin. Subsection 2.2.2

provides more details about the thermal decomposition of wood and wood-based composites.

### 2.2.1 Thermal Behaviors of Cellulose and Lignin

The thermal behavior of the commercial cellulose and lignin are shown in Figure 2.1. From room temperature to 120°C, the derivative curves presented one peak which corresponds to evaporation of the water occupying the intercellular vacuum. On the Figure 2.1, one peak of the degradation was observed after the departure of the free water because the cellulose is a homo-polymer of glucose. It is a semi-crystalline polymer (Browne et al., 1958). The degradation of the cellulose began around 250°C but presents a thin peak on the TGD thermos-gram indicating the purity of this polymer. It was nearly decomposed totally into volatile product at 400°C as shown in Table 2.2.

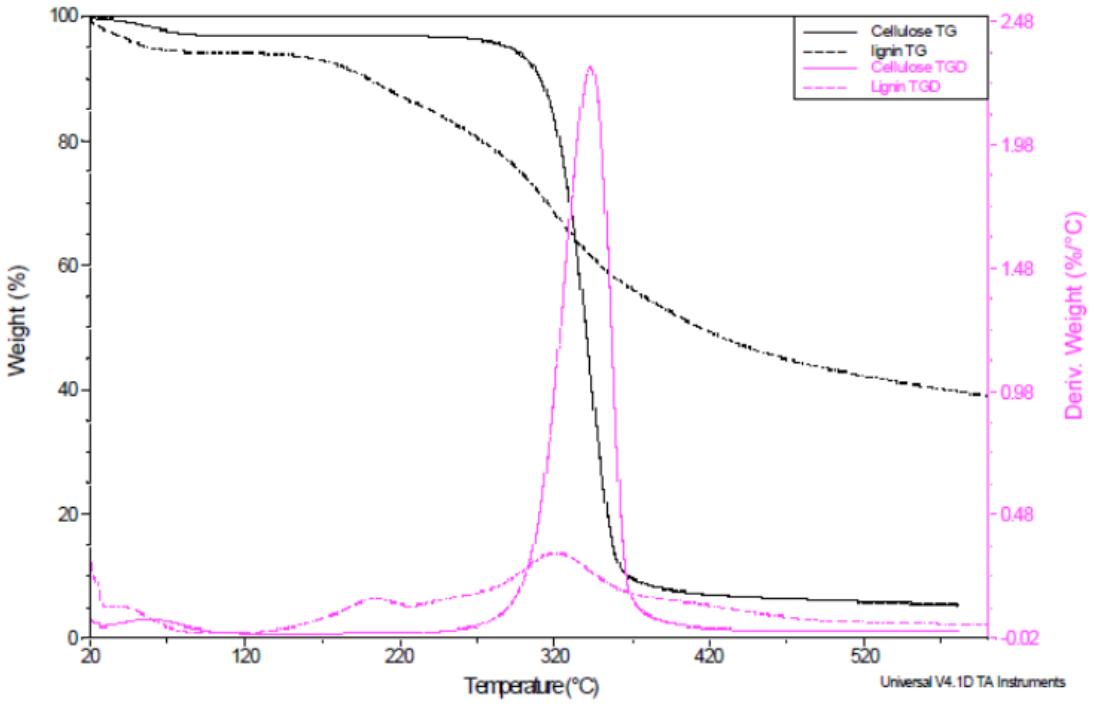


Figure 2.1. Thermo-grams (TG and TGD) of cellulose and lignin (Tantely et at., 2014)

The lignin is a polyphenolic polymer formed with three elementary motifs, the coumarylic, sinapylic, and coniferylic alcohols. It has a tri-dimensional structure. The polymerisation of the lignin is randomly shared at the vegetable secondary wall and its structure varies from one species to one another. Even if the lignin is less stable than the cellulose, its degradation is very slow with the high rate of non-volatile products. Several studies confirmed the extensiveness of the range of the degradation of the lignin in two or three stages, as shown in Table 2.3 (Tantely et al., 2014).

Table 2.2. Stages of cellulose degradation (Tantely et at., 2014)

| Stages of degradation | Temperature range | Maximum peak | Loss of mass |
|---|---|---|---|
| Only one stage | 250°C – 400°C | 343°C | 90.5% |

Mass of sample: 19.9mg; beginning of the degradation 250°C; nonvolatile residue at 500°C: 7% (Tantely et al., 2014).

Table 2.3. Stages of Lignin degradation (Tantely et at., 2014)

| Stages of degradation | Temperature range | Maximum peak | Loss of mass |
|---|---|---|---|
| $1^{st} stage$ | 115°C – 225°C | 202°C | 7.7% |
| $2^{st} stage$ | 225°C – 360°C | 321°C | 28.1% |
| $3^{st} stage$ | 360°C – 500°C | 400°C | 14.8% |

Mass of sample: 5.41mg; beginning of the degradation 125°C; nonvolatile residue at 500°C: 43% (Tantely et al., 2014).

### 2.2.2 Thermal Decomposition of Wood

From the physical point of view, wood is a complex structure with anisotropic properties. The chemical and physical properties of wood such as moisture content, chemical composition, density and crystallinity are factors that affect the characteristics of thermal decomposition and degradation kinetics. In this section, a discussion of the general thermal degradation process for wood is followed by a more specific review of the use of these methods to analyze the thermal degradation of wood and its components (Brall et al., 1970). In reporting the exothermic reactions in wood, it was defined three phase points (Kollmann, 1960):

(1) Flame point, 225° to260℃, at which decomposition gases will burn if an ignition source is present.

(2) Burning point, 260° to290℃, at which burning occurs with a steady flame.

(3) Flash point, 330° to470℃, the range of spontaneous ignition.

Amy (Amy, 1961) described the general course of pyrolysis of lignocellulosic materials. After the last traces of water were removed, which required a temperature of about 140℃, four classes of products were produced by wood carbonization: non-condensable gases, pyroligneous products, tar, charcoal (Amy et al., 1961). Gases were evolved at temperatures between 200℃, and 400° to 450℃, with a maximum at about 350° to 400℃. The rate of production of pyroligeneous material passed through a maximum between 250° to300℃, and virtually ceased at about 300℃. Tar formed between about 300℃, and 400° to 450℃. Some gases, primarily hydrogen, continued to be evolved above 400℃. Charcoal, which contains practically all the original ash,

was not completely carbonized even at 1500℃ (Beall et al., 1970). The water in the wood is presented in three forms: free water, linked water, and water of constitution. The free water evaporates without energy contribution while the bound water and the water of constitution from the chemical bounds with the constituents of the wood cell wall. Therefore, the temperature range of drying of wood lays out from room temperature to about 120℃. It always remains a humidity rate corresponding to water in linkage with the hydrophilic constituents.

The most comprehensive literature review to date on the thermal decomposition of wood was by Browne (Browne, 1958). This review covered pyrolysis, combustibility, theories of flame-proofing, fire-retarded ion mechanisms, and theories of glow prevention. He divided the pyrolysis processes into four zones, or temperature ranges, all of which can be present simultaneously in wood of appreciable thickness: Zone A, below 200℃, in which only non-combustible gases, primarily water vapor, with traces of carbon dioxide, formic and acetic acids, and glyoxal are produced. Dehydation of sorbed water is complete. Zone B, from 200° to 280℃, in which the same gases as in zone A are produced, but with a greatly reduced quantity of water vapor, and some carbon monoxide. At this point the reactions are endothermic, and the products are almost entirely nonflammable. Zone C, from 280° to 500℃, in which active pyrolysis takes place under exothermic conditions leading to secondary reactions among the products. The products are largely combustible, and include the highly flammable tars in the form of smoke particles. The charcoal residue catalyzes secondary react ions. Zone D, above 500℃, in which the residue consists primarily of charcoal, which

provides an extremely active site for further secondary reactions (Browne, 1958). In some cases, to achieve pyrolysis conditions, nitrogen atmosphere was applied. Nitrogen was used as the carrying and protective gas, protecting the micro-balance against possible pollutants.

Table 2.4. Temperature ranges of wood pyrolysis (FPL, 2010)

| Temperature range | Decomposition processes |
|---|---|
| $> 100℃$ | The evaporation of chemically unbound water |
| $160 - 200℃$ | The three polymeric components of wood begin to decompose slowly. Gases formed at this stage are non-combustible (mainly $H_2O$) |
| 200-225°C | Wood pyrolysis is still very slow, and most of the gases produced are non-combustible. |
| 225-275°C | The main pyrolysis begins and flaming combustion will occur with the aid of a pilot flame. |
| 280-500°C | Gases produced are now volatile (CO, methane etc.) and smoke particles are visible. Char forms rapidly as the physical structure of wood breaks down. |
| >500°C | Volatile production is complete. Char continues to smolder and oxidize to form CO, CO2 and H2O. |

## 2.3 Combustion Properties of Wood and Wood-Based Composites

Wood is one of the most sustainable, aesthetically pleasing and environmentally benign materials (FPL, 2010). The demand to use wood and wood-based products for applications in both residential and non-residential building construction has increased over recent years (FPL, 2010). However, due to the inherent combustibility of such products, they often contribute to unwanted fires, resulting in numerous injuries and fatalities (FPL, 2010). The use of wood is, therefore, limited by various safety requirements and regulations pertaining to its combustibility and spread of fire

characteristics (Cohen, 2008).

### 2.3.1 Natural Woods

As mentioned in Section 2.2., woods are divided into two broad classes, hardwoods and softwoods. Softwood is the source of about 80% of the world's production of timber, mainly used for dimensional lumber (e.g., framing lumber) and panels (e.g., OSB and plywood). Hardwood applications include furniture, flooring, boat building, and other special uses such as tools and musical instruments.

In general, woods having higher density and moisture content have better fire performance. The lower lignin content of hardwoods compared with softwoods reduces the residual char content. As with many fire retardants, the fire performance of wood is improved by increasing the residual char content. The limited extractive contents of hardwood species reduce their overall variability in flame spread and heat release compared with the softwoods (Lampin-Maillet, 2010).

### 2.3.2 Wood-Based Composites

The primary component of wood-based composite is the wood element, often 94% or more by mass. Common elements for conventional wood-based composites include veneers, strands, particles, and fibers. Specific products produced include panel products such as plywood, oriented strand board (OSB), particleboard, and fiberboard. Typical adhesives used in wood-based composites are PF (phenol formaldehyde) and PMDI (Polymeric Methylene Diphenyl Diisocyanate). Wood-based composites are used for a number of nonstructural and structural applications in product lines ranging

from panel for interior covering purposes to panels for exterior uses and in furniture and support structures in buildings (FPL, 2010).

In general, wood-based composites having higher density and moisture content thus better fire performance. The lowered flammability of wood-based composite panels enables them to be used in high-performance applications (FPL, 2010).

# CHAPTER 3: EXPERIMENTAL DESIGN AND PROCEDURES

## 3.1 Properties Test Questions

The experiment was divided into fuel properties test, pyrolysis properties test and combustion properties test. Controlling factors included MC level related to the materials (internal), as well as experimental temperature, heat flux and heating rate related to testing conditions (external).

Specifically, for fuel properties, there was one controlling factor MC level for specimen thickness area, and bulk density as parameters. For pyrolysis properties, there were three controlling factors (MC level, temperature and heating rate) for the value of thermal conductivity, E (activation energy) and A (pre-exponential factor) as parameters. For combustion properties, there were two controlling factors (MC level, and heat flux) for the values of ignition time, critical heat flux, peak heat release rate (PHRR), effective heat of combustion (EHC), mass loss and flameout time as parameters. Table 3.1 shows the questions need to be answered for the relationship between each controlling factor and parameter:

Table 3.1. Controlling Factors and Parameters

| Properties | Controlling factor | Relationship | Parameters |
|---|---|---|---|
| Fuel | MC level | Need to answer: Increase, Decrease, or Non-Influence | Thickness, Area, Density |
| Pyrolysis | MC level<br>Temperature<br>Heating Rate | | Pre-exponential factor (ln(A)), Activation Energy (E), Thermal Conductivity |
| Combustion | MC Level<br>Heat Flux | | Time to Ignition (TII), Critical Heat Flux (CHF), Peak of Heat Release Rate (PHRR), Effective Heat of Combustion (EHC), Mass Loss (ML), Mass Loss Rate (MLR), Time to Flameout (TTF) |

## 3.2 Experimental Specimens (selected structural fuels)

### 3.2.1 Selection of Structural Fuels

The JFSP project team went through a rigorous process to select the structural fuels for this study, with inputs from the whole project team and a technical panel. The main basis for the selection was that the chosen fuels should be representative of typical residential building construction in wildfire prone areas that have a high ignition potential and were thought to be capable of generating a large amount of firebrands. Among the selected structural fuels, seven fuels were used for this thesis, as shown in Table 3.2.

Table 3.2. Material Designation

| Designation | Short | Description |
|---|---|---|
| A | SYP | Framing Lumber Southern Yellow Pine: Produced at Canfor – New South Mill, |
| B | SPF | Framing Lumber Spruce-Pine-Fir: no |
| C | OSB-PF | OSB Sheathing. PF face and pMDI core: no |
| D | OSB- | OSB Siding. pMDI adhesive: LP Corporation, |
| E | OSB-H | Advantech OSB Sheathing. pMDI adhesive: Huber Engineered Woods LLC. TECO Mill |
| F | CDX | Sheathing Plywood (CDX) with PF adhesive, |
| G | HB | Hardboard Siding: LP Corporation. Roaring |

### 3.2.2 Descriptions of Selected Fuels

#### 3.2.2.1 Framing Lumbers

Framing lumber included Southern Yellow Pine (SYP) and Spruce-Pine-Fir (SPF). SYP is one of the strongest and most versatile species of wood, and has been used widely in buildings (FPL, 2010). SYP is one of the strongest softwood structural lumber species and has excellent load-bearing capacity and fastener-holding ability (FPL, 2010). SPF is also one of the most common and cost effective framing lumber. Similar to SYP, SPF is strong, lightweight, easy to work, and can hold nails well (FPL, 2010).

#### 3.2.2.2 Wood-Based Composites

The primary component of a wood-based composite is the wood element, often

94% or more by mass. Common elements for conventional wood-based composites include veneers, strands, particles, and fibers. Specific products addressed include panel products such as sheathing plywood (CDX) with PF adhesive, OSB sheathing with PMDI adhesive, and hardboard siding. Wood-based composites are used for a number of nonstructural and structural applications in product lines ranging from panels for interior covering purposes to panels for exterior uses and in furniture (Nicole, 1999).

#### 3.2.2.3 Plywood

Plywood panels are used in various applications, including construction sheathing, furniture, and cabinet panels. The properties of plywood depend on the quality of the veneer plies, the order of layers, the adhesive used, and the degree to which bonding conditions are controlled during production. It has significant bending strength both along the panel and across the panel, excellent dimensional stability along its length and across its width. In uses where internal knotholes and voids may pose a problem, such as in small pieces, plywood can be ordered with a solid core and face veneers. There are some studies about plywood combustibility. Plywood samples in the cone calorimeter undergo a piloted ignition procedure, during which the plywood is heated sufficiently to vaporize and form a flammable pre-mixed system, then ignited by a spark. The ignition time was a function of incident heat flux. The tests revealed that the minimum heat flux required for ignition elm-plywood was about 14.53kW/ $m^2$ which is lower than so-called the flashover heat flux at floor level of 20kW/ $m^2$, and for pine-plywood was about 21.95kW/ $m^2$ which is beyond 20kW/ $m^2$. It was observed that the elm-plywood was of higher fire risk than pine-plywood under 20kW/$m^2$

(Maranghides, 2011).

#### 3.2.2.4 Oriented Strand-Board

Oriented strand-board (OSB) is an engineered structural-use panel manufactured from thin wood strands bonded together with water-resistant resin, typically PF (phenol formaldehyde) or pMDI (polymeric Methylene Diphenyl Diisocyanate). It is used extensively for roof, wall and floor sheathing in residential and commercial construction. OSB panels are usually made up of three layers of strands, the outer faces having longer strands aligned in the long-direction of the panel and a core layer that is perpendicular or laid randomly using the smaller strands or fines. The orientation of different layers of aligned strands gives OSB its unique characteristics, including greater bending strength and stiffness in the orientation, and layered construction allows OSB to be engineered to suit different uses. OSB is extremely flammable because it is made up of glue holding wooden chips together. The glue is flammable (Thompson, 2001).

#### 3.2.2.5 Hardboard

Hardboard (HB), also known as high-density fiberboard or HDF, is an EWP that can be used for a number of purposes and projects. It is made from small wood fibers and wood pulp that is pressed until it is densely impacted and then baked for added stability. It is stronger and harder than most EWPs. Unlike particleboard, hardboard does not crack or split (FPL, 2010). During construction, hardboard is often used to protect other less durable wood before it is finished.

### 3.2.3 Fuel Properties

Fuel properties in this study included bulk density and moisture content level.

The density of wood and wood-based composites is primarily dependent on the species but it will also vary by individual tree and within that individual tree. Any moisture in the wood will also affect the density. In this study, the average bulk density of each sample was calculated from its mass and volume recorded prior to testing (Spearpoint, 2001).

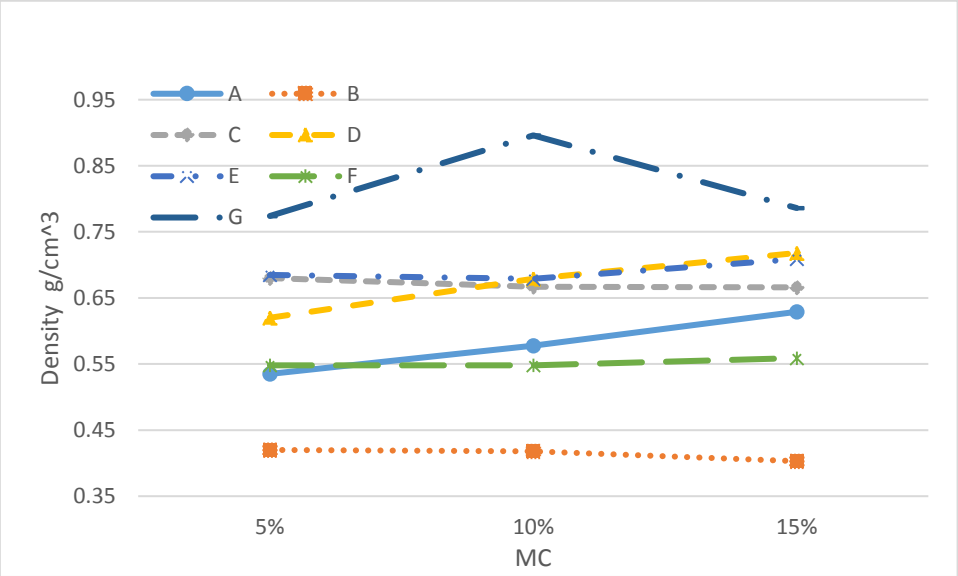


Figure 3.1. Density of selected fuels vs.MC

### 3.3 Specimen Moisture Content and Its Control

For the moisture content, it` has influence on the mass and size distribution of the firebrands (Manzello, 2009), as well as, the thermal conductivity and specific heat and thus the ignition characteristics of wood. The MC of a wood or wood-based composite can be calculated as the following

$$Moisture\ content = \frac{M_{wet} - M_{dry}}{M_{dry}} \times 100 \qquad \text{Equation (1)}$$

Where $M_{wet}$ and $M_{dry}$ are the masses of the sample before and after drying in the oven.

### 3.3.1 MCs Levels of As Received Specimens

The procedure for obtaining the MC level of a specimen was per ASTM D4442 Standard Test Methods for Direct Moisture Content Measurement of Wood and Wood-Based Materials (ASTM D4442, 2016). Method A - Primary Oven-Drying Method per ASTM D4442-15 was used to get the MCs levels of the as-received specimens. To prevent drying or uptake of moisture, each specimen was weighed immediately after receiving and cutting. If the specimen could not be weighed immediately, it was placed in two layers of plastic bag to protect it from moisture change until it could be weighed. Seven samples were used to measure the MC levels. The initial mass of the replicate samples were used to get the average mass before drying in the oven. Then, the specimens were placed in an oven heated to $103 \pm 2$ °C (214 to 221 °F), and kept there until no appreciable weight change occurred in 4-h weighing intervals.（The Sartorius M-prove was used to measure the sample weight, which offered 210 grams weighing capacity with readability to 0.01g.） After that, the mass of the oven-dried sample after were measured. The constant or oven-dry mass and the (original) mass of the specimen when cut were used to determine the percentage of MC of the specimen per Equation 1 (Richard, 1999). Table 3.2 shows the obtained MC levels of the as-received specimens.

Table 3.3. Specimen MC Level (as-received)

| Material | Specimen and MC Level Per ASTM D4442-15 (%) | | | | | | | Ave.(%) |
|---|---|---|---|---|---|---|---|---|
| A | A101 | A102 | A103 | A104 | A105 | A106 | A107 | 13.5 |
| | 17% | 14% | 13.7% | 13.9% | 8.7% | 13.6% | 13.8% | |
| B | B101 | B102 | B103 | B104 | B105 | B106 | B107 | 11.7 |
| | 18% | 11% | 7.8% | 11% | 11.4% | 11% | 10.7% | |
| C | C101 | C102 | C103 | C104 | C105 | C106 | C107 | 7.8 |
| | 26% | 4% | 4.3% | 4.4% | 4% | 4.3% | 4.7% | |
| D | D101 | D102 | D103 | D104 | D105 | D106 | D107 | 3.5 |
| | 4% | 2.7% | 3% | 3.2% | 4.8% | 3.2% | 3% | |
| E | E101 | E102 | E103 | E104 | E105 | E106 | E107 | 6.0 |
| | 4% | 6% | 4% | 5% | 4.5% | 12.5% | 3.7% | |
| F | F101 | F102 | F103 | F104 | F105 | F106 | F107 | 7.3 |
| | 7% | 1% | 6.3% | 6.7% | 7.6% | 6.2% | 6.3% | |
| G | G101 | G102 | G103 | G104 | Stable result for G, thus only four replicates | | | 5.7 |
| | 5.5% | 5.6% | 5.7% | 5.6% | | | | |

Table 3.3 shows that the MC levels of as-received wood in the experiment (SYP and SPF) were in the 10-15% range, and the MC levels of engineered wood-based composites were in the 5-10% range, except Material D (OSB-siding) with an average MC level of 3.5%.

### 3.3.2 MC Control to Desired Levels

For this study, three nominal MC levels were used to examine the effect of MC level on thermal degradation and combustion properties: 5%, 10%, and 15%. The 5% MC level represent a typical MC level of in-door structural fuels in a building. The 10% MC level represents a typical MC level of some exterior structural components (or possibly in-door components in a new construction). The 15% level represents a high level of MC in some exterior structural components or structural fuels in a new

construction (FPL, 2010). It should be noted that these values (5%, 10%, and 15%) are nominal values, the actual MC levels may vary from these nominal values.

An environmental chamber was used to condition the specimens to the pre-determined MC levels. A 4-$ft^3$ benchtop programmable environmental chamber from Espec (Model BTL-433, Serial Number IC-385) was used, as shown in Figure 3.2. The chamber has a temperature range of -20 to +180°C (-4 to +354°F) and a humidity range of 10% - 95% RH. The temperature fluctuation at control sensor is ±0.5, and the humidity fluctuation at control sensor is ±5.

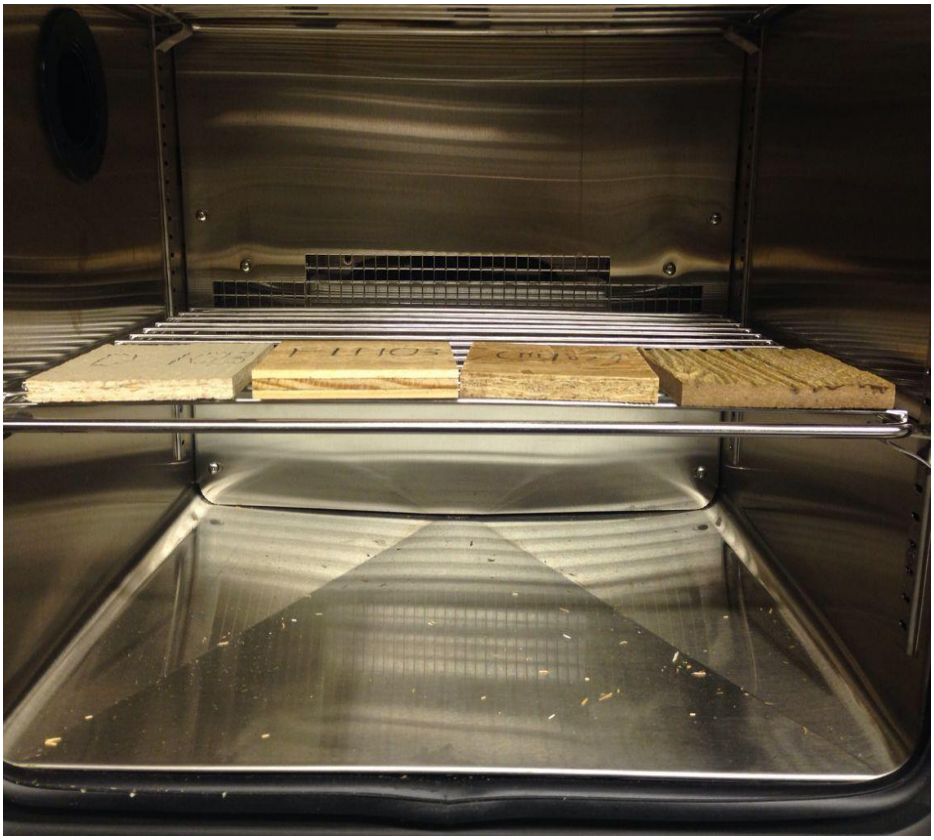

Figure 3.2. Samples in the environmental chamber

According to Green (2008), low temperature and high humidity were used to convert oven-dried samples into 5%, 10% and 15%. The result indicate lower

temperature leads to higher MC level (Green, 2008). From Table 3.2, the MC levels of as-received woods (A and B) are in the 10-15% range, it would be easy to get any pre-determined MC levels. The MC levels of engineered wood-based composites are in the 5-10% range, in order to get the 10% and 15% MC level, we would need the environmental chamber to improve the MC level. For Material D (OSB-siding) with an average MC level of 3.5%, we had to put it in the environmental chamber to get the 5%, 10%, 15% MC level.

According to ASTM D4933 Standard Guide for Moisture Conditioning of Wood and Wood-Based Materials, we followed the standard procedures for conditioning and equilibrating wood and wood-based materials to constant moisture content. (Specifically, Equilibrium Determination, Periodic Weighing and Endpoint Fluctuations). However, it was not easy to use the environmental chamber to increase the moisture content in the engineered wood-based composites. Table 3.3 showed that it took 20 days for some to achieve to the range of 5-10%. Thus an alternative method that can accelerate the conditioning process was needed.

Table 3.4. Samples MC Control (Using an Environmental Chamber)

| Time | 2016/3/1 | | | 15:00 | |
|---|---|---|---|---|---|
| h | C101 | D101 | E101 | F101 | G101 |
| 0 | 73.98 | 56.77 | 131.16 | 69 | 85.68 |
| 4 | 74.29 | 57.02 | 131.5 | 69.48 | 85.97 |
| 50 | 74.55 | 57.18 | 131.88 | 69.62 | 86.41 |
| 97 | 74.57 | 57.22 | 132 | 69.66 | 86.44 |
| 118 | 74.59 | 57.24 | 132.07 | 69.7 | 86.48 |
| 168 | 74.69 | 57.3 | 132.25 | 69.72 | 86.58 |
| 190 | 74.95 | 57.53 | 132.7 | 70.14 | 86.8 |
| 287 | 75.08 | 57.63 | 132.83 | 70.15 | 86.89 |
| 336 | 75.46 | 57.89 | 133.36 | 70.56 | 87.33 |
| 480 | 76.28 | 57.97 | 133.69 | 70.67 | 88.42 |
| MC | 11.20% | 5.70% | 8% | 9.90% | 9% |

A water-soaking and subsequent conditioning method was used to get the pre-determined high MC levels for wood-based composites. Materials C, F, and G were conditioned this way to get the 15% MC level, and materials D and E were ere conditioned this way to get both the 10% and 15% MC level. In this process, the samples were first soaked in water as shown in Figure 3.3. . After 20 hours, they were dried in the environmental chamber until the expected MC level was achieved. Table 3.4 shows some of the data. When necessary, a sample was put to the oven and dried to remove excessive water. When a sample achieved a pre-determined MC level, it was sealed by two layers of plastic bags for storage and the mass of the sample was recorded.

This mass was used to compare with the mass of the sample right before test to monitor that mass loss was insignificant during storage.

Figure 3.3. Soaking sample material in the water

It should be noted that this process may bring differences between average moisture (the one was measured) and the surface moisture.

Table 3.5. Soaking sample material mass change

| time | A | B | C | D | E | F | G | hours |
|---|---|---|---|---|---|---|---|---|
| 10:00 | 97.09 | 68.8 | 81.13 | 65.18 | 132.5 | 60.5 | 85.03 | 0 |
| 11:00 | 119.76 | 77.9 | 87.87 | 70.6 | 143.9 | 85.43 | 90.92 | 1 |
| 13:00 | 124.53 | 82.1 | 92.37 | 72.11 | 155.7 | 90.02 | 92.17 | 2 |
| 15:00 | 130.17 | 85.2 | 94.7 | 73.02 | 161.08 | 95.33 | 93.18 | 5 |
| 17:00 | 133.57 | 86.89 | 97.93 | 74.18 | 165.7 | 96.87 | 94.23 | 7 |
| 18:00 | 134.5 | 87.55 | 98.07 | 74.42 | 165.9 | 97 | 94.38 | 8 |
| 20:00 | 134.7 | 87.56 | 98.19 | 74.44 | 166.2 | 97.07 | 94.4 | 10 |
| next day | Chamber | | | | | | | |
| 10:00 | 128.89 | 87.15 | 97.89 | 74.19 | 157 | 91.02 | 94.42 | 24 |
| 13:00 | 128.94 | 86.72 | 97.16 | 72.35 | 155.99 | 90.47 | 92.63 | 27 |
| 18:00 | 129.15 | 86.86 | 93 | 71.4 | 155.42 | 89.94 | 92.35 | 32 |
| | 50% | 41% | 23.60% | 13.40% | 24.30% | 59.50% | 14.80% | |

## 3.4 Experimental Procedures

For fuel properties test, the one controlling factor was the MC level. For the pyrolysis properties test, there were three controlling factors: MC level, temperature, and heating rate. For the combustion properties test, there were two controlling factors: MC level and heat flux level. Table 3.5 shows the properties to be measured in the experiments. .

Table 3.6. Properties to be Measured

| Fuel Properties | Thermal Properties | Combustion Properties |
|---|---|---|
| $v$, ρ | Pyrolysis Kinetics(A and E) | PHRR, critical heat flux |
| | | ML, MLR, EHC |
| $M_{wet}, M_{dry}$, MC | Thermal conductivity ($k$) | TTI, Flame out time |

The sample identification used in this study is explained in Figure 3.4 and Tables 3.6 and 3.7:

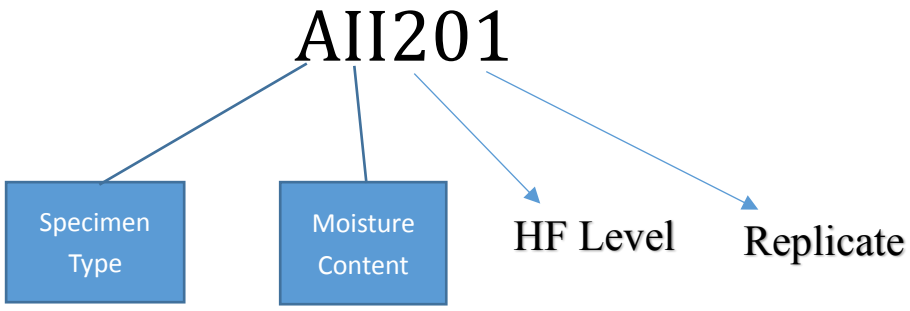


Figure 3.4. Sample material label guide

Table 3.7. Sample material label guide

| Parameter | | | |
|---|---|---|---|
| Moisture Content | | Heat Flux Level | |
| II | 5% | 1 | 20(kW/m^2) |
| III | 10% | 2 | 30(kW/m^2) |
| IV | 15% | 3 | 50(kW/m^2) |

Table 3.8. Combustion Test Scope (Small-scale Material Characterization)

| # | **Description** | **Moisture** | **Heat Flux** | **Material ID** |
|---|---|---|---|---|
| A | SPIB SYP | MC=5% | 20, 30, 50 | AII101-103,AII201-203,AI301-303 |
| | | MC=10% | | AIII101-103,AIII201-203,AIII301-303 |
| | | MC=15% | | AIV101-103,AIV201-203,AIV301-301 |
| B | CMSA SPF | MC=5% | 20, 30, 50 | BII101-103,BII201-203,BII301-303 |
| | | MC=10% | | BIII101-103,BIII201-203,BIII301-303 |
| | | MC=15% | | BIV101-103,BIV201-203,BIV301-303 |
| C | OSB PF | MC=5% | 20, 30, 50 | CII101-103,CII201-203,CII301-303 |
| | | MC=10% | | CIII101-103,CIII201-203,CIII301-303 |
| | | MC=15% | | CIV101-103,CIV201-203,CIV301-303 |
| D | OSB SIDING PMDI | MC=5% | 20, 30, 50 | DII101-103,DII201-203,DII301-303 |
| | | MC=10% | | DIII101-103,DIII201-203,DIII301-303 |
| | | MC=15% | | DIV101-103,DIV201-203,DIV301-303 |
| E | PMDI ADHESIVE OSB | MC=5% | 20, 30, 50 | EII101-103,EII201-203,EII301-303 |
| | | MC=10% | | EIII101-103,EIII201-203,EIII301-303 |
| | | MC=15% | | EIV101-103,EIV201-203,EIV301-303 |
| F | CDX SYP | MC=5% | 20, 30, 50 | FII101-103,FII201-203,FII301-303 |
| | | MC=10% | | FIII101-103,FIII201-203,FIII301-303 |
| | | MC=15% | | FIV101-103,FIV201-203,FIV301-303 |
| G | HARDBOARD SIDING | MC=5% | 20, 30, 50 | GII101-103,GII201-203,GII301-303 |
| | | MC=10% | | GIII101-103,GIII201-203,GIII301-303 |
| | | MC=15% | | GIV101-103,GIV201-203,GIV301-303 |

TGA was performed at three different heating rate levels (5, 15, and 25℃/min)

so that the thermal degradation kinetics of fuels would be investigated over a range of heating conditions. It is known that the heating rate affects both the location of the TGA curve and the maximum decomposition rate. Thermal conductivity measurements were conducted for three replicates in 25 and 100℃ so that the fuel's conductivity and diffusivity properties could be quantified in a range of temperatures. The combustion test using the Cone Calorimeter used three replicates at each heat flux level for each fuel MC level. Since the critical heat flux depends on the fuel type and MC level, each fuel was tested to determine as appropriate for this type of fuel according to its combustion results from the test at the critical heat flux level.

The following thermal degradation properties were measured for each fuel at designed MC levels through small-scale thermal analysis experiments: thermal degradation kinetics (measured by mass loss and mass loss rate), and temperature-dependent thermal conductivity. Before testing, structural properties (geometry and dimensions) of the fuel were be measured. The small-scale combustion experiments were performed using a Cone Calorimeter. After the specimens were ready for testing, ASTM E1354 was used for specimen preparation, testing, and protocol for data collection. The following combustion properties were measured: heat release rate (HRR, including peak and average values, PHRR), mass loss (ML) and mass loss rate (MLR), effective heat of combustion (EHC), and time to ignition (TTI). Ambient temperature, and relative humidity were measured for each test.

Quantitative data analysis were performed for the small-scale thermal analysis, fuel structural property measurements, and combustion tests.

## 3.5 Data Analysis

### 3.5.1 Pyrolysis Properties

Pyrolysis kinetics can be used to calculate the activation energies of different pyrolysis phases, which could be measured by TGA (Kollmann, 1960). Previous studies used data on weight loss as a function of temperature generated from TGA equipment to study pyrolysis kinetics of woody biomass. For example, the isothermal method used constant temperatures while non-isothermal heating ramps the temperature from ambient to the target temperature at a given heating rate. The rate of decomposition is a function of temperature and conversion

$$\frac{d_\alpha}{d_t} = f(T, \alpha) \qquad \text{Equation (2)}$$

It is possible to rewrite the right hand side of it by two functions, where the first one is dependent on temperature and the second one is a function of conversion

$$\frac{d_\alpha}{d_t} = k(T)g(\alpha) \qquad \text{Equation (3)}$$

The temperature dependent function $k(T)$ is usually expressed by the Arrhenius equation

$$k(T) = Aexp(\frac{-E}{RT}) \qquad \text{Equation (4)}$$

Where A is the pre-exponential factor, E is the activation energy, and R is the universal gas constant. There are various possibilities how to express the conversion function g (α). In this study, the form used was as follows

$$g(\alpha) = (1-\alpha)^n \ \frac{-E}{RT}) \qquad \text{Equation (5)}$$

where n is the reaction order. Combining previous equations, the decomposition kinetic equation is obtained (Gasparovic,2010)

Combining all previous equations, the decomposition kinetic equation is obtained as the following (Gasparovic et al., 2010)

$$\frac{d_\alpha}{d_t} = Aexp(\frac{-E}{RT})(1-\alpha)^n \qquad \text{Equation (6)}$$

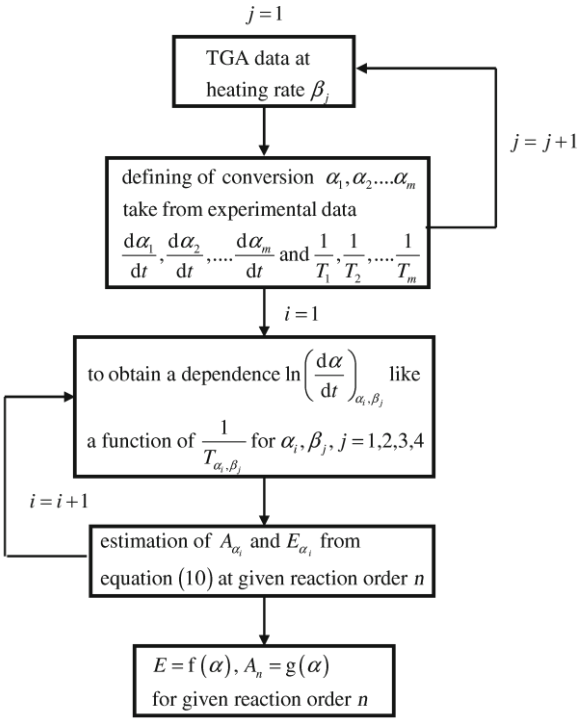


Figure 3.5. Block diagram for the estimation of A and E (Gasparovic et al., 2010)

A common practice for obtaining the Arrhenius parameters is to graphically fit the TGA curves using the equation above. We could rewrite the equation into

$$\frac{d_w^2}{d_t d_T} = -Anw^{n-1}\frac{d_W}{d_T}\exp\left(-\frac{E}{RT}\right) - Aw^n\exp(-\frac{E}{RT})\frac{E}{RT^2} \qquad \text{Equation (7)}$$

It could be modified because at the temperature point corresponding to peak mass loss rate $\frac{d_w^2}{d_t d_T} = 0$

$$\frac{1}{\beta}Anw^{n-1}\exp\left(-\frac{E}{RT}\right) = \frac{E}{RT^2} \qquad \text{Equation (8)}$$

Where $\beta = \partial T/\partial t$ is the heating rate. Using TGA results at different heating rates, it could be solved for Arrhenius parameters A, n and E (Yu and Zhou, 2010).

There are many methods for analyzing non-isothermal solid-state kinetic data from TGA (Slopiecka, 2012). These methods can be divided into two types: model-fitting and model-free (iso-conversional) methods, as summarized in Table 3.8 (Khawam, 2005). A model fitting method fits different models to the data so that a model is chosen when it gives the best statistical fit as the model from which the kinetic parameters are calculated. A conversional method requires several kinetic curves to perform the analysis. Calculations from several curves at different heating rates are performed on the same value of conversion, which allows to calculate the activation energy for each conversion point.

Table 3.9. Methods for studying solid-state kinetics (Khawam, 2005)

| Model-fitting | | Model-free | |
|---|---|---|---|
| Isothermal | Non-isothermal | Isothermal | Non-isothermal |
| – Conventional | – Differential<br>– Freeman–Carroll<br>– Coats–Redfern | – Standard<br>– Friedman<br>– AIC | – Kissinger<br>– Flynn–Wall and Ozawa (FWO method) |

There are many model fitting methods that extract the three kinetic parameters known as the kinetic triplet (A, E and model) from non-isothermal data. These methods were used extensively earlier in solid-state kinetic analysis and they continue to appear. These methods have been critically evaluated (Khawam, 2005) and it's been shown that the sole use of these methods is not recommended because:

1. They assume a constant kinetic triplet (A, E and model).

2. They involve fitting three parameters (A, E and model) which are determined from a single run (i.e., one hating rate).

3. They involve a single heating rate which is not always sufficient to determine reaction kinetics.

The use of single-heating rate data for the determination of kinetic parameters should be avoided. At least three heating rates are necessary in order to correctly describe the course of the reaction (Marek, 1999).

The advantage of the model free analysis is founded on its simplicity and on the avoidance of errors connected with the choice of a kinetic model. Disadvantage of these methods are a series of measurements at different heating rate which must be made for the same samples mass and the same volume flow of inert gas and their fluctuation can cause of errors. From a mathematical point-of-view, model-fitting methods that use multi-heating rate data and assume a multi-step nature of the process can describe the course of a solid reaction sufficiently well (Marek, 1999).

Pyrolysis heat is negative for exothermic reactions and positive for endothermic reactions, which can be measured by DSC. In the study of Pyrolysis Kinetics of Physical Components of Wood and Wood-Polymers Using Isoconversion Method, Cellulose showed activation energy values in the range of 208 to 381 $\frac{kJ}{mol}$ during decomposition whereas xylan and lignin had maximum activation energy values of 348 $\frac{kJ}{mol}$ and 801 $\frac{kJ}{mol}$ at fractional conversions of 0.4 and 0.5, respectively. The activation energy requirement for wood components remained within the range of 233 $\frac{kJ}{mol}$ to 388

$\frac{kJ}{mol}$ until 365℃ and then peaked to roughly $943\frac{kJ}{mol}, 499\frac{kJ}{mol} and\ 298\frac{kJ}{mol}$ for bark, sapwood and heartwood at 375℃ where major energy input for lignin decomposition is needed. Also, it was observed that the isoconversion methods may not work for all the fractional conversion values for individual wood polymers but the method worked well for the wood components (Jin et al., 2013);

While thermal conductivity $k$ is a measure of the rate of heat flow through a material subjected to unit temperature difference across unit thickness (Michael, 1999):

$$k = \frac{rate\ of\ heat\ flow}{thickness} \qquad \text{Equation (9)}$$

Here, we measured it using DTC (Direct Thermal Conductivity Measurement).

### 3.5.2 Combustion Properties

The Cone Calorimeter was developed by NIST during the 1990s as an apparatus primarily for measuring the HRR of small-scale specimens. The method has been published as ASTM E 1354, ISO 5660, and in various specialized standards. Because of the uniform exposure provided to specimens, it has become widely used for measuring additional fire properties: mass loss rate, ignitability, smoke production rate, and toxic gas production (Babrauskas, 2003).

Fires differ greatly in their heat and mass transport, defined by characteristics such as applied heat flux. The developing stage of fire growth is characterized by an external heat flux (around 20–60 kW/m$^2$), while a fully-developed stage of fire growth is characterized by a high external heat flux (>50 kW/m$^2$). So we selected 20 kW/m$^2$, 30 kW/m$^2$ and 50 kW/m$^2$ as our cone calorimeter test heat flux (Schartel, 2007). The cone calorimeter used for this study is shown in Figure 3.6.

Figure 3.6. Cone Calorimeter in UNCC

## 3.6 Data Collection and Analysis

### 3.6.1 Data Collection and Analysis for Pyrolysis Properties

The Flynn-Wall-Ozawa (FWO) method (Slopiecka, 2012) allows to obtain apparent activation energy (E) from a plot of natural logarithm of heating rates, $ln\beta$,

versus $1000/T$, which represents the linear relation with a given value of conversion at different heating rates.

$$\ln(\beta) = \ln\left(\frac{A_\alpha E_\alpha}{R g_{(\alpha)}}\right) - 5.331 - 1.052\frac{E_\alpha}{RT_{\alpha i}} \quad \text{Equation (10)}$$

Assume $\frac{1}{T_{\alpha i}} = 0$

$$y = \ln\left(\frac{AE}{R g_{(\alpha)}}\right) - 5.331 \quad \text{Equation (11)}$$

$$A = \frac{Rg}{E} e^{y+5.331} \quad \text{Equation (12)}$$

$$g_{(\alpha)} = \int_0^\alpha \frac{d_\alpha}{(1-\alpha)^n} = \frac{1-(1-\alpha)^{1-n}}{1-n} \quad n \neq 1 \quad \text{Equation (13)}$$

$$g_{(\alpha)} = \int_0^\alpha \frac{d_\alpha}{1-\alpha} = -\ln(1-\alpha) \quad n = 1 \quad \text{Equation (14)}$$

Here, according to the standard requirement, based on the assumption that the decomposition obeys first-order kinetics.

$$A = \frac{Rg}{E} e^{y+5.331} = -\frac{Rg}{E} e^{y+5.331} \quad \text{Equation (15)}$$

Where $g_{(\alpha)}$ is constant at a given value of conversion. The subscript $i$ and $\alpha$ denotes given value of heating rate and given value of conversion, respectively. The activation energy $E_\alpha$ is calculated from the slope$-1.052E_\alpha/R$. To determine the kinetic parameters, we chose the same value of $\alpha$ from range 0.05 to 0.7 for all curves at different heating rate and we found the corresponding temperature.

The applicability of the method to other types of thermal analyses has been discussed, and the method of the conversion of the data to other conditions of temperature change has been suggested.

Procedures in ASTM E1641 were used in this study. ASTM E1641 is generally applicable to materials with well-defined decomposition obeys profiles, namely, a smooth, continuous mass change with a single maximum rate. This test is normally

applicable to decomposition occurring in the range from 400 to 1300K (nominally 100 to 1000°C).

This test method is based upon the general rate equation that takes the form of:

$$\frac{d_\alpha}{d_T} = A(1-\alpha)\exp\left[-\frac{E}{RT}\right]/\beta \qquad \text{Equation (16)}$$

Where:

α =fraction reacted(dimensionless), A= pre-exponential factor($min^{-1}$),

β =heating rate(K/min), E=activation energy(J/mol), R=gas constant(=8.316J/(mol K)), T= absolute temperature(K), exp=Euler's number exponential, and $\frac{d_\alpha}{d_T}$ =rate of change of α with T.

Using the method of Ozawa, Flynn and Wall, it may be solved for activation energy:

$$\mathrm{E} = \left(\frac{\mathrm{R}}{\mathrm{b}}\right)\Delta\log(\beta)/\Delta(1/\mathrm{T}) \qquad \text{Equation (17)}$$

Using a point of constant conversion from a series of decomposition curves obtained at different heat rates, $\Delta\log(\beta)/\Delta(1-\mathrm{T})$ was obtained by linear regression.

Assuming an initial value of b=0.457, a first approximation of activation energy ($E'$) was obtained, this approximate activation energy was then used to determine a new value of $b'$ using the following table. After$\frac{E}{RT} > 60$, we used MATLAB to analyze data above, got the tendency curve of a and b, and estimated a and b value.

Based upon the general rate equation:

$$\frac{d_\alpha}{d_t} = A(1-\alpha)\exp\left[-\frac{E}{RT}\right]/\beta \qquad \text{Equation (18)}$$

Solved for activation energy:

$$E = \left(\frac{R}{b}\right)\Delta\log[\beta]/\Delta(1/T) \qquad \text{Equation (19)}$$

Pre-exponential factor (A):

$$A = \left(-\frac{\beta R}{E}\right)[\ln[1-\alpha]]10^{a} \qquad \text{Equation (20)}$$

First order

$$g_{(\alpha)} = \int_0^{\alpha} \frac{d_\alpha}{1-\alpha} = -\ln(1-\alpha) \quad n = 1 \qquad \text{Equation (21)}$$

We would take the data after 100℃

We divided the curve into two periods: before 240℃ and after 240℃

The iterative process was continued until the value of activation energy no longer changes with the next iteration.

For first order reactions (n=1), the value of the pre-exponential factor (A) may be determined using$A = (-\beta R/E)(\ln[1-\alpha])10^{a}$, a= the Doyle approximation value. For OSB Sheathing, PF face and pMDI core, we used steps in the appendix to get the following table:

Table 3.10. $1000/T \sim \alpha$ for CII 5, 15, 25 K/min heating rate

| | 5 K/min heating rate | | 15 K/min heating | | 25 K/min heating | |
|---|---|---|---|---|---|---|
| α | $\ln\frac{d_T}{d_t}$ | 1000/T | $\ln\frac{d_T}{d_t}$ | 1000/T | $\ln\frac{d_T}{d_t}$ | 1000/T |
| 0.1 | -2.49 | 1.85 | -1.39 | 1.82 | -0.87 | 1.79 |
| 0.15 | | 1.79 | | 1.76 | | 1.73 |
| 0.2 | | 1.75 | | 1.72 | | 1.69 |
| 0.25 | | 1.72 | | 1.69 | | 1.66 |
| 0.3 | | 1.7 | | 1.66 | | 1.64 |
| 0.35 | | 1.67 | | 1.64 | | 1.615 |
| 0.4 | | 1.65 | | 1.62 | | 1.6 |
| 0.45 | | 1.63 | | 1.6 | | 1.58 |
| 0.5 | | 1.62 | | 1.58 | | 1.56 |
| 0.55 | | 1.6 | | 1.565 | | 1.54 |
| 0.6 | | 1.58 | | 1.545 | | 1.53 |
| 0.65 | | 1.54 | | 1.52 | | 1.5 |
| 0.7 | | 1.42 | | 1.43 | | 1.42 |
| 0.75 | | 1.19 | | 1.28 | | 1.28 |

Using the method in the appendix, we got the following figures for activation energy and pre-exponential factor under different heating rate of CII:

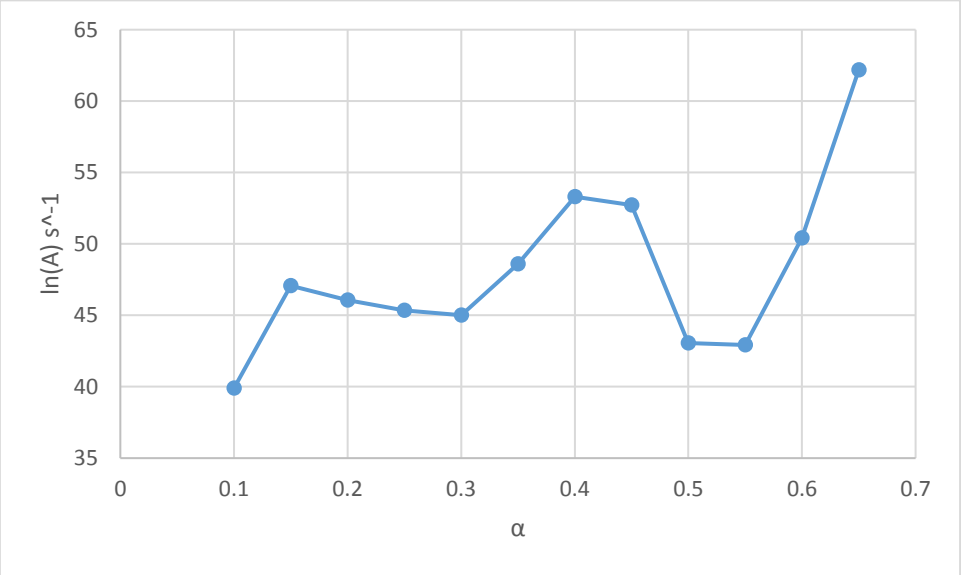


Figure 3.7. CII 5 K/min heating rate ln (A)

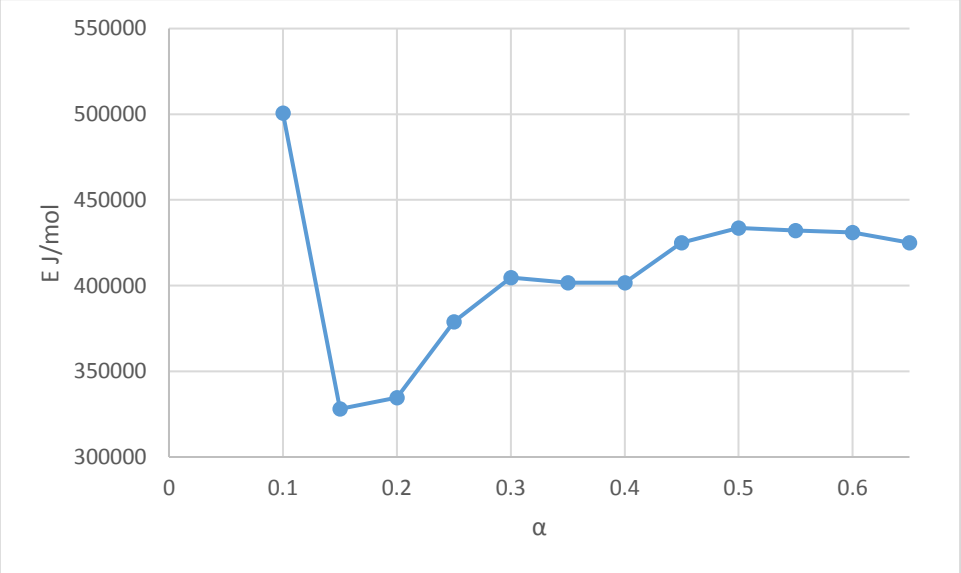


Figure 3.8. CII 5 K/min heating rate E

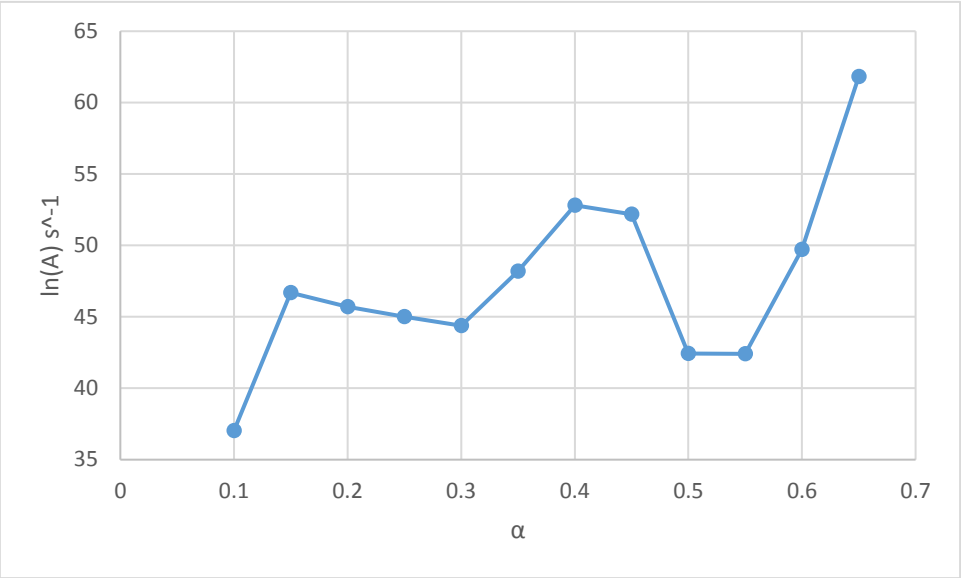


Figure 3.9. CII 15 K/min heating rate ln (A)

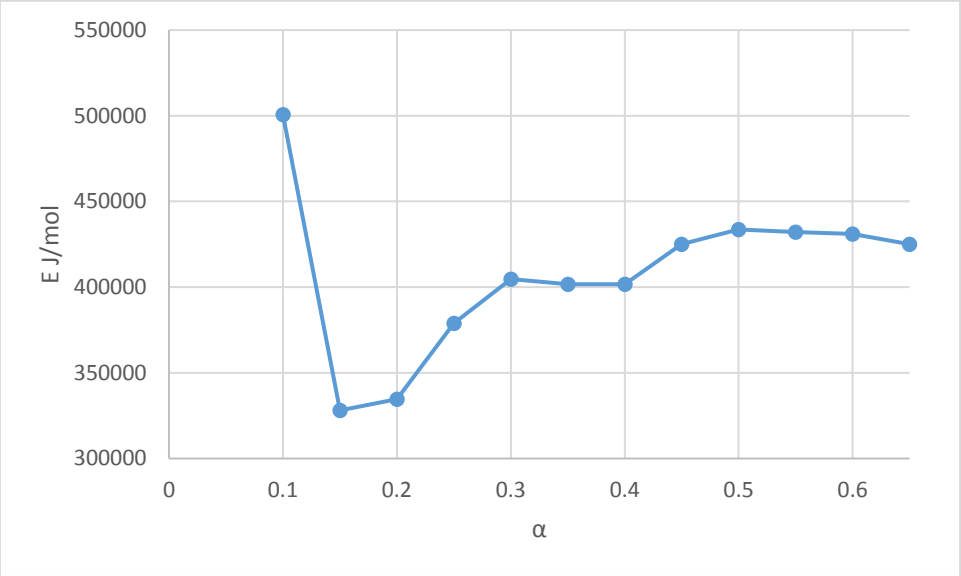


Figure 3.10. CII 15 K/min heating rate E

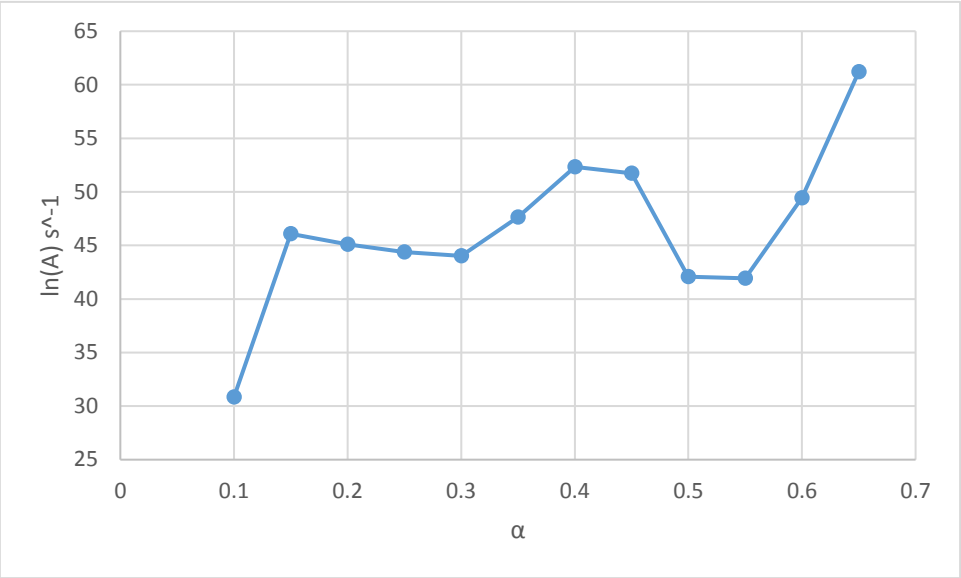


Figure 3.11. CII 25 K/min heating rate ln (A)

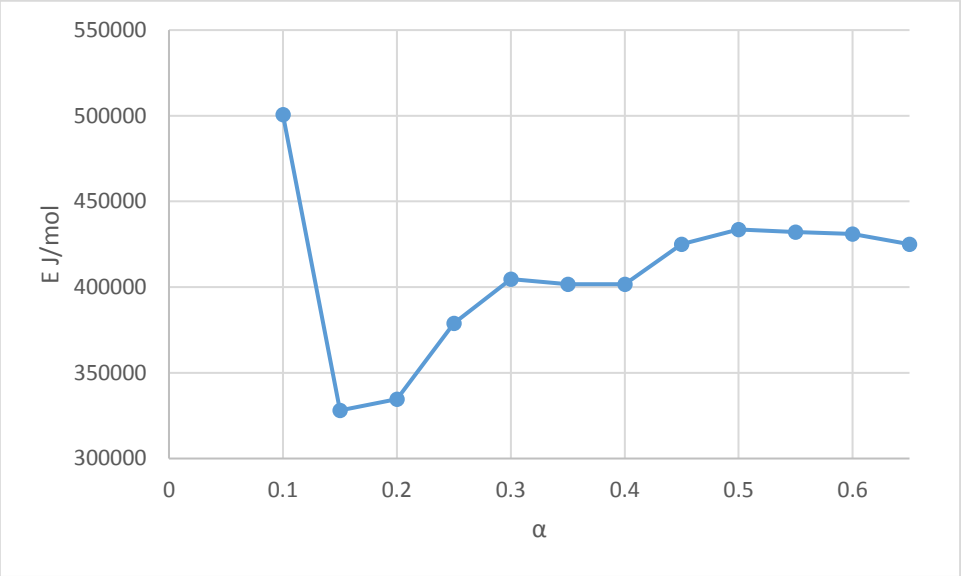


Figure 3.12. CII 25 K/min heating rate E

As a result, FWO shows a reasonable curve. So that we can get the variation of E, which can be referred to (Jin, 2013)

### 3.6.2 Data Collection and Analysis for Combustion Properties

Data collection and analysis followed procedures in ASTM E1354. The 180-s mean HRR readings shall be compared for the three specimens. If any of these mean readings differ by more than 10 % from the average of the three readings, then a further

set of three specimens shall be tested. In such cases, report the averages for the set of six readings. According to this principle, we selected the effective data, and got combustion properties for each sample. For example, the combustion properties of sample CII are shown in Tables 3.11, 3.12, and 3.13 for heat flux levels of 20, 30 and 50 kW/m$^2$ respectively.

Table 3.11. CII kW/m$^2$ cone calorimeter data

| Test | t(ig) (s) | t(fo) (s) | HRR(peak) (KW/m^2) | HRR(180) (KW/m^2) | MLR(av) (g/s·m^2) | EHC(av) (MJ/kg) |
|---|---|---|---|---|---|---|
| Mean | 192 | 1168 | 193.95 | 128.92 | 6.52 | 13.93 |
| 1 | 230 | 1284 | 228.68 | 123.26 | 3.38 | 13.93 |
| 2 | 184 | 1207 | 181.33 | 132 | 7.72 | 14 |
| 3 | 161 | 1012 | 171.83 | 131.48 | 8.46 | 13.86 |

Table 3.12. CII 30 kW/m$^2$ cone calorimeter data

| Test | t(ig) (s) | t(fo) (s) | HRR(peak) (KW/m^2) | HRR(180) (KW/m^2) | MLR(av) (g/s·m^2) | EHC(av) (MJ/kg) |
|---|---|---|---|---|---|---|
| Mean | 76.3 | 788 | 206.76 | 141.37 | 9.18 | 13.59 |
| 1 | 69 | 672 | 235.99 | 143.85 | 10.24 | 14.1 |
| 2 | 76 | 939 | 179.6 | 135.69 | 7.82 | 12.88 |
| 3 | 84 | 752 | 204.69 | 144.58 | 9.49 | 13.8 |

Table 3.13. CII 50kw/m^2 Cone calorimeter data

| Test | t(ig) (s) | t(fo) (s) | HRR(peak) (KW/m^2) | HRR(180) (KW/m^2) | MLR(av) (g/s·m^2) | EHC(av) (MJ/kg) |
|---|---|---|---|---|---|---|
| Mean | 24.3 | 926.7 | 303.75 | 201.56 | 7.75 | 15.87 |
| 1 | 28 | 960 | 270.47 | 186.99 | 7.35 | 15.13 |
| 2 | 21 | 900 | 315.45 | 202.64 | 7.96 | 15.91 |
| 3 | 24 | 920 | 325.33 | 215.05 | 7.94 | 16.58 |

The critical heat flux (CHF) for ignition for the CII samples can be obtained by using the TTI values of the samples at 20, 30 and 50 kW/m$^2$. Firstly, the function between heat flux and TTI was built in the Figure 3.13. From the function, the interception value was obtained.

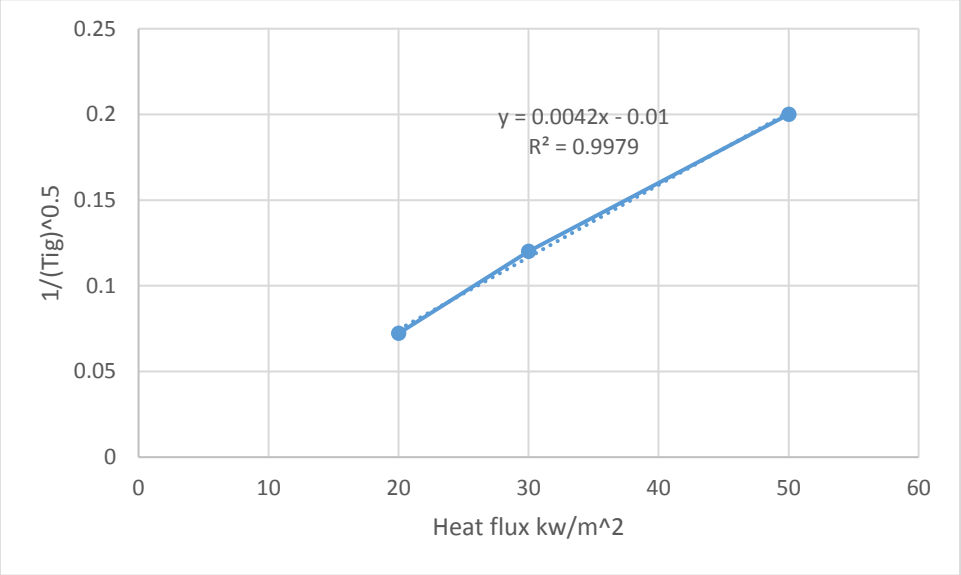


Figure 3.13. CII Critical heat flux

The integral analysis for ignition assumed an ignition based on a critical temperature of the structure due to an applied radiative heat flux (Spearpoint, 2001).

The following assumptions were made for the ignition model:

a. Ignition occurs when the surface temperature achieves critical value, $T_{ig}$.

b. Solid is inert up to ignition.

c. Solid is infinitely thick

After the basic theory, we could get heat flux is found from

$$\dot{q}_{cr}^{"} = \frac{(\dot{q}_i^{"})_{intercept}}{0.76} \qquad \text{Equation (22)}$$

To get the critical heat flux, from Figure 3.13, the interception value was obtained, according to equation (22), the CHF was obtained. In the same way, the CHF values for other samples were obtained using the above process.

# CHAPTER 4: RESULTS AND DISCUSSIONS

## 4.1 Fuel Properties

Dry wood undergoes small changes in dimension with normal changes in relative humidity. More humid air will cause slight swelling, and drier air will cause slight shrinkage (FPL, 2010). The changes in mass and dimensions of the wood or wood-based composite will affect the bulk density of the material.

### 4.1.1 Thickness of Selected Fuels

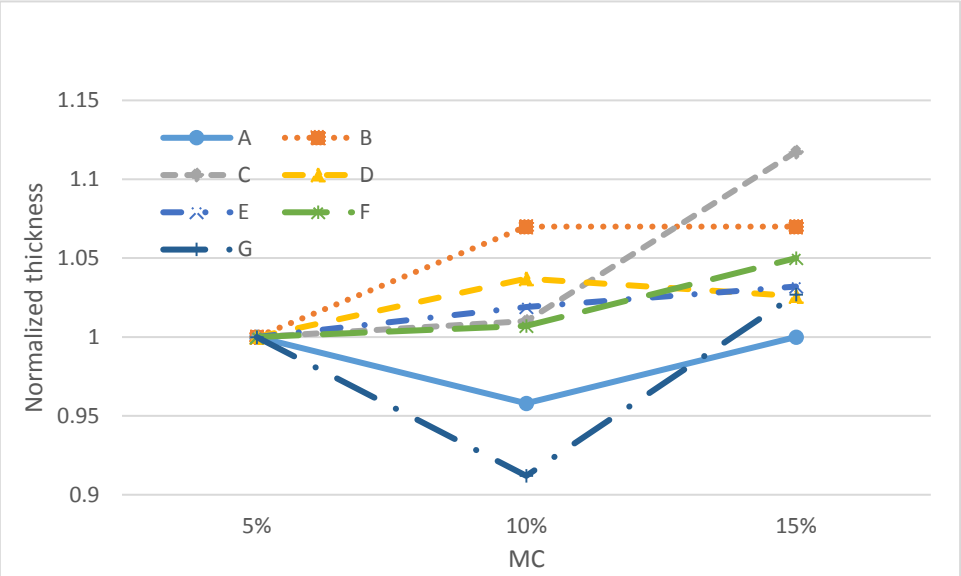


Figure 4.1. Normalized thickness vs.MC

Figure 4.1 shows the normalized thickness of the selected structural fuels as a function of the three pre-determined MC levels. All the data points were average values from three replicates. The average thickness of SYP (Material A) decreased from MC

5% to 10%, increased from MC10% to 15%. The average thickness of SPF (Material B) increased as the MC increased. The average thickness of OSB-PF (Material C) increased as the MC increased. The average thickness of OSB-Siding (Material D) increased from MC 5% to 10%, but decreased from MC 10% to 15%. The average thickness of OSB-H (Material E) increased as the MC increased. The average thickness of CDX (Material F) increased as the MC increased. The average thickness of HB (Material G) decreased from MC 5% to 10%, but increased from MC 10% to 15%.

### 4.1.2 Area of Selected Fuels

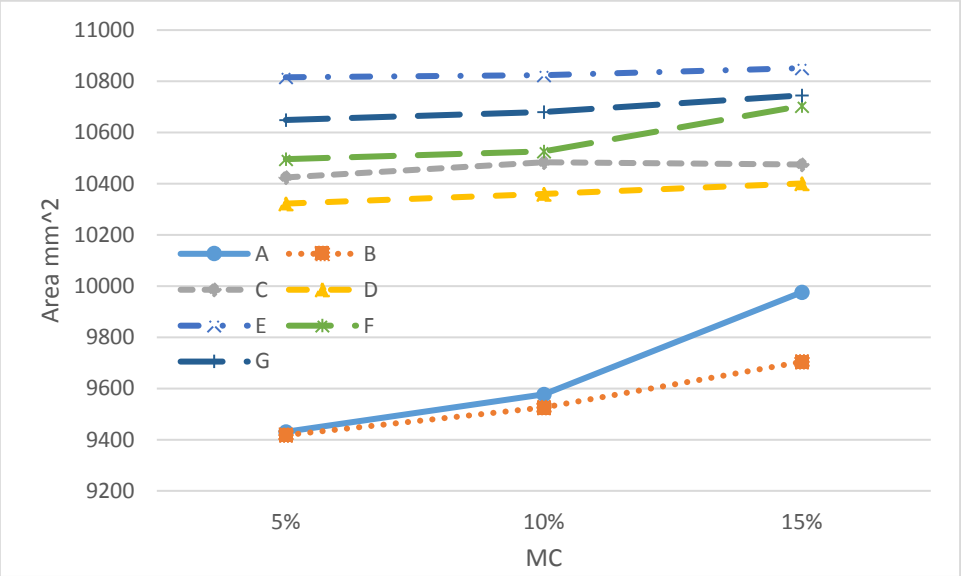


Figure 4.2. Area of selected structural materials vs.MC

Figure 4.2 shows the changes of area as a function of MC levels. The area of all selected structural materials increased as the MC level increased.

### 4.1.3 Density of Selected Fuels

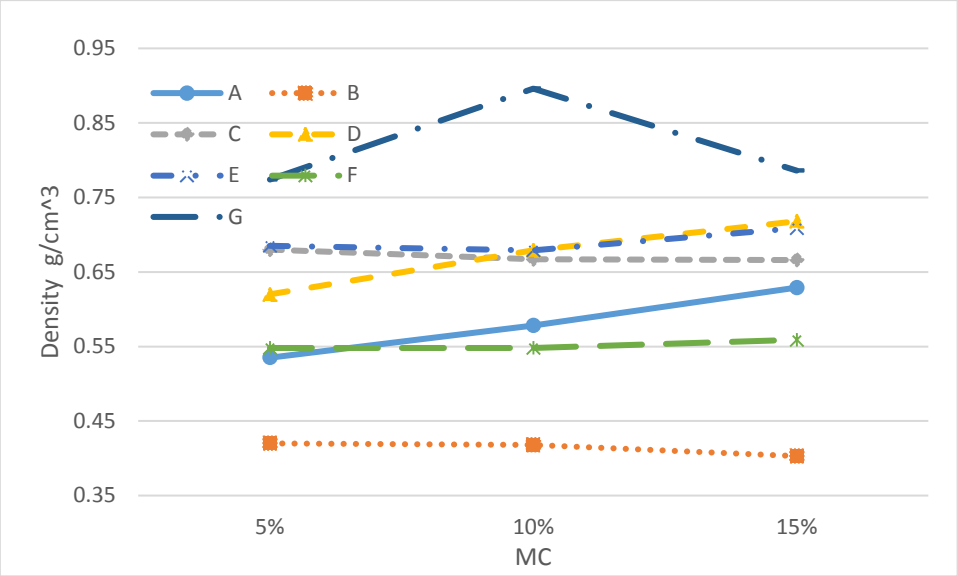


Figure 4.3. Density of selected structural materials vs.MC

The density at a MC level (i.e., density based on the mass of a specimen including moisture and its volume at the same moisture content) was used in this study (ASTM D2395-14). The density of a material was determined by dividing the mass (in grams) to the volume (in $cm^3$) of the specimen at a specific MC level. Figure 4.3 shows the bulk density of the materials as a function of MC levels. Each data point was the average from three replicates. The density of OSB-H, OSB-Siding and OSB-PF were close. The density of HB was the biggest, and the density of SPF was the smallest. As the MC level increased, the density of SYP, OSB-Siding, OSB-H and CDX increased slightly, while SPF and OBS-sheathing decreased slightly. The density of HB had the highest density at MC level 10%.

## 4.2 Thermal and Pyrolysis Properties

### 4.2.1 Thermal Conductivity

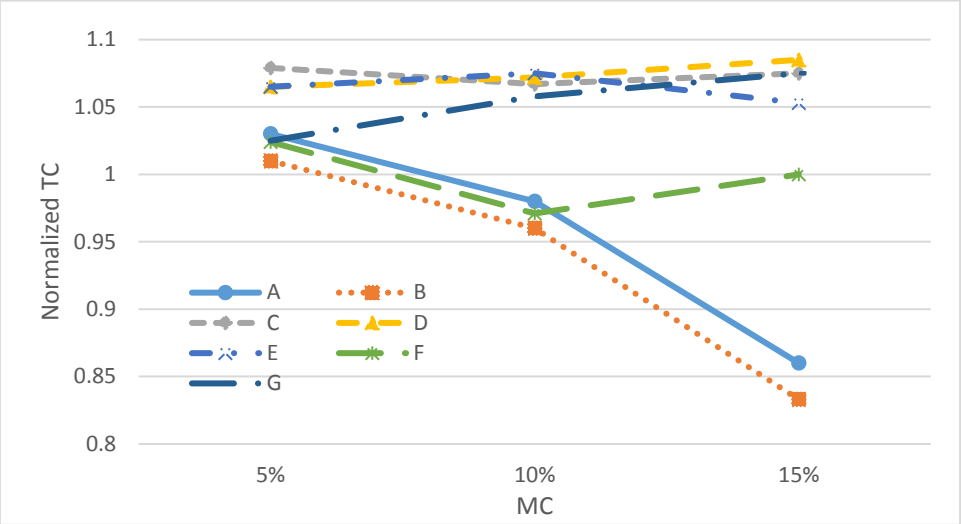


Figure 4.4. Normalized thermal conductivity vs.MC

Figure 4.4 shows the normalized thermal conductivity of the materials as a function of MC levels. All data points were the average from three replicates. The thermal conductivity of water is much bigger than woods and wood-based composites (FPL, 2010FPL, 2010). As temperature increased from 25°C to 100°C, the thermal conductivity increased except SYP, SPF and CDX.

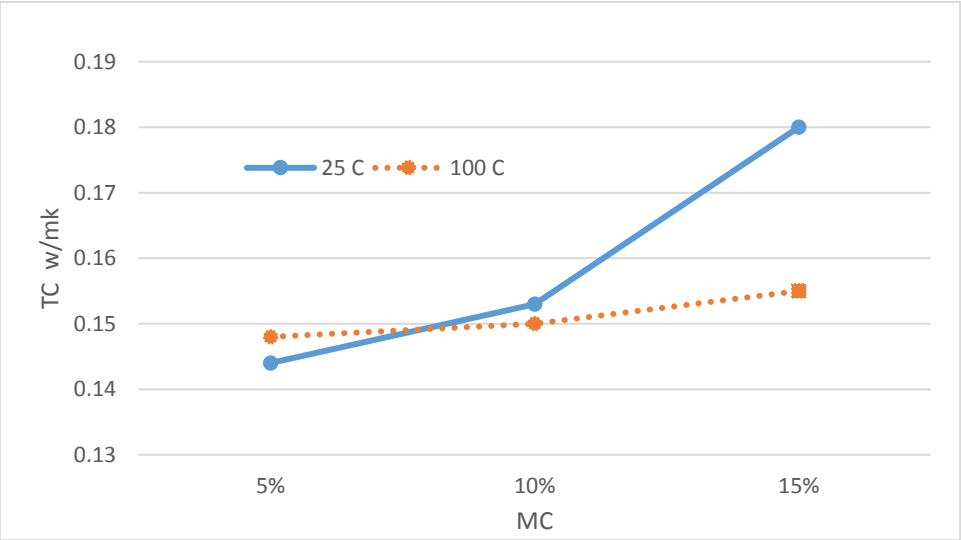


Figure 4.5. SYP (Material A) thermal conductivity vs.MC

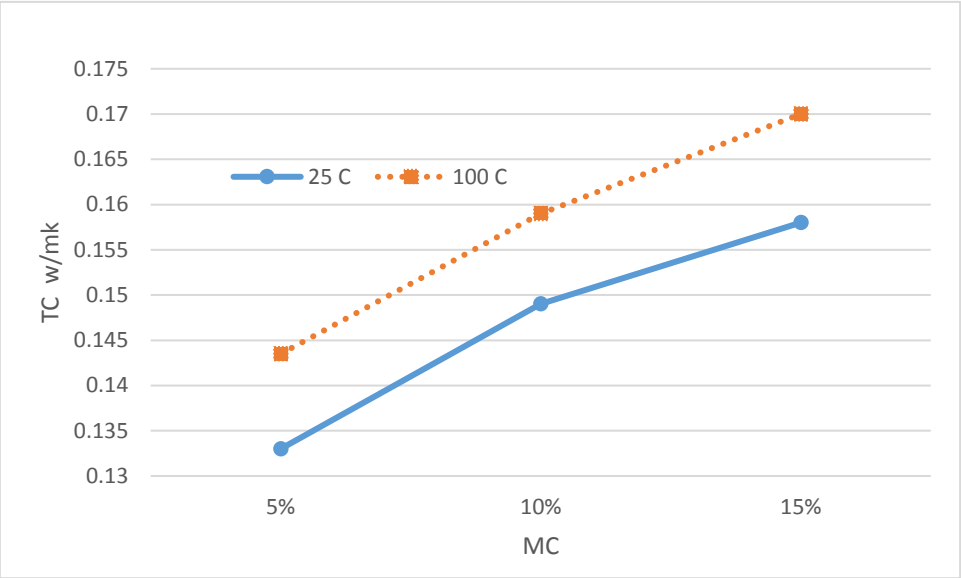


Figure 4.6. OSB-PF (Material C) thermal conductivity vs.MC

The effects of MC levels and temperature on thermal conductivity of materials A (SYP) and C (OSB-PF) are shown in Figures 4.5 and 4.6. All data points are average values from three replicates. The effects of MC levels and temperature on thermal conductivity of materials are shown in Appendix B. The thermal conductivity of woods and wood-based composites increased as the MC level increased. Overall, temperature had smaller impact on thermal conductivity than MC level.

### 4.2.2 Pre-Exponential Factor (A)

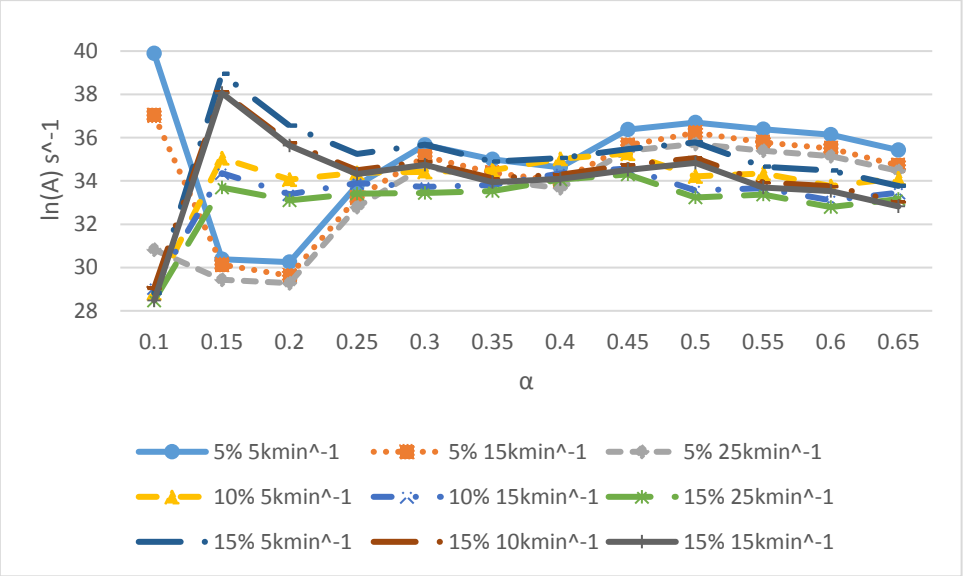


Figure 4.7. SYP (Material A) ln (A) vs.MC

Figures 4.7-4.13 show the pre-exponential factor (A) of the Arrhenius equation as a function of MC levels for materials A-G. α is the fraction reacted (or pyrolysized) or conversion factor of the material. The details about data analysis for the pyrolysis parameters are in Appendix A. From Figure 4.7, when $\alpha < 0.15$,The ln(A) value of SYP decreased at 5% MC, increased at 10% and 15% MC. When$0.15 < \alpha < 0.25$, the ln(A) value of SYP increased at 5% MC, decreased at 10% and 15% MC. When $0.25 < \alpha < 0.65$, the ln(A) value of SYP at all MC levels tended to be stable. The ln(A) value of SYP increased as the heating rate increased.

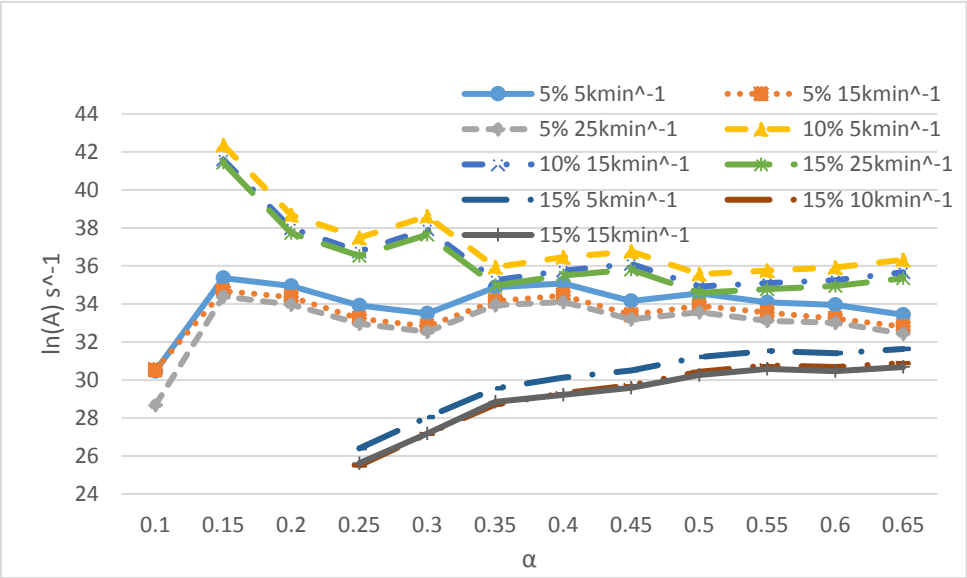


Figure 4.8. SPF (Material B) ln (A) vs.MC

From Figure 4.8,when$0.15 < \alpha < 0.65$ , the ln(A) value of SPF decreased at 10% MC, increased at 15% and kept stable at 5%. The ln(A) value increased from 5% MC to 10% MC, decreased rapidly from 10% MC to 15% MC. The ln(A) value of SPF increased as the heating rate increased.

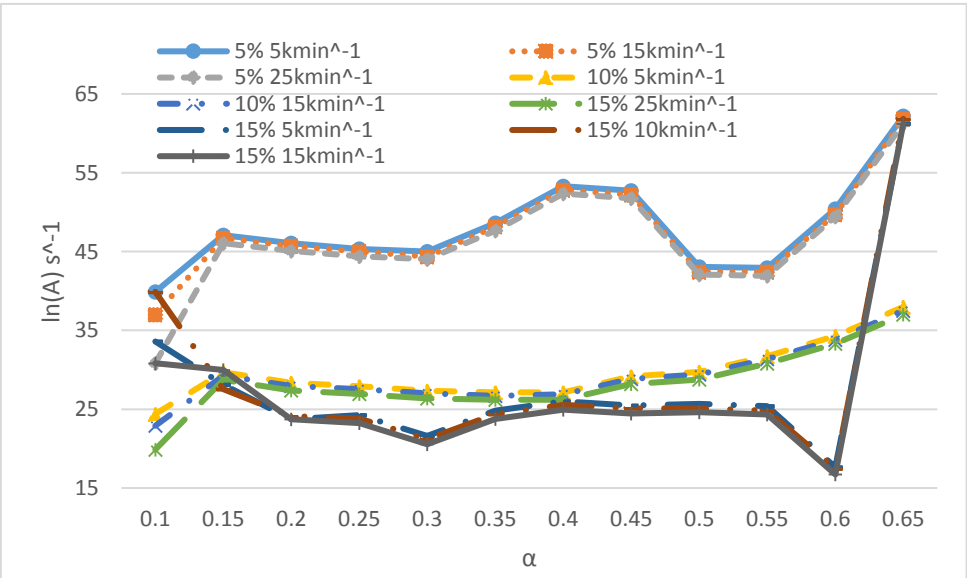


Figure 4.9. OSB-PF (Material C) ln (A) vs.MC

From Figure 4.9,when $\alpha < 0.15$, the ln(A) value of OSB-PF increased at 5%

and 10% MC, decreased at 15% MC. When $0.15 < \alpha < 0.6$, the ln(A) value of OSB-Siding kept stable at 5% , 10% and 15% MC levels. The ln(A) value of OSB-PF increased as the heating rate increased.

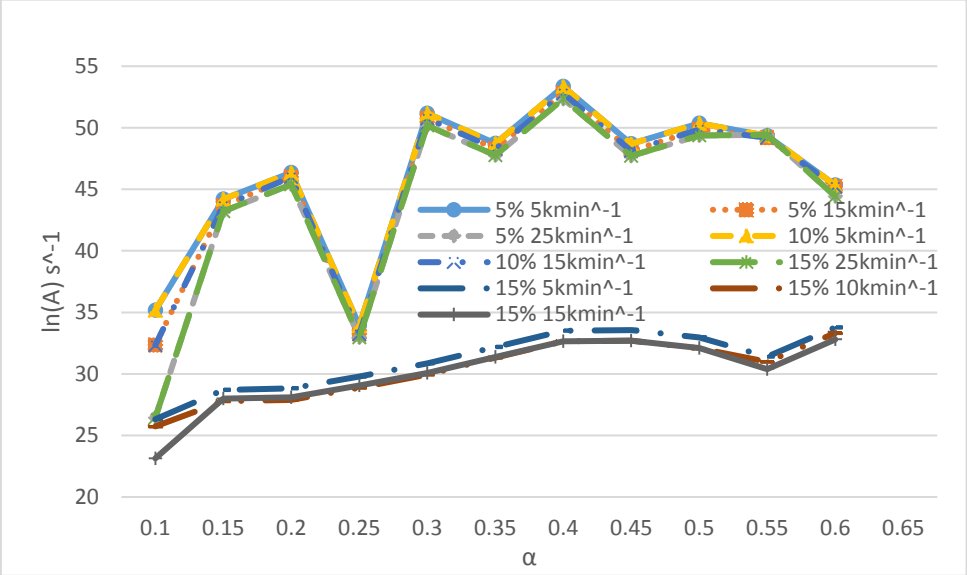


Figure 4.10. OSB-Siding (Material D) ln (A) vs.MC

From Figure 4.10, the ln(A) value of OSB-Siding kept almost the same from MC 5% to 10%, decreased from MC 10% to 15%. The ln(A) value of OSB-Siding increased as the heating rate increased.

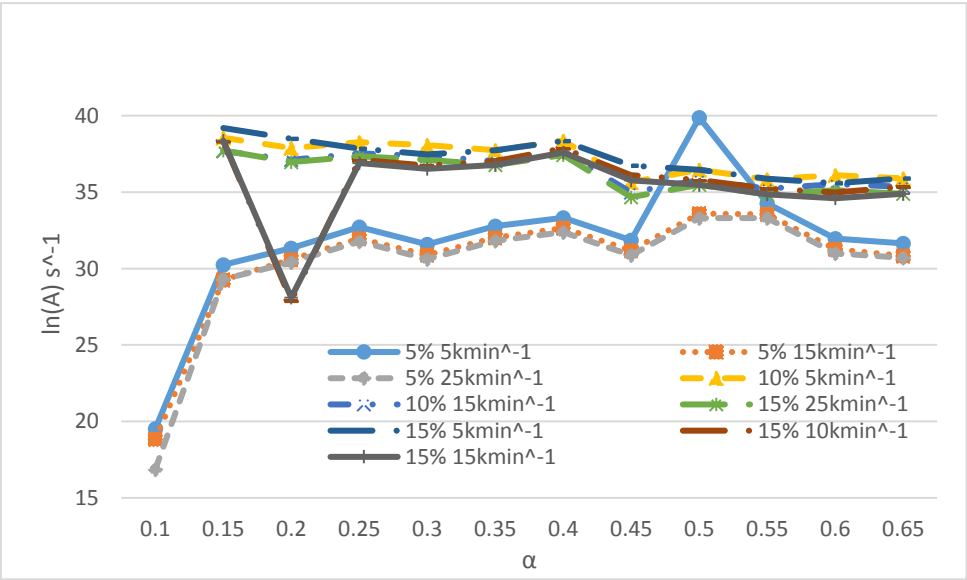


Figure 4.11. OSB-H (Material E) ln (A) vs.MC

From Figure 4.11, the ln(A) value of OSB-H increased from MC 5% to 10%, kept stable from MC 10% to 15%. The ln(A) value of OSB-H increased as the heating rate increased.

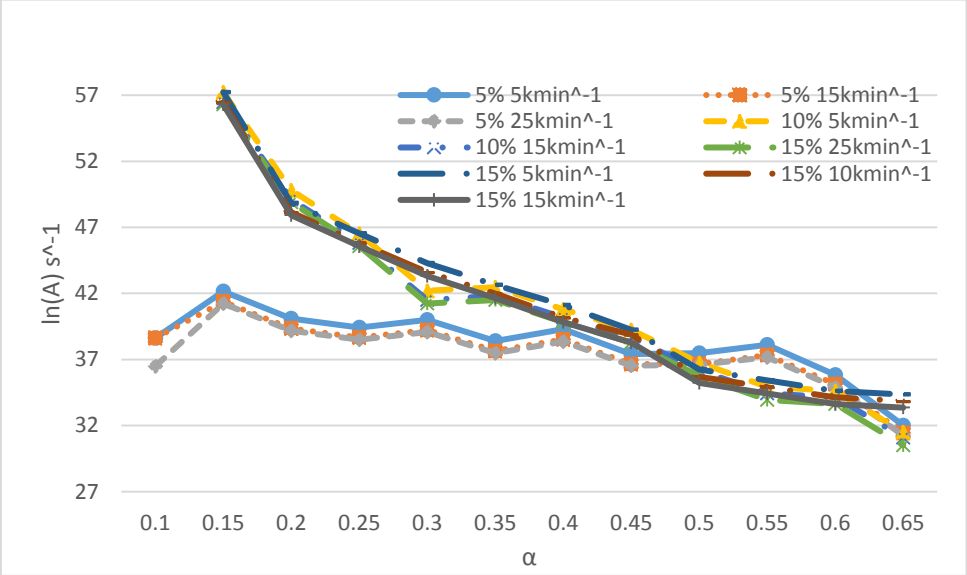


Figure 4.12. CDX (Material F) ln (A) vs.MC

From Figure 4.12, the ln (A) value of CDX increased from MC 5% to 10%, kept almost same from MC 10% to 15%. The ln (A) value of CDX increased as the heating rate increased.

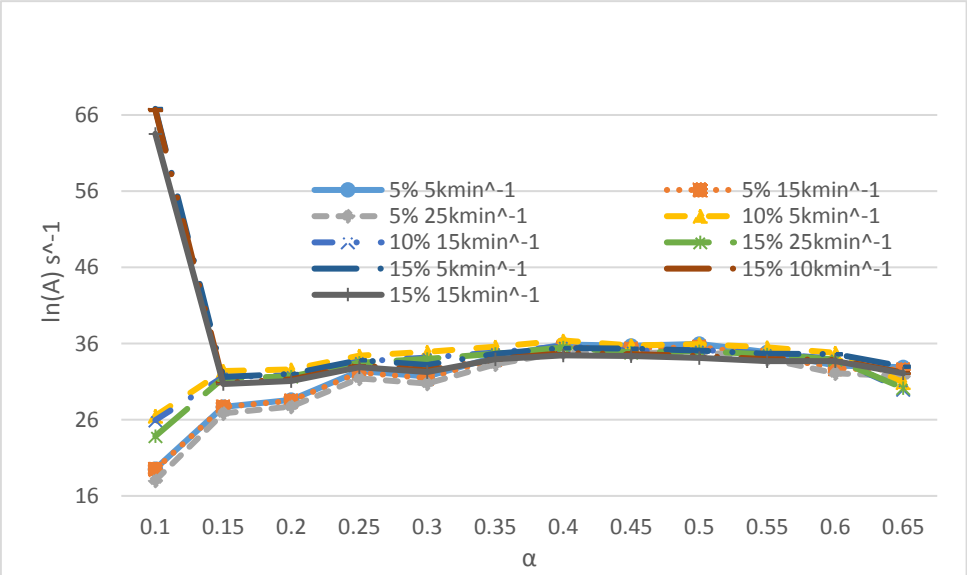


Figure 4.13. HB (Material G) ln (A) vs.MC

From Figure 4.13,when $\alpha < 0.15$, the ln(A) value of HB increased at 5% and 10% MC, decreased at 15% MC. When $0.15 < \alpha < 0.6$, the ln(A) value of HB kept stable at all MC levels. The ln(A) value of HB increased as the heating rate increased.

In summary, the ln(A) values varied in the early stage of pyrolysis, but appeared to be more stable when the conversion factor α was 0.25 or higher. Both MC level and heating rate had strong effect on the Pre-exponential factor.

When $\alpha < 0.15$, the ln(A) value of HB increased of 5% and 10% MC, decreased of 15% MC; when$0.15 < \alpha < 0.6$,the ln(A) value of HB kept stable of 5% , 10% and 15% MC; the ln(A) value of hb increased as the heating rate increased.

### 4.2.3 Activation Energy (E)

Figures 4.14-4.20 show the activation energy (E) as a function of MC levels for materials A-G.

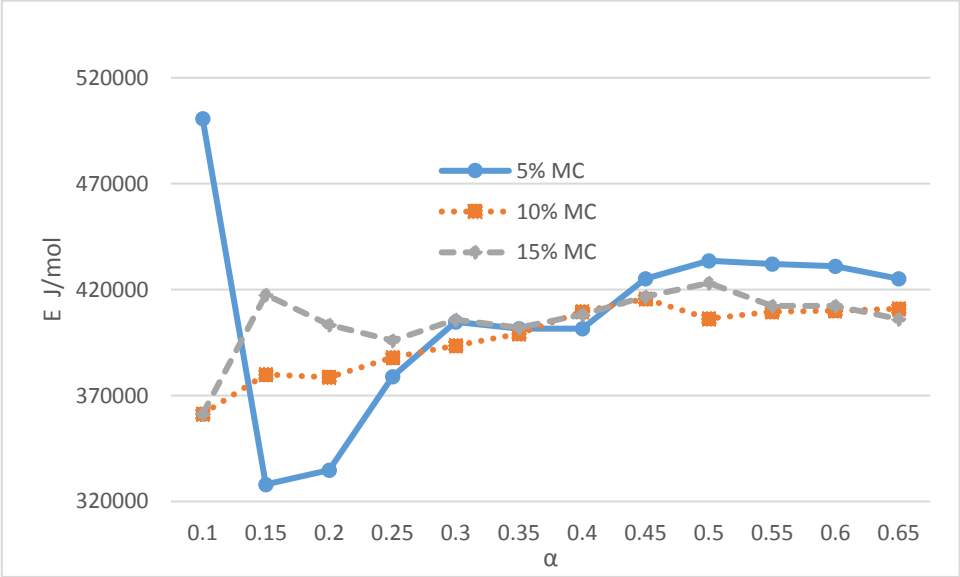


Figure 4.14. SYP (Material A) activation energy vs.MC

From Figure 4.14, the activation energy of SYP showed similar values for all MC levels when $\alpha > 0.25$.

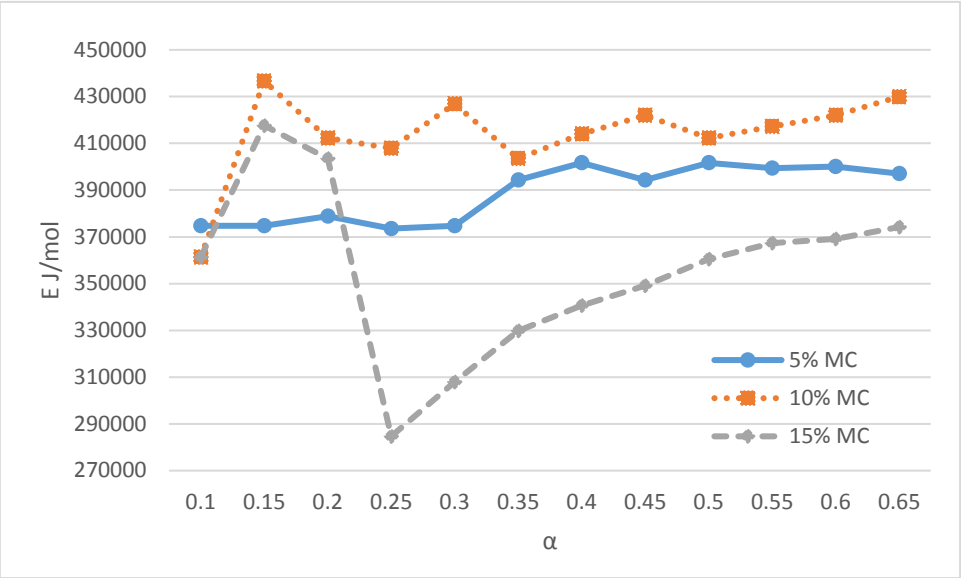


Figure 4.15. SPF (Material B) activation energy vs.MC

From Figure 4.15, the activation energy of SPF showed similar values in 5% MC level and 10% MC level. The conversion had a strong effect on the activation energy in 15% MC.

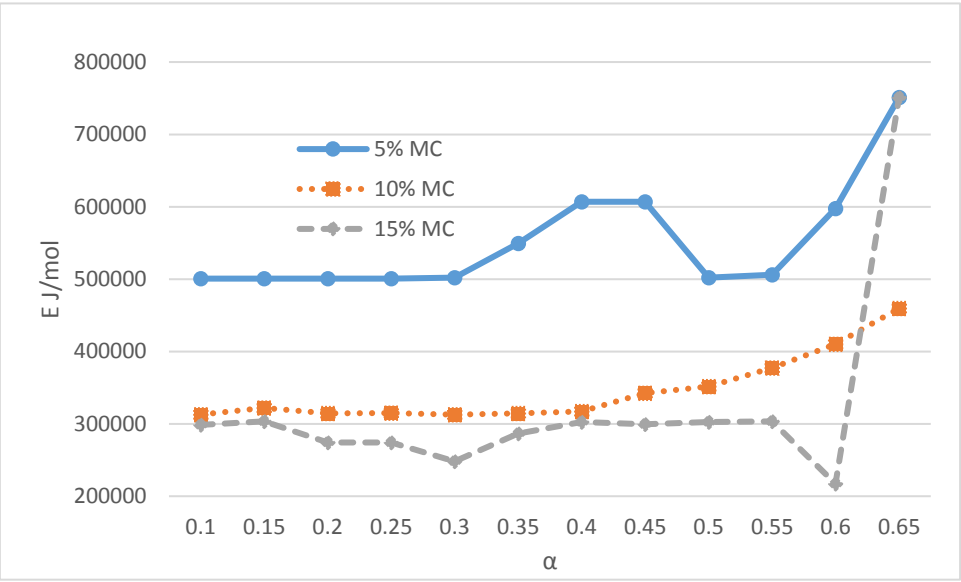


Figure 4.16. OSB-PF (Material C) activation energy vs.MC

From Figure 4.16, the activation energy of OSB-PF showed similar values in 10% MC level and 15% MC level, which were much lower than the value in 5% MC level.

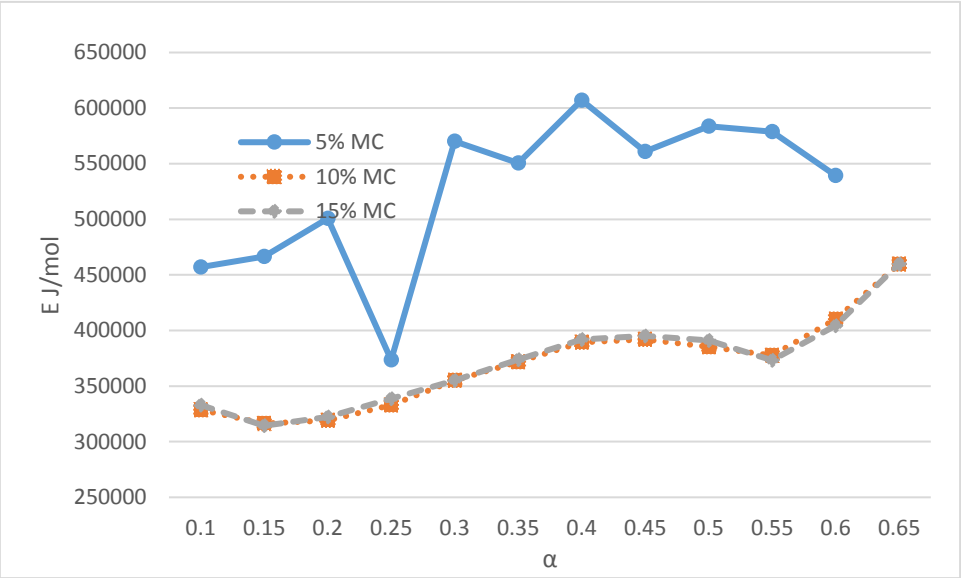


Figure 4.17. OSB-Siding (Material D) activation energy vs.MC

From Figure 4.17, the activation energy of OSB-Siding showed same values in 10% MC level and 15% MC level, which were much lower than the value in 5% MC level.

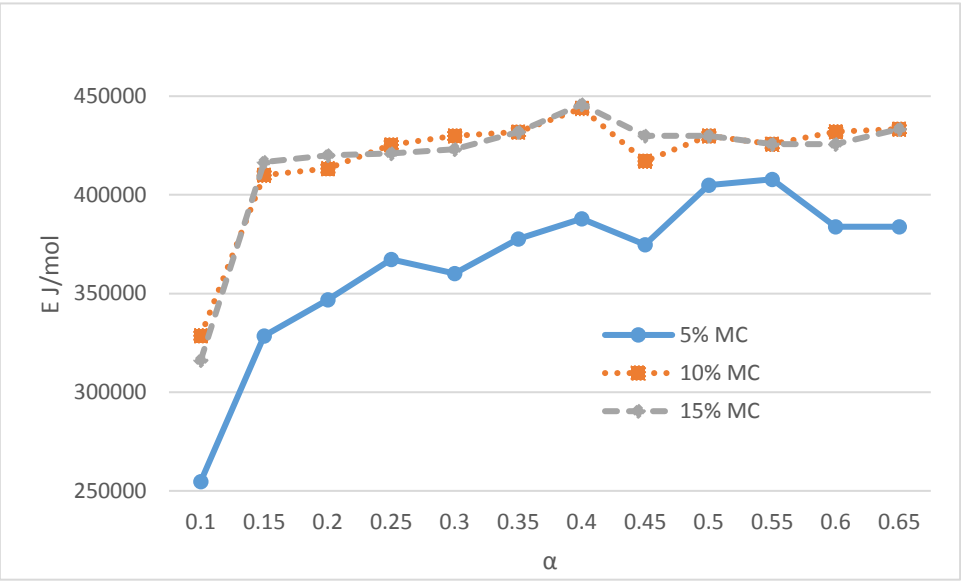


Figure 4.18. OSB-H (Material E) activation energy vs.MC

From Figure 4.18, the activation energy of OSB-H showed similar values in 10% MC level and 15% MC level, which were much higher than the value in 5% MC level.

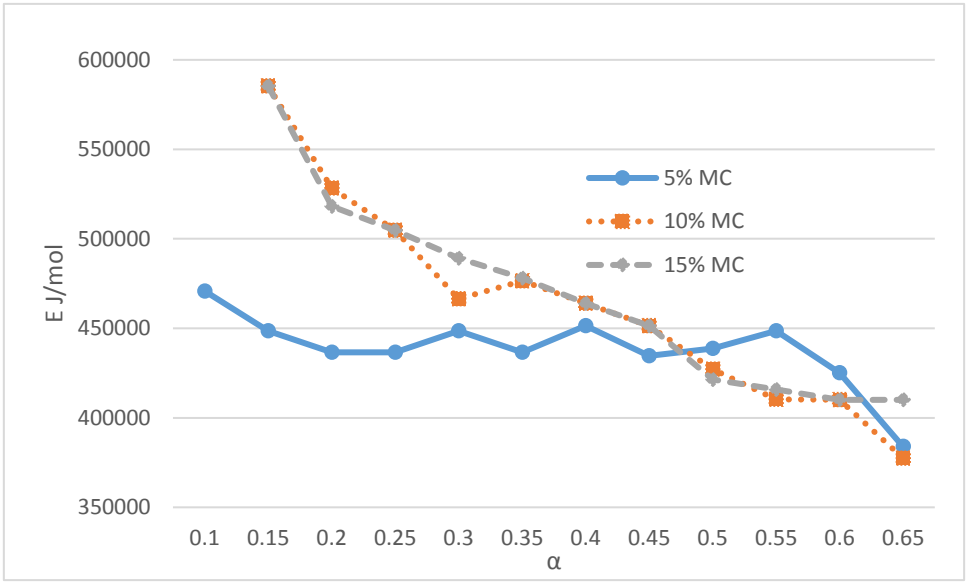


Figure 4.19. CDX (Material F) activation energy vs.MC

From Figure 4.19, the activation energy of CDX showed similar values in 10% MC level and 15% MC level.

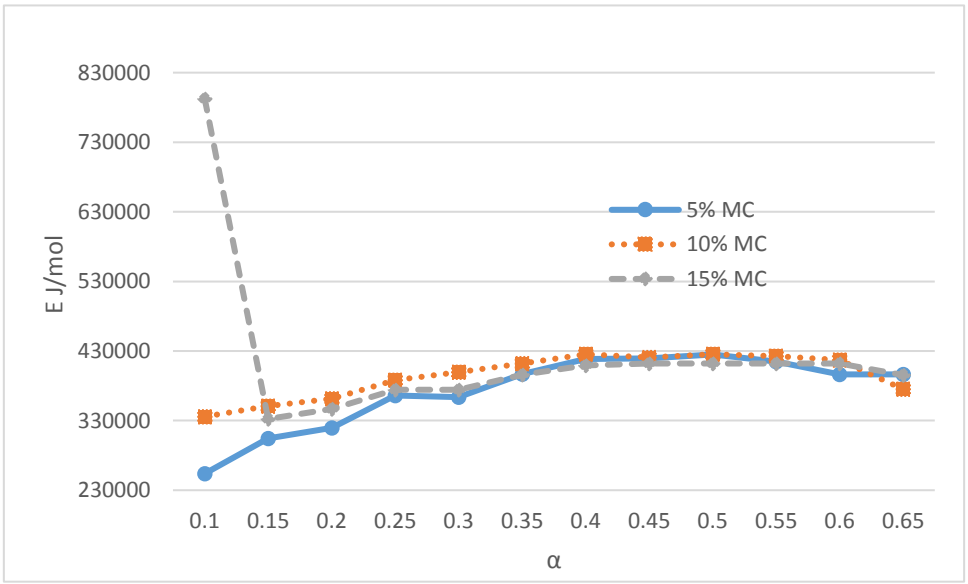


Figure 4.20. HB (Material G) activation energy vs.MC

From Figure 4.20, the activation energy of HB showed similar values for all MC levels when $\alpha>0.15$.

In summary, the activation energy values varied in the early stage of pyrolysis, but appeared to be more stable when the conversion factor α was 0.25 or higher. This is similar to pre-exponential factor. MC level had insignificant effect on the activation energy of SYP, CDX, and HB, but had some effect on the activation energy of SPF and OSB materials.

## 4.3 Combustion Properties

Basic combustion properties included Time to Ignition (TTI or $t_{ig}$ ), Heat Release Rate (HRR) at 180 seconds, Peak Heat Release Rate (PHRR), Critical Heat Flux (CHF) for ignition, Effective Heat of Combustion (EHC), Mass Loss (ML), Mass Loss Rate (MLR), and Time to Flameout (TTF or $t_{fo}$).

Table 4.1 summarizes the TTI values (in seconds) of materials A-G at the three heat flux levels (20, 30, and 50 kW/m$^2$) and three MC levels (5%, 10%, and 15%). These same values were plotted in Figure 4.21 for SYP and Figure 4.22 for OSB-PF, as well as the figures for other materials in Appendix C.

### 4.3.1 Time to Ignition (TTI)

Table 4.1. TII (time to ignition) of the selected fuels

| Ignition time (s) | HF(kW/m$^2$) | 20 | 30 | 50 |
|---|---|---|---|---|
| A | 5% | 192 | 34 | 24 |
| | 10% | 357 | 71 | 25 |
| | 15% | 703 | 65 | 31 |
| B | 5% | 233 | 32 | 10 |
| | 10% | 307 | 56 | 15 |
| | 15% | 465 | 49 | 17 |
| C | 5% | 192 | 70 | 24 |
| | 10% | 258 | 85 | 25 |
| | 15% | 317 | 101 | 31 |
| D | 5% | 329 | 65 | 21 |
| | 10% | 406 | 142 | 31 |
| | 15% | 625 | 119 | 33 |
| E | 5% | 301 | 56 | 20 |
| | 10% | 343 | 98 | 29 |
| | 15% | 461 | 104 | 36 |
| F | 5% | 191 | 32 | 13 |
| | 10% | 210 | 77 | 22 |
| | 15% | 306 | 76 | 32 |
| G | 5% | 206 | 63 | 20 |
| | 10% | 206 | 97 | 26 |
| | 15% | 375 | 115 | 30 |

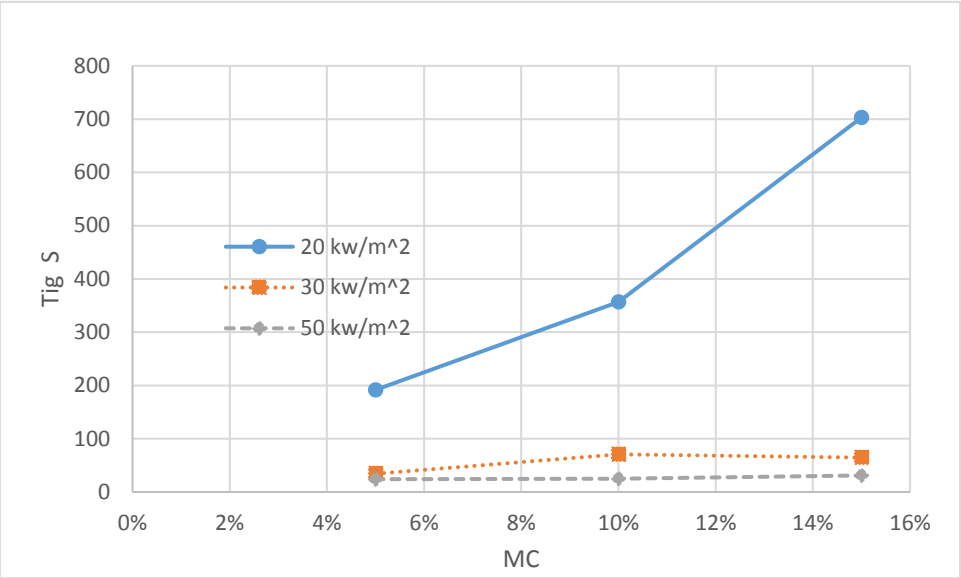


Figure 4.21. SYP (Material A) ignition time vs.MC

From Figure 4.21, at 20 kW/m$^2$, the TTI of SYP increased significantly as the MC level increased. At higher HF levels (30 and 50 kW/m$^2$), the effect of MC level on TTI is insignificant. As the heat flux decreased, the TTI values decreased, but close at higher HF values of 30 and 50 kW/m$^2$.

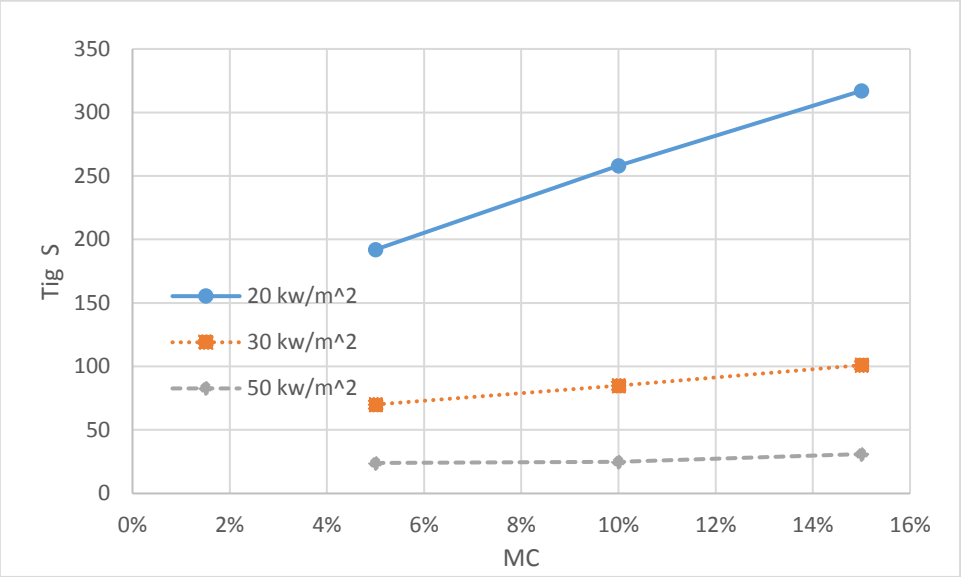


Figure 4.22. OSB-PF (Material C) ignition time vs.MC

From Figure 4.22, the TTI of OSB-PF increased almost linearly as the MC level increased at HF levels of 20 and 30 kW/m$^2$. The TTI showed slight increase at 50 30

$kW/m^2$ as the MC increased As heat flux increased, the TTI of OSB-PF decreased significantly.

Similar figures showing the effects of MC and HF on TTI of other materials were plotted in Appendix C. In general, heat flux had significant effect on TTI, the higher the heat flux levels, the smaller the TTI values. MC levels had significant effect at low heat flux levels (20 or 30 $kW/m^2$).

### 4.3.2 Heat Release Rate at 180s (HRR_180s)

The Heat Release Rate at 180s (HRR_180s) for materials A-G tested at three HF levels and three MC levels are shown in Tables 4.2 to 4.8 and Appendix D.

Table 4.2. SYP (Material A) percent change of ave HRR 180s

| A HRR 180 | heat flux | 5% MC | 10% MC | 15% MC |
|---|---|---|---|---|
| | 20Kw/m^2 I | 1% | 1% | -1% |
| | 20Kw/m^2 II | 5% | 6% | 6% |
| | 20Kw/m^2 III | -3% | -7% | -5% |
| | 30Kw/m^2 I | 4% | -6% | -8% |
| | 30kw/m^2 II | -1% | 8% | 11% |
| | 30Kw/m^2 III | -3% | -3% | -3% |
| | 50Kw/ m^2 I | -5% | -1% | 2% |
| | 50Kw/m^2 II | 5% | 1% | -4% |
| | 50Kw/m^2 III | 0% | -1% | 2% |

From Table 4.2, each percent change of ave HRR 180s of SYP was less than 11%, which almost fitted the requirement of E 1354 ASTM standards.

Table 4.3. SPF (Material B) percent change of ave HRR 180s

| B HRR 180 | heat flux | 5% MC | 10% MC | 15% MC |
|---|---|---|---|---|
| | 20Kw/m^2 I | -4% | 4% | -1% |
| | 20Kw/m^2 II | 10% | -5% | 6% |
| | 20Kw/m^2 III | -6% | 2% | -5% |
| | 30Kw/m^2 I | -3% | 1% | -8% |
| | 30kw/m^2 II | 3% | -7% | 11% |
| | 30Kw/m^2 III | 0% | 6% | -3% |
| | 50Kw/ m^2 I | 2% | 2% | 2% |
| | 50Kw/m^2 II | 3% | 3% | -4% |
| | 50Kw/m^2 III | -5% | -5% | 2% |

From Table 4.3, each percent change of ave HRR 180s of SPF was less than 11%, which almost fitted the requirement of E 1354 ASTM standards.

Table 4.4. OSB-PF (Material C) percent change of ave HRR 180s

| C HRR 180 | heat flux | 5% MC | 10% MC | 15% MC |
|---|---|---|---|---|
| | 20Kw/m^2 I | -4% | 4% | 7% |
| | 20Kw/m^2 II | 2% | -5% | -9% |
| | 20Kw/m^2 III | 2% | 2% | 2% |
| | 30Kw/m^2 I | 2% | 1% | -3% |
| | 30kw/m^2 II | -4% | -7% | 5% |
| | 30Kw/m^2 III | 2% | 6% | -2% |
| | 50Kw/ m^2 I | -7% | 2% | 1% |
| | 50Kw/m^2 II | 1% | 3% | 6% |
| | 50Kw/m^2 III | 7% | -5% | -7% |

From Table 4.4, each percent change of ave HRR 180s of OSB-PF was less than 9%, which fitted the requirement of E 1354 ASTM standards.

Table 4.5. OSB-Siding (Material D) percent change of ave HRR 180s

| D HRR 180 | heat flux | 5% MC | 10% MC | 15% MC |
|---|---|---|---|---|
| | 20Kw/m^2 I | 3% | 4% | 12% |
| | 20Kw/m^2 II | -3% | -2% | -10% |
| | 20Kw/m^2 III | 0% | -2% | -2% |
| | 30Kw/m^2 I | -12% | 3% | 1% |
| | 30kw/m^2 II | 4% | -2% | -1% |
| | 30Kw/m^2 III | 8% | -1% | 1% |
| | 50Kw/ m^2 I | -11% | -2% | 5% |
| | 50Kw/m^2 II | 12% | -2% | -4% |
| | 50Kw/m^2 III | -1% | 4% | 0% |

From Table 4.5, each percent change of ave HRR 180s of OSB-Siding was less than 12%, which almost fitted the requirement of E 1354 ASTM standards.

Table 4.6. OSB-H (Material E) percent change of ave HRR 180s

| E HRR 180 | heat flux | 5% MC | 10% MC | 15% MC |
|---|---|---|---|---|
| | 20Kw/m^2 I | -1% | -2% | 7% |
| | 20Kw/m^2 II | 0% | 0% | -5% |
| | 20Kw/m^2 III | 2% | 1% | -2% |
| | 30Kw/m^2 I | -3% | 8% | -9% |
| | 30kw/m^2 II | 2% | -8% | -3% |
| | 30Kw/m^2 III | 1% | 1% | 12% |
| | 50Kw/ m^2 I | -11% | -6% | 1% |
| | 50Kw/m^2 II | 12% | 5% | -1% |
| | 50Kw/m^2 III | -1% | 1% | 0% |

From Table 4.6, each percent change of ave HRR 180s of OSB-H was less than 12%, which almost fitted the requirement of E 1354 ASTM standards.

Table 4.7. CDX (Material F) percent change of ave HRR 180s

| F HRR 180 | heat flux | 5% MC | 10% MC | 15% MC |
|---|---|---|---|---|
| | 20Kw/m^2 I | -3% | -5% | 12% |
| | 20Kw/m^2 II | -5% | -3% | 4% |
| | 20Kw/m^2 III | 8% | 8% | -3% |
| | 30Kw/m^2 I | -2% | -12% | -4% |
| | 30kw/m^2 II | 11% | 10% | -6% |
| | 30Kw/m^2 III | -10% | 3% | 8% |
| | 50Kw/ m^2 I | -13% | -1% | 2% |
| | 50Kw/m^2 II | 4% | 5% | -1% |
| | 50Kw/m^2 III | 9% | -4% | -1% |

From Table 4.7, each percent change of ave HRR 180s of CDX was less than 13%, which almost fitted the requirement of E 1354 ASTM standards.

Table 4.8. HB (Material G) ratio of ave HRR 180s

| G HRR 180 | heat flux | 5% MC | 10% MC | 15% MC |
|---|---|---|---|---|
| | 20Kw/m^2 I | -9% | -9% | -9% |
| | 20Kw/m^2 II | 3% | 3% | 3% |
| | 20Kw/m^2 III | 6% | 6% | 6% |
| | 30Kw/m^2 I | -1% | 3% | -1% |
| | 30kw/m^2 II | -1% | -2% | -1% |
| | 30Kw/m^2 III | 2% | -1% | 2% |
| | 50Kw/ m^2 I | -12% | 5% | -7% |
| | 50Kw/m^2 II | 5% | -3% | 5% |
| | 50Kw/m^2 III | 7% | -2% | 3% |

From Table 4.8, each percent change of ave HRR 180s of CDX was less than 12%, which almost fitted the requirement of E 1354 ASTM standards.

### 4.3.3 Critical Heat Flux

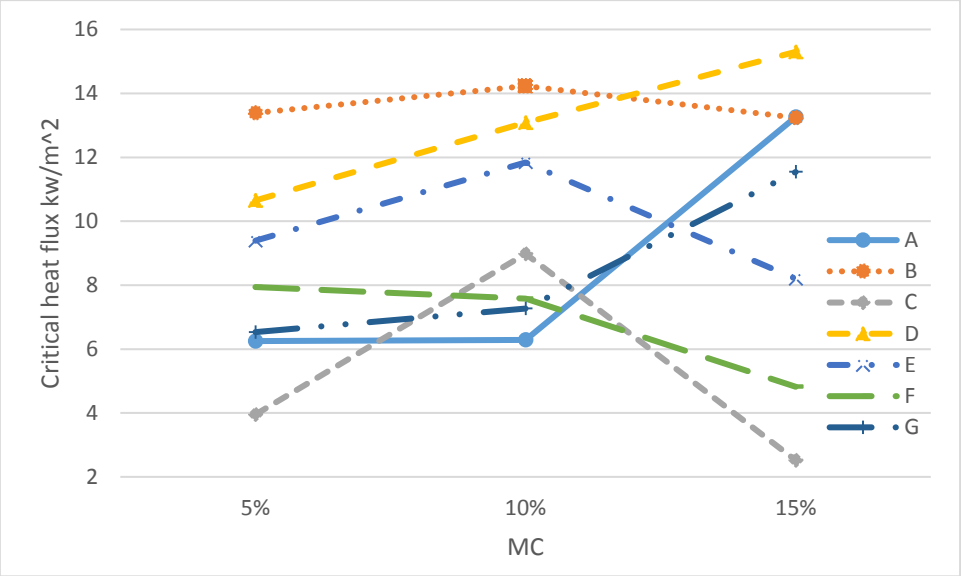


Figure 4.23. Critical heat flux of selected fuels vs.MC

The critical heat flux (CHF) for ignition values of all materials were plotted and shown in Figure 4.23. The CHFs of SYP and OSB-Siding increased as the MC level increased. The CHFs of CDX and HB decreased as the MC level increased. TheCHFs of SPF, OSB-PF and OSB-H increased from MC 5% to MC 10% level, but decreased from MC 10% to MC 15%.

### 4.3.4 Peak of Heat Release Rate (PHRR)

The PHRR values for all materials are summarized in Table 4.9. The same PHRR values were plotted in Figure 4.24 for SYP and Figure 4.25 for OSB-PF. The plots for other materials are shown in Appendix E.

Table 4.9. PHRR of the selected fuels

| PHRR (Kw/m^2) | HF(kW/m$^2$) | 20 | 30 | 50 |
|---|---|---|---|---|
| SYP | 5% | 160.21 | 182.8 | 176.68 |
| | 10% | 162.36 | 169.59 | 190.81 |
| | 15% | 131.83 | 158.48 | 200.75 |
| SPF | 5% | 174.88 | 192.64 | 230.36 |
| | 10% | 152.63 | 204.33 | 185.08 |
| | 15% | 112.59 | 168.43 | 182.84 |
| OSB-PF | 5% | 193.95 | 206.76 | 303.76 |
| | 10% | 164.41 | 221.63 | 290.35 |
| | 15% | 166.38 | 179.91 | 251.81 |
| OSB-Siding | 5% | 255.25 | 242.35 | 339.85 |
| | 10% | 252.94 | 226.96 | 269.19 |
| | 15% | 191.85 | 168.31 | 221.19 |
| OSB-H | 5% | 301.01 | 192.61 | 289.66 |
| | 10% | 208.26 | 217.15 | 249.94 |
| | 15% | 213.52 | 201.33 | 253.8 |
| CDX | 5% | 162.09 | 188.32 | 319.2 |
| | 10% | 143.78 | 201.87 | 281.91 |
| | 15% | 155.35 | 151.95 | 203.15 |
| HB | 5% | 170.17 | 217.05 | 370.89 |
| | 10% | 170.17 | 215.27 | 321.74 |
| | 15% | 141.66 | 187.42 | 387 |

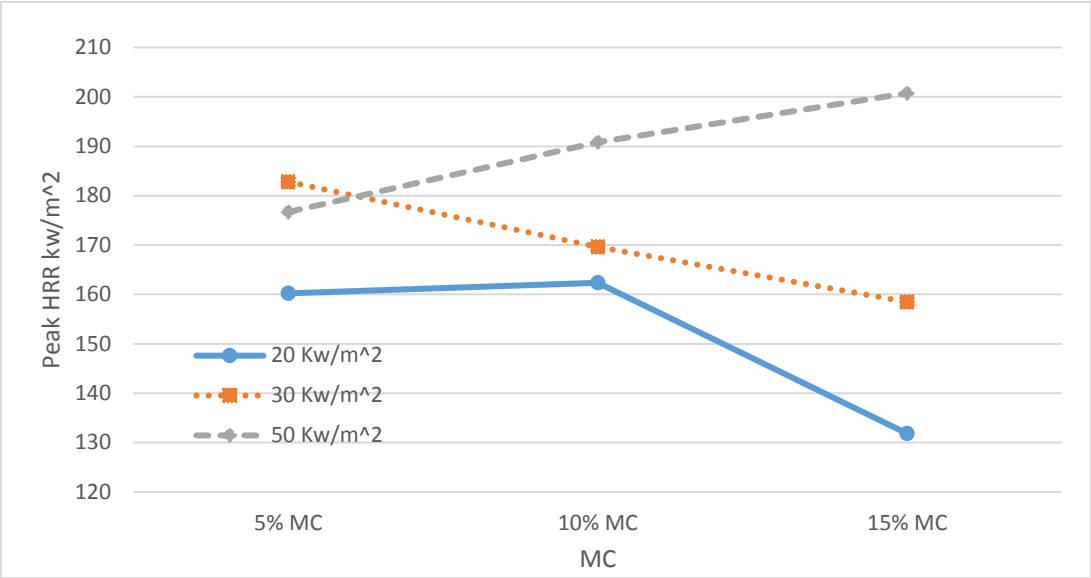


Figure 4.24. SYP (Material A) PHRR vs.MC

From Figure 4.24, the PHRR of SYP increased as the heat flux increased in 10% MC level and 15% MC level. The MC had a strong effect on the PHRR of SYP.

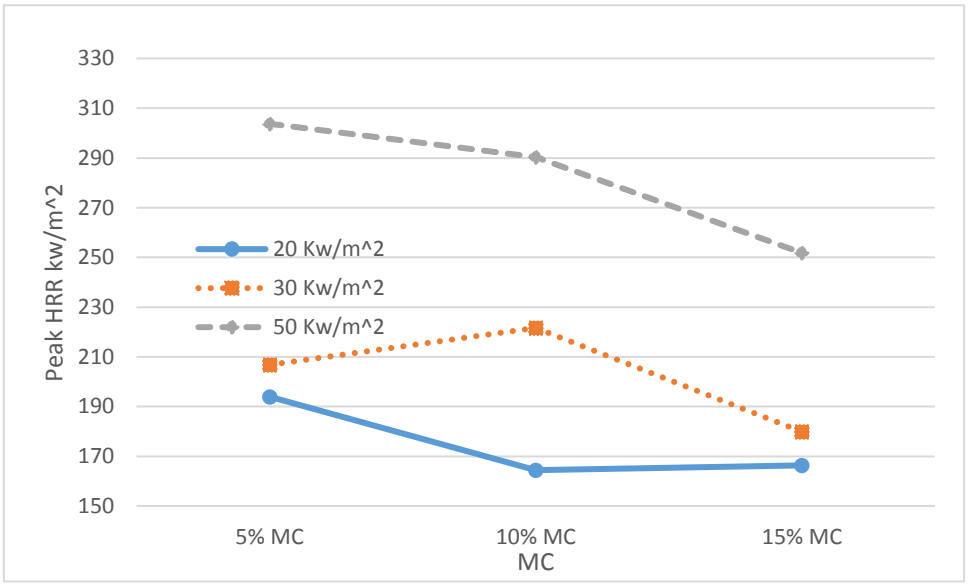


Figure 4.25. OSB-PF (Material C) PHRR vs.MC

From Figure 4.25, the PHRR of OSB-PF increased as the heat flux increased, especially from 30 kw/ m^2 to 50 kw/m^2. The MC had a strong effect on the PHRR of SYP.

In general, the PHRR of all selected structural materials increased as the heat flux level increased, and decreased as the MC level increased, although with a few exceptions.

### 4.3.5 Effective Heat of Combustion (EHC)

The EHC values for all materials are summarized in Table 4.10. The same EHC values were plotted in Figure 4.26 for SYP and Figure 4.27 for OSB-PF. The plots for other materials are shown in Appendix F.

Table 4.10. EHC of the selected fuels

| EHC (MJ/kg) | HF(kW/m$^2$) | 20 | 30 | 50 |
|---|---|---|---|---|
| SYP | 5% | 14.09 | 13.89 | 7.88 |
| | 10% | 14.32 | 14.12 | 12.23 |
| | 15% | 14.83 | 13.62 | 13.97 |
| SPF | 5% | 14.29 | 14.26 | 14.62 |
| | 10% | 13.70 | 13.10 | 13.89 |
| | 15% | 10.99 | 12.80 | 13.39 |
| OSB-PF | 5% | 13.93 | 13.59 | 15.87 |
| | 10% | 13.89 | 13.87 | 13.50 |
| | 15% | 9.88 | 12.85 | 10.42 |
| OSB-Siding | 5% | 14.77 | 10.78 | 14.46 |
| | 10% | 14.46 | 10.40 | 14.22 |
| | 15% | 14.31 | 12.70 | 10.34 |
| OSB-H | 5% | 17.41 | 9.55 | 11.50 |
| | 10% | 18.32 | 17.37 | 18.71 |
| | 15% | 26.83 | 18.50 | 18.94 |
| CDX | 5% | 16.16 | 13.30 | 14.57 |
| | 10% | 13.58 | 13.88 | 14.06 |
| | 15% | 13.40 | 7.54 | 10.05 |
| HB | 5% | 14.73 | 13.94 | 15.53 |
| | 10% | 14.73 | 13.24 | 12.30 |
| | 15% | 13.28 | 13.24 | 14.33 |

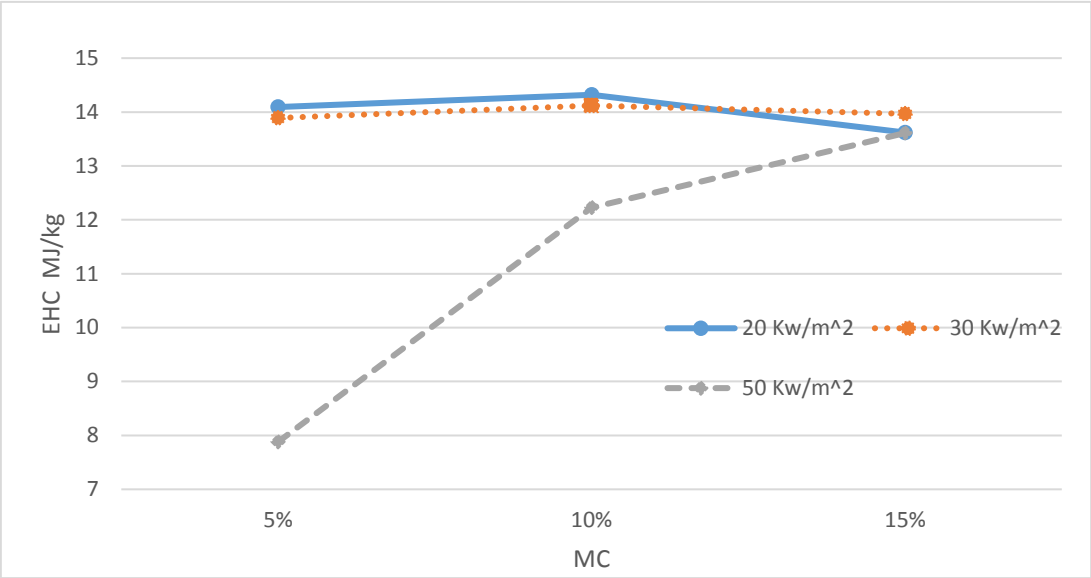


Figure 4.26. SYP (Material A) EHC vs.MC

From Figure 4.26, the EHC of SYP showed similar value in 20 kw/m^2 and 30 kw/m^2, which were much higher than the value in 50 kw/m^2, the MC had a strong effect on the EHC of SYP in 50 kw/m^2.

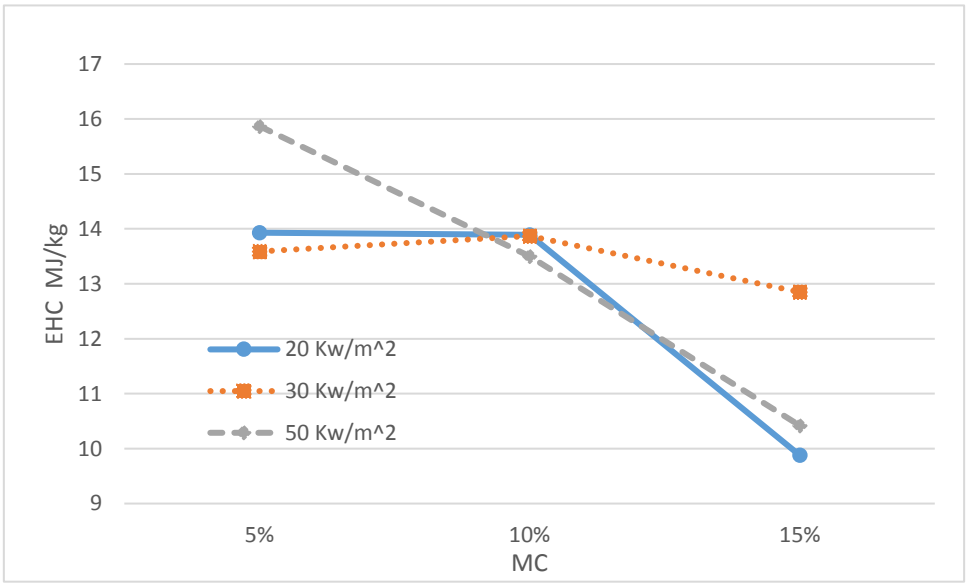


Figure 4.27. OSB-PF (Material C) EHC vs.MC

From Figure 4.27, the EHC of OSC-PF decreased as the MC level increased.

In general, as the MC level increased, the EHC of materials also increased. HF levels had less effect on the EHC values.

### 4.3.6 Mass Loss (ML)

The ML values for all materials are summarized in Table 4.11. The same ML values were plotted in Figure 4.28 for SYP and Figure 4.29 for OSB-PF. The plots for other materials are shown in Appendix G.

Table 4.11. ML (mass loss) of selected fuels

| ML | HF(kW/m$^2$) | 20 | 30 | 50 |
|---|---|---|---|---|
| SYP | 5% | 74.80% | 80.80% | 79.97% |
| | 10% | 79.14% | 78.85% | 80.43% |
| | 15% | 75.95% | 87.64% | 79.03% |
| SPF | 5% | 72.73% | 74.37% | 77.27% |
| | 10% | 73.01% | 79.42% | 78.81% |
| | 15% | 72.18% | 76.85% | 78.60% |
| OSB-PF | 5% | 73.07% | 76.10% | 81.51% |
| | 10% | 72.12% | 75.20% | 81.28% |
| | 15% | 72.67% | 76.06% | 81.32% |
| OSB-Siding | 5% | 70.93% | 73.64% | 76.78% |
| | 10% | 69.19% | 74.48% | 77.62% |
| | 15% | 67.13% | 71.12% | 78.34% |
| OSB-H | 5% | 58.71% | 59.06% | 75.47% |
| | 10% | 53.39% | 58.46% | 59.93% |
| | 15% | 21.76% | 54.43% | 61.46% |
| CDX | 5% | 70.93% | 67.85% | 77.83% |
| | 10% | 72.38% | 77.81% | 79.26% |
| | 15% | 71.10% | 74.52% | 79.67% |
| HB | 5% | 74.61% | 77.46% | 83.93% |
| | 10% | 74.61% | 75.32% | 79.92% |
| | 15% | 75.69% | 77.49% | 81.46% |

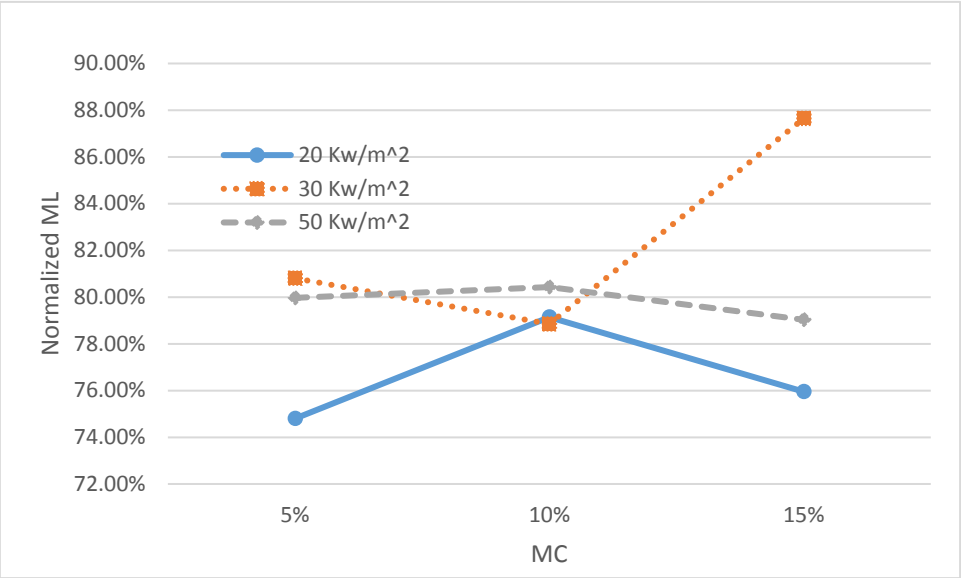


Figure 4.28. SYP (Material A) Normalized ML vs.MC

From Figure 4.28, the ML of SYP in 20 kw/m^2 and 50 kw/m^2 increased from MC 5% to MC 10%, decreased from MC 10% to 15%, while the ML of SYP in 30 kw/m^2 showed the opposite tendency.

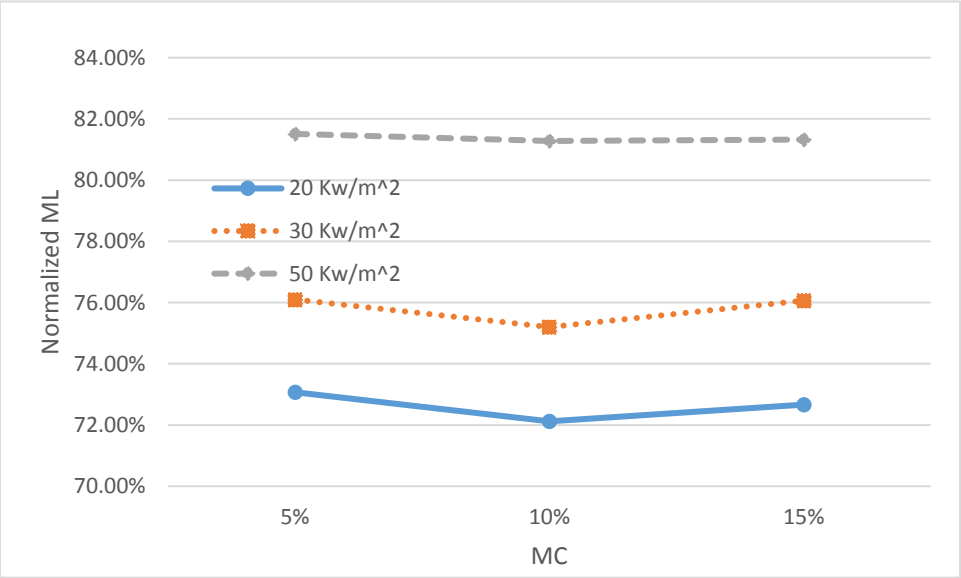


Figure 4.29. OSB-PF (Material C) Normalized ML vs.MC

From Figure 4.29, the ML of OSB-PF increased as the heat flux increased, the MC had no strong effect on the ML of OSB-PF.

In summary, the ML of materials increased as the HF level increased. MC

levels showed less effect on ML.

### 4.3.7 Mass Loss Rate (MLR)

The MLR values for all materials are summarized in Table 4.12. The same MLR values were plotted in Figure 4.30 for SYP and Figure 4.31 for OSB-PF. The plots for other materials are shown in Appendix H.

Table 4.12. MLR (mass loss rate) of selected fuels

| MLR (g/s*m^2) | HF(kW/m$^2$) | 20 | 30 | 50 |
|---|---|---|---|---|
| SYP | 5% | 6.18 | 8.48 | 14.87 |
| | 10% | 6.61 | 8.21 | 11.03 |
| | 15% | 5.98 | 7.91 | 9.59 |
| SPF | 5% | 4.55 | 5.01 | 6.74 |
| | 10% | 4.7 | 5.06 | 6.74 |
| | 15% | 4.36 | 4.97 | 6.27 |
| OSB-PF | 5% | 6.52 | 9.18 | 7.75 |
| | 10% | 6.53 | 9.55 | 10.42 |
| | 15% | 6.06 | 8.3 | 13.23 |
| OSB-Siding | 5% | 6.95 | 13.28 | 13.3 |
| | 10% | 6.66 | 12.78 | 35.06 |
| | 15% | 6.03 | 24.98 | 35.42 |
| OSB-H | 5% | 5.52 | 12.24 | 13.59 |
| | 10% | 2.92 | 5.73 | 6.92 |
| | 15% | 2.45 | 5.46 | 5.89 |
| CDX | 5% | 6.06 | 8.75 | 13.11 |
| | 10% | 5.87 | 8.49 | 11.4 |
| | 15% | 6.57 | 8.63 | 4.69 |
| HB | 5% | 6.57 | 8.53 | 9.4 |
| | 10% | 6.57 | 9.23 | 13.48 |
| | 15% | 5.96 | 8.29 | 11.73 |

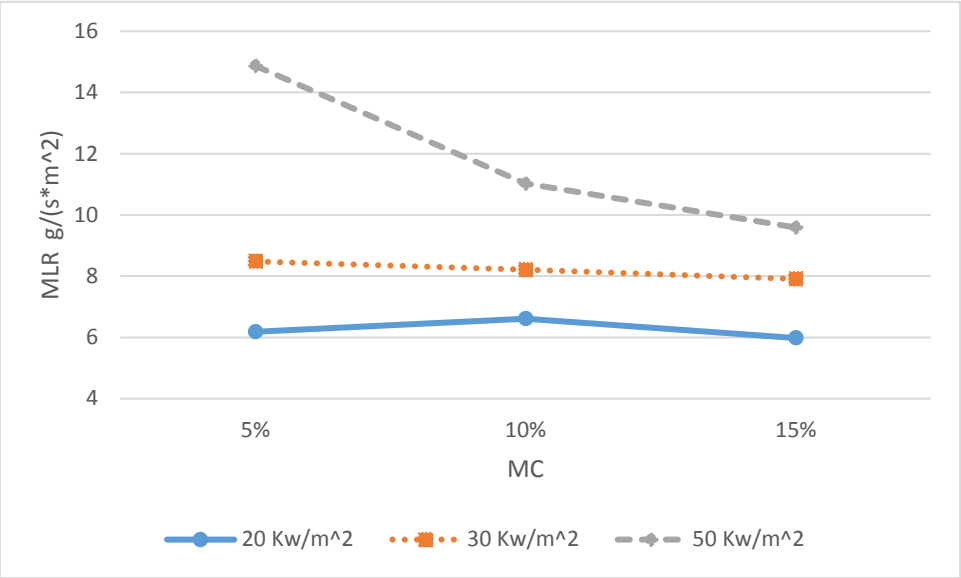


Figure 4.30. SYP (Material A) MLR vs.MC

From Figure 4.30, the MLR of SYP increased as the heat flux increased, the MC had strong effect on the ML of OSB-PF in 50 kw/m^2.

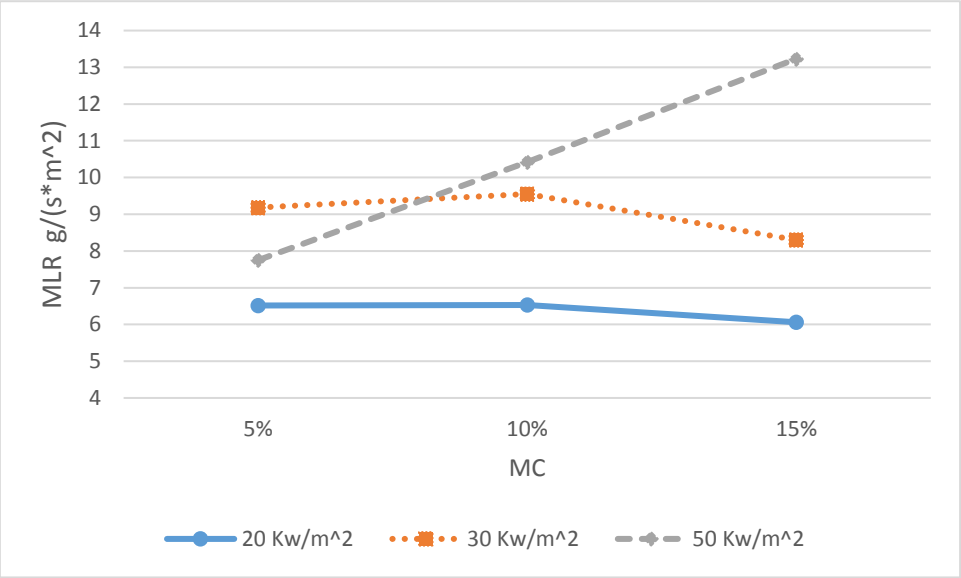


Figure 4.31. OSB-PF (Material C) MLR vs.MC

From Figure 4.31, the MLR of SYP increased as the heat flux increased in 10% MC and 15% MC, the MC had strong effect on the MLR of SYP in 50 kw/m^2.

In summary, the MRL of materials increased as the HF level increased. MC levels showed less effect on MLR.

### 4.3.8 Time to Flameout (TTF)

The TTF values for all materials are summarized in Table 4.13. The same TTF values were plotted in Figure 4.32 for SYP and Figure 4.33 for OSB-PF. The plots for other materials are shown in Appendix I.

Table 4.13. Flameout time of selected fuels

| Tfo (s) | HF(kW/m$^2$) | 20 | 30 | 50 |
|---|---|---|---|---|
| SYP | 5% | 1443.3 | 1153 | 868.3 |
| | 10% | 1616.7 | 1090 | 981.7 |
| | 15% | 1950 | 1406.3 | 1004.7 |
| SPF | 5% | 1486 | 1228 | 844 |
| | 10% | 1479 | 1304.7 | 1015.7 |
| | 15% | 1856 | 1346.7 | 1075.7 |
| OSB-PF | 5% | 1168 | 706 | 402 |
| | 10% | 1159 | 751 | 746 |
| | 15% | 1423 | 992 | 802 |
| OSB-Siding | 5% | 998 | 818.3 | 441.3 |
| | 10% | 1109.7 | 876.3 | 597 |
| | 15% | 1363.7 | 953.7 | 691 |
| OSB-H | 5% | 1917.7 | 1558.7 | 1197 |
| | 10% | 1943.3 | 1713.3 | 1408 |
| | 15% | 1716 | 1764.3 | 1740.3 |
| CDX | 5% | 1027 | 805 | 469 |
| | 10% | 1217.3 | 822 | 566.3 |
| | 15% | 1112 | 441.7 | 1714.7 |
| HB | 5% | 1312 | 924.3 | 864.3 |
| | 10% | 1312 | 932 | 715.7 |
| | 15% | 1620 | 1056 | 716.3 |

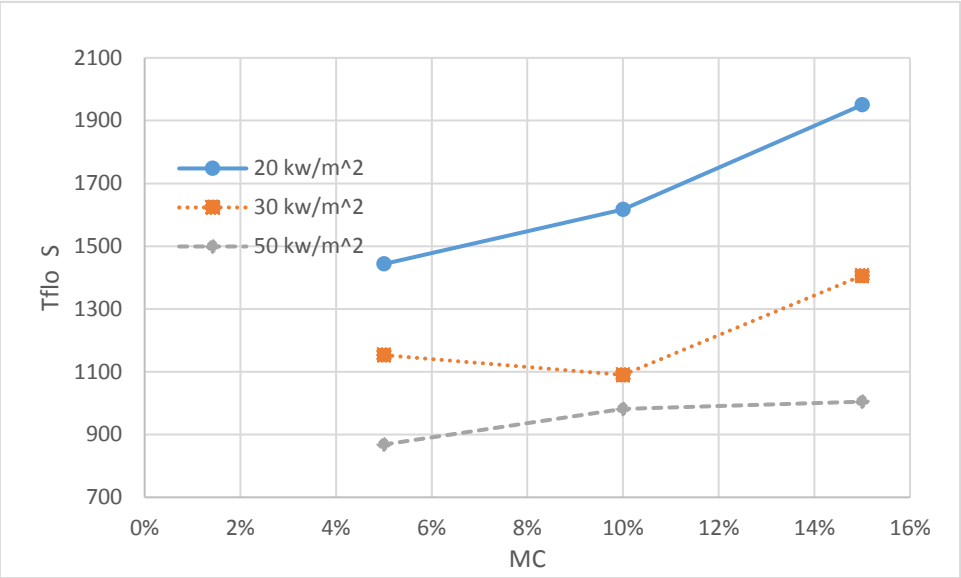


Figure 4.32. SYP (Material A) flameout time vs.MC

From Figure 4.32, the flameout time of SYP increased as the MC level increased (except 30 kw/m^2). As heat flux increased, the TTF decreased significantly.

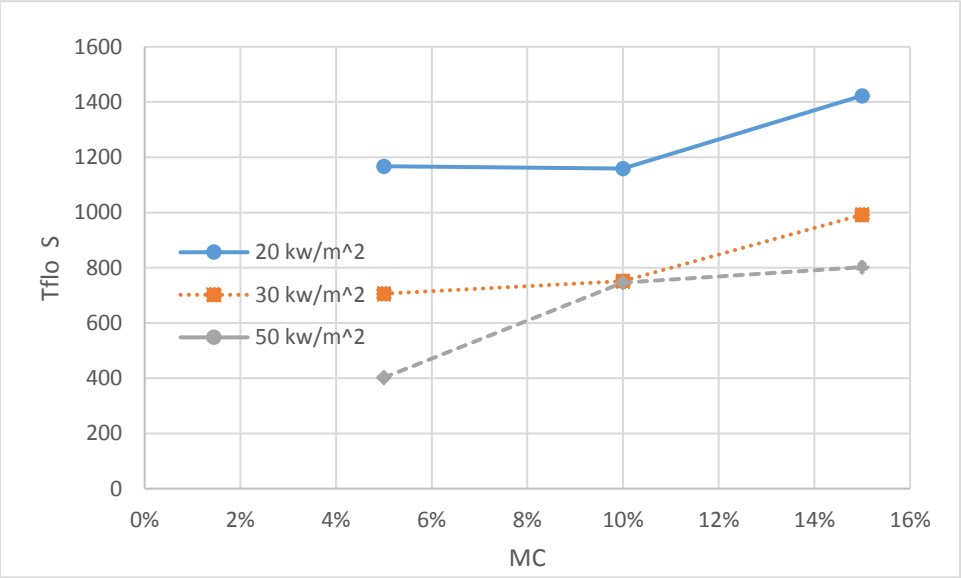


Figure 4.33. OSB-PF (Material C) flameout time vs.MC

From Figure 4.33, the flameout time of OSB-PF increased as the MC level increased. As heat flux increased, the TTF decreased.

In summary, the TTF of all materials increased as the MC level increased, but decreased as the heat flux increased.

# CHAPTER 5: CONCLUSIONS AND FUTURE WORK

## 5.1 Conclusions

For the fuel properties test, 46 replicates were tested for the sample MC level, and 63 replicates were tested for the selective material dimensions. ; For the pyrolysis properties test, 189 replicates were tested for TGA, and 42 replicates were tested for the thermal conductivity. For the combustiion properties test, 189 replicates were tested using the cone calorimeter. The following subsections summarize major conclusions from this research.

### 5.1. 1 Fuel Properties

MC levels changed the thickness and area of samples. The average thickness of SYP and HB decreased from MC 5% to 10%, increased from MC10% to 15%. The average thickness of SPF, OSB-PF, OSB-H and CDX increased as the MC increased. The average thickness of OSB-Siding increased from MC 5% to 10%, decreased from MC 10% to 15%. The area of all selected structural materials increased as the MC level increased. As the MC level increased, the density of SYP, OSB-Siding, OSB-H and CDX increased slightly, while SPF and OBS-sheathing decreased slightly. HB had the highest density at MC level 10%.

### 5.1. 2 Thermal and Pyrolysis Properties

The thermal conductivity of woods and wood-based composites increased as the MC level increased. At temperature range between 25℃ and 100℃, temperature had smaller impact on the thermal conductivity than MC level.

The pyrolysis properties were affected by both the MC levels and heating rate levels. The pre-exponential factor and activation energy values varied in the early stage of pyrolysis, but appeared to be more stable when the conversion factor α was 0.25 or higher. Both MC level and heating rate had strong effect on the pre-exponential factor for all materials. MC level had insignificant effect on the activation energy of SYP, CDX, and HB, but had some effect on the activation energy of SPF and OSB materials.

### 5.1. 3 Combustion Properties

The MC levels and HF levels had strong effect on the combustion properties of the selected structural fuels.

Heat flux had significant effect on TTI, the higher the heat flux levels, the smaller the TTI values. MC levels had significant effect at low heat flux levels (20 or 30 kW/m2).

The CHFs of SYP and OSB-Siding increased as the MC level increased. The CHFs of CDX and HB decreased as the MC level increased. The CHFs of SPF, OSB-PF and OSB-H increased from MC 5% to MC 10% level, but decreased from MC 10% to MC 15%.

The PHRR of all selected structural materials increased as the heat flux level increased, and decreased as the MC level increased, although with a few exceptions.

As the MC level increased, the EHC of materials also increased. HF levels had less effect on the EHC values.

The ML and MRL of materials increased as the HF level increased. MC levels showed less effect on ML and MLR.

The TTF of all materials increased as the MC level increased, but decreased as the heat flux increased.

## 5.2 Future Work

As the first step of the JFSP firebrand production project, this thesis measured the pyrolysis and combustion properties of some selected structural fuels. More detailed statistical analysis (such as ANOVA) should be performed to provide more insightful correlations among these controlling factors and variables. Analysis work is also needed to understand how the fuel's material, pyrolysis and combustion properties are related to its firebrand production characteristics.

# REFERENCES


1. Amy, L. (1961). The physico-chemical bases of the combustion of cellulose and ligneous materials. Cah. Du Centre Tech. du Bois No. 45. 30 pp.(Fr.)

2. Anna, L.B. (2003) Flammability of native understory species in pine flatwood and hardwood hammock ecosystems and implications for the wildland--urban interface. International Journal of Wildland Fire,13,355-365

3. ASTM D2395-14e1 Standard Test Methods for Density and Specific Gravity (Relative Density) of Wood and Wood-Based Materials. West Conshohocken, PA: ASTM International, 2014.

4. ASTM E1354-16a Standard Test Method for Heat and Visible Smoke Release Rates for Materials and Products Using an Oxygen Consumption Calorimeter, ASTM International, West Conshohocken, PA, 2016.

5. ASTM E1591-7. Standard Guide for Obtaining Data for Deterministic Fire Models, West Conshohocken, PA: ASTM International, 2009.

6. ASTM E 1641-15. Standard Test Method for Decomposition Kinetics by Thermo-gravimetry Using the Ozawa/Flynn/Wall Method, West Conshohocken, PA: ASTM International, 2016.

7. Brown, A., Manzello, S. L., Suzuki, J., Hayashi, Y., & Suzuki, S. (January 01, 2014). Firebrands generated from a full-scale structure burning under well-controlled laboratory conditions. Fire Safety Journal, 63, 43-51.

8. Beall, F. C., & Eickner, H. W. (1970) Thermal Degradation of Wood Components, Forest Products Laboratory, Forest Service, U.S. Department of Agriculture.

9. Browne, F. L. (1958). Theories on the combustion of wood and its control. U.S.Forest Prod. Lab, Rep. 2136, 59 pp., Madison, Wis.

10. Babrauskas, V. (2003). Ignition handbook: Principles and applications to fire safety engineering, fire investigation, risk management and forensic science. Issaquah, WA: Fire Science Publishers.

11. Brown, A., Manzello, S. L., Suzuki, J., Hayashi, Y., & Suzuki, S. (2014). Firebrands generated from a full-scale structure burning under well-controlled laboratory conditions. Fire Safety Journal, 63, 43-51.

12. Brown, A., Manzello, S. L., Suzuki, J., Hayashi, Y., & Suzuki, S. (2014). Firebrands generated from a full-scale structure burning under well-controlled laboratory conditions. Fire Safety Journal, 63, 43-51.

13. Caton, S. E., Hakes, R. S. P., Gorham, D. J., Zhou, A., & Gollner, M. J. (2016). Review of pathways for building fire spread in the Wildland urban interface part I: Exposure conditions. Fire Technology. doi:10.1007/s10694-016-0589-z

14. Cohen, J., (2008). The wildland-urban interface fire problem: a consequence of the fire exclusion paradigm. Forest Hist Today Fall pp 20–26

15. NFPA. (2008). Deadliest/large-loss fires, 25 largest fire losses in US history. Quincy, MA: National Fire Protection Association (NFPA).

16. FPL. (2010). Wood handbook—Wood as an engineer ing material. General Technical Report FPL-GTR-190. Madison, WI: U.S. Department of Agriculture, Forest Service, Forest Products Laboratory (FPL).

17. Gašparovič, L., Koreňová, Z., & Jelemenský, Ľ. (2010). Kinetic study of wood chips decomposition by TGA. Chemical Papers, 64, 2, 174-181.

18. Grishin, A. M., Filkov, A. I., Loboda, E. L., Reyno, V. V., Kozlov, A. V., Kuznetsov, V. T., Kasymov, D. P., ... Stolyarchuk, N. D. (January 01, 2014). A field experiment on grass fire effects on wooden constructions and peat layer ignition. International Journal of Wildland Fire, 23, 3, 445.

19. Green, D. W., & Evans, J. W. (2008). The immediate effect of temperature on the modulus of elasticity of green and dry lumber. Wood and Fiber Science, 40, 3, 374-383.

20. Gorte, R., (2013) The rising cost of wildfire protection. Bozeman, MT: Headwaters Economics.

21. Haynes, K., Handmer, J., McAneney, J., Tibbits, A., & Coates, L. (2010). Australian bushfire fatalities 1900-2008: exploring trends in relation to the ‘Prepare, stay and defend or leave early’ policy. Environmental Science and Policy, 13, 3, 185-194.

22. Janssens M. (1991) Fundamental thermos-physical characteristics of wood and their role in enclosure fire growth. PhD thesis, University of Cent, Belgium

23. Jin, W., Singh, K., & Zondlo, J. (2013). Pyrolysis Kinetics of physical components of wood and wood-polymers using Isoconversion method. Agriculture, 3(1), 12–32. doi:10.3390/agriculture3010012

24. Koo, E., Pagni, P. J., Weise, D. R., & Woycheese, J. P. (2010). Firebrands and spotting ignition in large-scale fires. International Journal of Wildland Fire Int. J. Wildland Fire, 19(7), 818. doi:10.1071/wf07119

25. Khawam, A. (2005), "Application of solid state-kinetics to desolvation reactions", Iowa University Doctorial Thesis, September 2007

26. Kissinger, H. E. (1956). Variation of peak temperature with heating rate in differential thermal analysis. Journal of Research of the National Bureau of Standards, 57, 4, 217.

27. Koo, E., Linn, R. R., Pagni, P. J., & Edminster, C. B. (2012). Modelling firebrand transport in wildfires using HIGRAD/FIRETEC. International Journal of Wildland Fire, 21,4, 396-417.

28. Lampin-Maillet, C., Jappiot, M., Long, M., Bouillon, C., Morge, D., & Ferrier, J. P. (2010). Mapping wildland-urban interfaces at large scales integrating housing density and vegetation aggregation for fire prevention in the South of France.Journal of Environmental Management, 91, 3.

29. Manzello, S. L., Park, S.-H., & Cleary, T. G. (2009). Investigation on the ability of glowing firebrands deposited within crevices to ignite common building materials. Fire Safety Journal, 44, 6, 894-900.

30. Kollmann, F. （1960）. Occurrence of exothermic reactions in wood. Holz als Rohund Werkstoff 18:193-200

31. Mashura, L.A. (2014) A Lesson from the Sea Isle City Beachfront Fire Flammability of OSB in New Construction

32. Manzello, S. L., & Foote, E. I. D. (2014). Characterizing Firebrand Exposure from Wildland-Urban Interface (WUI) Fires: Results from the 2007 Angora Fire. Fire Technology, 50, 1, 105-124.

33. Mulik, A. I., & Fauzi, F. (2013). Properties of Oriented Strand Board(OSB) Made from Mixing Bamboo, ARPN Journal of Science and Technology ISSN 2225-7217

34. Mell, W. E., Manzello, S. L., Maranghides, A., Butry, D., & Rehm, R. G. (2010). The wildland–urban interface fire problem – current approaches and research needs. International Journal of Wildland Fire, 19(2), 238. doi:10.1071/wf07131

35. Manzello, S. L., Maranghides, A., Shields, J. R., Mell, W. E., Hayashi, Y., & Nii,

D. (2009). Mass and size distribution of firebrands generated from burning Korean pine (Pinus koraiensis) trees. Fire and Materials, 33, 1, 21-31.

36. Marek. M. (1999), “Computational aspects of kinetic analysis. Part B: The ICTAC Kinetics Project- the decomposition kinetics of calcium carbonate revisited, or some tips on survival in the kinetic minefield”, Laboratory of Technical Chemistry, Swiss Federal Institute of Technology, ETH- Zentrum, CH-8092 Zurich, Switzerland

37. Manzello, S. (2014). Enabling the investigation of structure vulnerabilities to wind- driven firebrand showers in Wildland-Urban interface (WUI) fires. Fire Safety Science - Proceedings of the Eleventh International Symposium, 11, 83–96. doi:10.3801/iafss.fss.11-83

38. Manzello, S. L., Suzuki, S., & Hayashi, Y. (2012). Exposing siding treatments, walls fitted with eaves, and glazing assemblies to firebrand showers. Fire Safety Journal, 50, 25-34.

39. Martin, S. (1965). Diffusion-controlled ignition of cellulosic materials by intense radiant energy. Symposium (International) on Combustion, 10(1), 877–896.

40. Manzello, S. L., Cleary, T. G., Shields, J. R., & Yang, J. C. (2006). On the ignition of fuel beds by firebrands. Fire and Materials, 30, 1, 77-87.

41. Maranghides, A., & Mell, W. (2011). A Case Study of a Community Affected by the Witch and Guejito Wildland Fires. Fire Technology, 47, 2, 379-420.

42. Moghtaderi, B., & Fletcher, D.F. (1988). Flaming Combustion Characteristics of Wood-Based Materials.

43. Nicole, M.S., Cai, Z., & Charles,C. (1999). Wood-Based Composite Materials Panel Products, Glued-Laminated Timber, Structural Composite Lumber, and Wood-Nonwood Composite Matetials, General Technical Report FPL-GTR-190

44. Ozawa, T. (1965). A New Method of Analyzing Thermogravimetric Data.Bulletin of the Chemical Society of Japan, 38, 11, 1881-1886.

45. Poletto, M., Zattera, A. J., & Santana, R. M. C. (2012). Thermal decomposition of wood: Kinetics and degradation mechanisms. Bioresource Technology, 126, 7-12.

46. WPIF, TTF & NPPD (2006), Panel-guide

47. Quarles SL (2012) Vulnerabilities of buildings to wildfire exposures. pp 1–13.

http:// articles.extension.org/pages/63495/vulnerabilities-of-buildings-to-wildfire-exposure

48. Qiang, X., Martin, Z., Andrea, M., Cong, J., & Yong, J. (2013) Evaluation of plywood fire behaviour by ISO tests. European Journal of Environmental and Safety Sciences 2013 1(1): 1-7

49. Randall, B., Nelson, B., Byan, D., Steve, G., Steve, Q., Don, O., Michele, S., & Rick, S. (2015).Pathways for Building Fire Spread at the Wildland Urban Interface, The Fire Protection Research Foundation, Quincy. MA.

50. Slopiecka, K., Bartocci, P., & Fantozzi, F. (2012). Thermogravimetric analysis and kinetic study of poplar wood pyrolysis. Applied Energy, 97, 491-497.

51. Spearpoint, M. (2001). Predicting the piloted ignition of wood in the cone calorimeter using an integral model — effect of species, grain orientation and heat flux.Fire Safety Journal, 36, 4, 391-415.

52. Simms, D. L. (1962). Damage to cellulosic solids by thermal radiation.Combustion and Flame, 6, 303-318.

53. Suzuki, S., Manzello, S. L., & Hayashi, Y. (2013). The size and mass distribution of firebrands collected from ignited building components exposed to wind. Proceedings of the Combustion Institute, 34, 2, 2479-2485.

54. Stephens, S. L., & Ruth, L. W. (2005). Federal Forest-Fire Policy In The United States. Ecological Applications, 15(2), 532-542. doi:10.1890/04-0545

55. Schartel, B., & Hull, T. R. (2007). Development of fire-retarded materials—Interpretation of cone calorimeter data. Fire and Materials, 31, 5, 327-354.

56. Shi, L., & Chew, M. Y. (2012). Influence of moisture on autoignition of woods in cone calorimeter. Journal of Fire Sciences, 30(2), 158-169. doi:10.1177/0734904111431675

57. Suzuki, S., Manzello, S. L., Lage, M., & Laing, G. (2012). Firebrand generation data obtained from a full-scale structure burn. International Journal of Wildland Fire, 21(8), 961. doi:10.1071/wf11133

58. Suzuki, S., Manzello, S. L., & Hayashi, Y. (2013). The size and mass distribution of firebrands collected from ignited building components exposed to wind. Proceedings of the Combustion Institute, 34(2), 2479–2485. doi:10.1016/j.proci.2012.06.061

59. Shi, L., & Chew, M. Y. L. (2013). A review of fire processes modeling of combustible materials under external heat flux. Fuel, 106, 30-50.

60. Tantely, R., Fils, L. R., Georgette, R., Alain, B & Colette, L. (2016). Thermal Behavior of Three Woods of Madagascar by Thermogravimetric Analysis in Inert Atmosphere

61. Tsamba, A. J., Yang, W., & Blasiak, W. (2006). Pyrolysis characteristics and global kinetics of coconut and cashew nut shells. Fuel Processing Technology, 87, 6, 523-530.

62. Tolhurst, K., Duff, T., Chong, D., (2014) Using fire simulations to assess house vulnerability at the urban interface. Fire Note, Bushfire CRC pp 1–4.

63. Thompson C (2001) Notices. Fed Reg 66(3):751–777

64. Viegas, D. X., Almeida, M., Raposo, J., Oliveira, R., & Viegas, C. X. (2014). Ignition of Mediterranean Fuel Beds by Several Types of Firebrands. Fire Technology, 50 , 1, 61-77.

65. Yu, Z., & Zhou, A. (2010). Mass loss of fiber-reinforced polymer composites in fire. Proceedings of the SAMPE 2010 Conference, May 17-21, 2010, Seattle, WA.

# APPENDIX A: FWO DATA

Table A.1. Numerical Integration Constants

| E/RT | a | b | E/RT | a | b | E/RT | a | b |
|---|---|---|---|---|---|---|---|---|
| **8** | 5.370 | 0.540 | **47** | 23.774 | 0.453 | **86** | 41.829 | 0.448 |
| **9** | 5.898 | 0.528 | **48** | 24.226 | 0.452 | **87** | 42.292 | 0.448 |
| **10** | 6.417 | 0.519 | **49** | 24.678 | 0.452 | **88** | 42.755 | 0.448 |
| **11** | 6.928 | 0.511 | **50** | 25.130 | 0.452 | **89** | 43.218 | 0.448 |
| **12** | 7.433 | 0.505 | **51** | 25.581 | 0.451 | **90** | 43.681 | 0.448 |
| **13** | 7.933 | 0.500 | **52** | 26.031 | 0.451 | **91** | 44.144 | 0.448 |
| **14** | 8.427 | 0.494 | **53** | 26.482 | 0.451 | **92** | 44.607 | 0.448 |
| **15** | 8.918 | 0.491 | **54** | 26.932 | 0.450 | **93** | 45.070 | 0.448 |
| **16** | 9.406 | 0.488 | **55** | 27.382 | 0.450 | **94** | 45.533 | 0.448 |
| **17** | 9.890 | 0.484 | **56** | 27.832 | 0.450 | **95** | 45.997 | 0.448 |
| **18** | 10.372 | 0.482 | **57** | 28.281 | 0.450 | **96** | 46.460 | 0.448 |
| **19** | 10.851 | 0.479 | **58** | 28.731 | 0.449 | **97** | 46.923 | 0.448 |
| **20** | 11.328 | 0.477 | **59** | 29.179 | 0.449 | **98** | 47.386 | 0.448 |
| **21** | 11.803 | 0.475 | **60** | 29.628 | 0.449 | **99** | 47.849 | 0.448 |
| **22** | 12.276 | 0.473 | **61** | 30.251 | 0.449 | **100** | 48.312 | 0.448 |
| **23** | 12.747 | 0.471 | **62** | 30.714 | 0.449 | | | |
| **24** | 13.217 | 0.47 | **63** | 31.177 | 0.449 | | | |
| **25** | 13.686 | 0.469 | **64** | 31.640 | 0.449 | | | |
| **26** | 14.153 | 0.467 | **65** | 32.104 | 0.449 | | | |
| **27** | 14.619 | 0.466 | **66** | 32.567 | 0.449 | | | |
| **28** | 15.084 | 0.465 | **67** | 33.030 | 0.449 | | | |
| **29** | 15.547 | 0.463 | **68** | 33.493 | 0.449 | | | |
| **30** | 16.010 | 0.463 | **69** | 33.956 | 0.449 | | | |
| **31** | 16.472 | 0.462 | **70** | 34.419 | 0.449 | | | |
| **32** | 16.933 | 0.461 | **71** | 34.882 | 0.449 | | | |
| **33** | 17.394 | 0.461 | **72** | 35.345 | 0.449 | | | |
| **34** | 17.853 | 0.459 | **73** | 35.808 | 0.449 | | | |
| **35** | 18.312 | 0.459 | **74** | 36.271 | 0.449 | | | |
| **36** | 18.77 | 0.458 | **75** | 36.735 | 0.448 | | | |
| **37** | 19.228 | 0.458 | **76** | 37.198 | 0.448 | | | |
| **38** | 19.684 | 0.456 | **77** | 37.661 | 0.448 | | | |
| **39** | 20.141 | 0.456 | **78** | 38.124 | 0.448 | | | |
| **40** | 20.597 | 0.456 | **79** | 38.587 | 0.448 | | | |
| **41** | 21.052 | 0.455 | **80** | 39.050 | 0.448 | | | |
| **42** | 21.507 | 0.455 | **81** | 39.513 | 0.448 | | | |
| **43** | 21.961 | 0.454 | **82** | 39.976 | 0.448 | | | |
| **44** | 22.415 | 0.454 | **83** | 40.439 | 0.448 | | | |
| **45** | 22.868 | 0.453 | **84** | 40.902 | 0.448 | | | |
| **46** | 23.321 | 0.453 | **85** | 41.366 | 0.448 | | | |

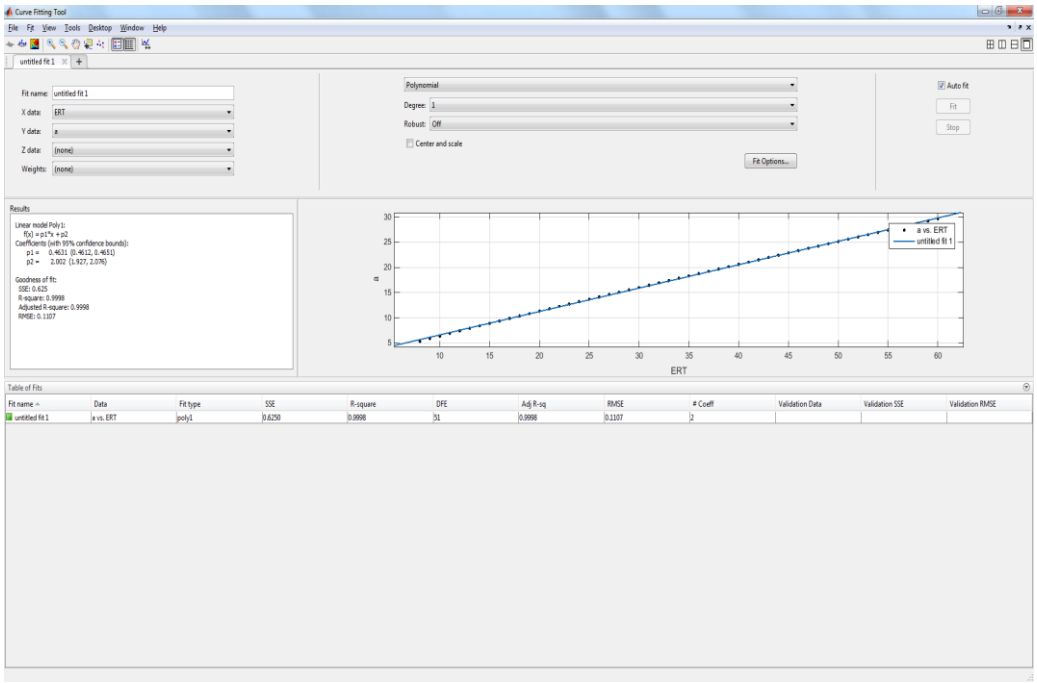


Figure A.1. The relationship between a and E/RT

$$a = 0.4631\left(\frac{E}{RT}\right) + 2 \quad R^2 = 1$$ Equation (23)

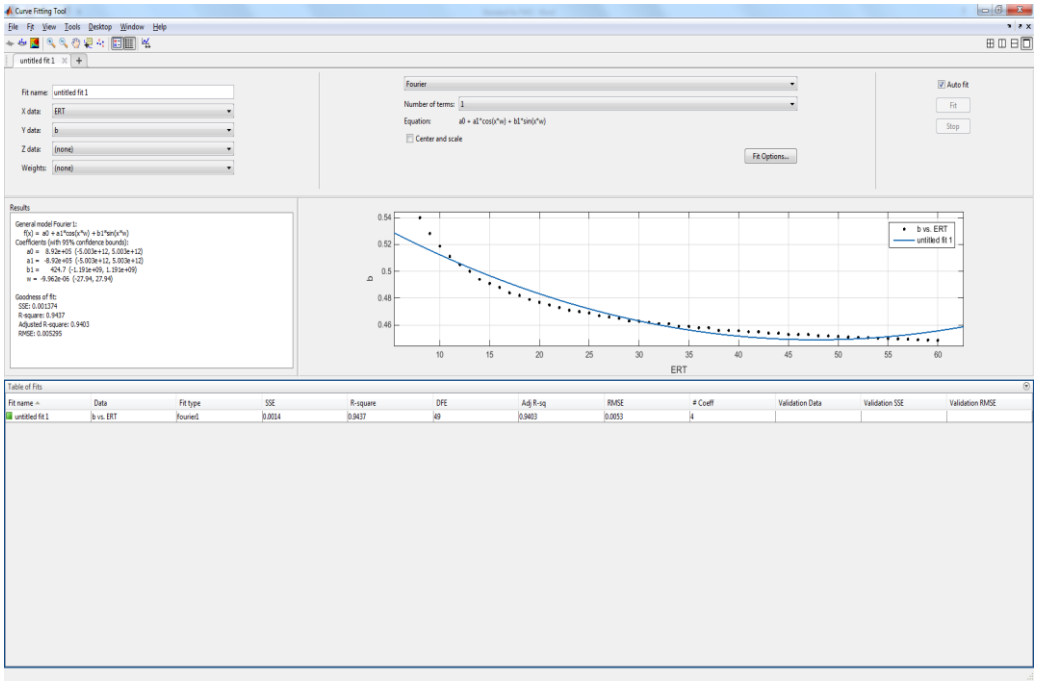


Figure A.2. The relationship between b and E/RT

While, after $\frac{E}{RT} = 60$, b turns out to be constant

The following steps would show the way I analyzed specimen.

For OSB Sheathing, PF face and pMDI core

1. For CII 5 K/min heating rate

$$\alpha = \frac{m_o - m_i}{m_o - m_\infty} = \frac{1-\frac{m_i}{m_o}}{1-\frac{m_\infty}{m_o}} = \frac{1-C}{1-24.2\%} = 1.319 - \frac{C}{75.8\%} \qquad \text{Equation (24)}$$

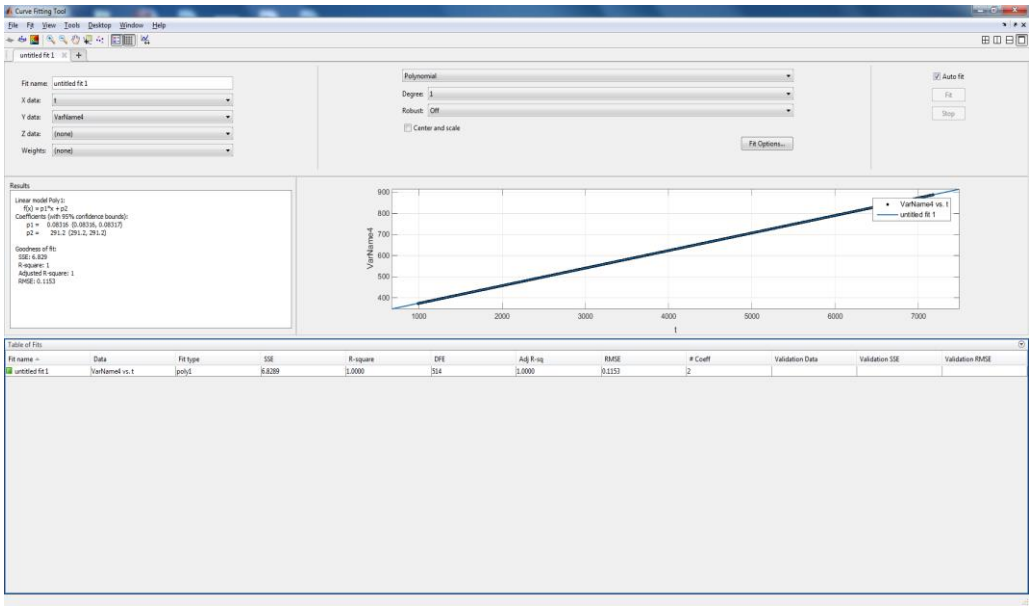


Figure A.3. The relationship of CII 5 K/min between T and t

$$T = 0.083t + 291.2 \qquad R^2 = 1 \qquad \text{Equation (25)}$$

So, when 5 K/min heating rate $\frac{d_T}{d_t} = 0.083$

$$\ln\left(\frac{d_T}{d_t}\right) = \ln(\beta) = -2.49 \qquad \text{Equation (26)}$$

2. For CII 15 K/min heating rate

$$\alpha = \frac{m_o - m_i}{m_o - m_\infty} = \frac{1-\frac{m_i}{m_o}}{1-\frac{m_\infty}{m_o}} = \frac{1-C}{1-22.55\%} = 1.14 - \frac{C}{87.5\%} \qquad \text{Equation (27)}$$

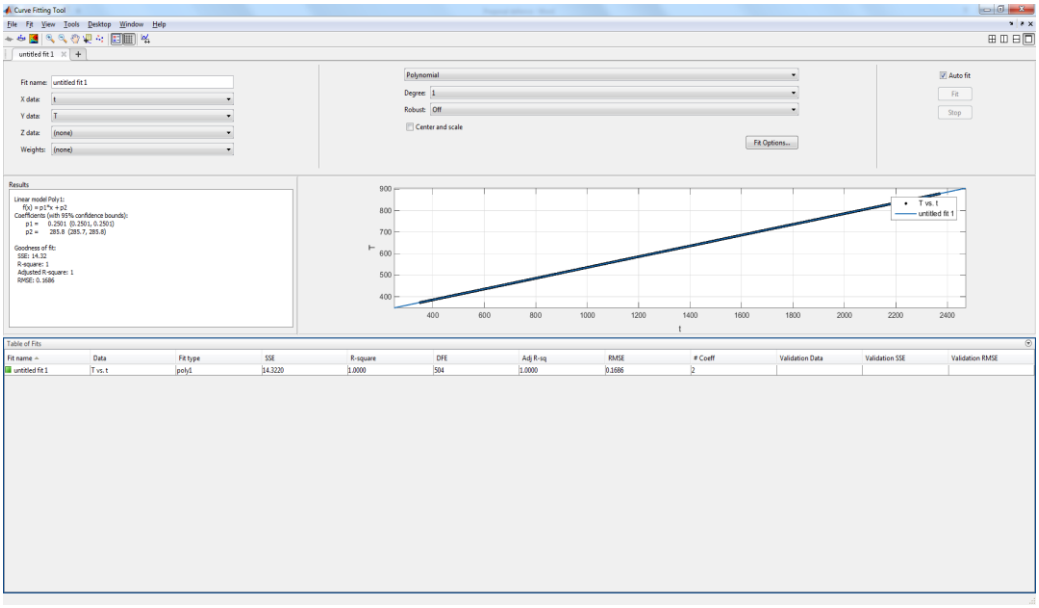


Figure A.4. The relationship of CII 15 K/min between T and t

$$T = 0.25t + 286 \qquad R^2 = 1 \qquad \text{Equation (28)}$$

So, when 15 K/min heating rate $\frac{d_T}{d_t} = 0.25$

$$\ln\left(\frac{d_T}{d_t}\right) = -1.39 \qquad \text{Equation (29)}$$

3. For CII 25 K/min heating rate

$$\alpha = \frac{m_o - m_i}{m_o - m_\infty} = \frac{1-\frac{m_i}{m_o}}{1-\frac{m_\infty}{m_o}} = \frac{1-C}{1-22.44\%} = 1.29 - \frac{C}{77.56\%} \qquad \text{Equation (30)}$$

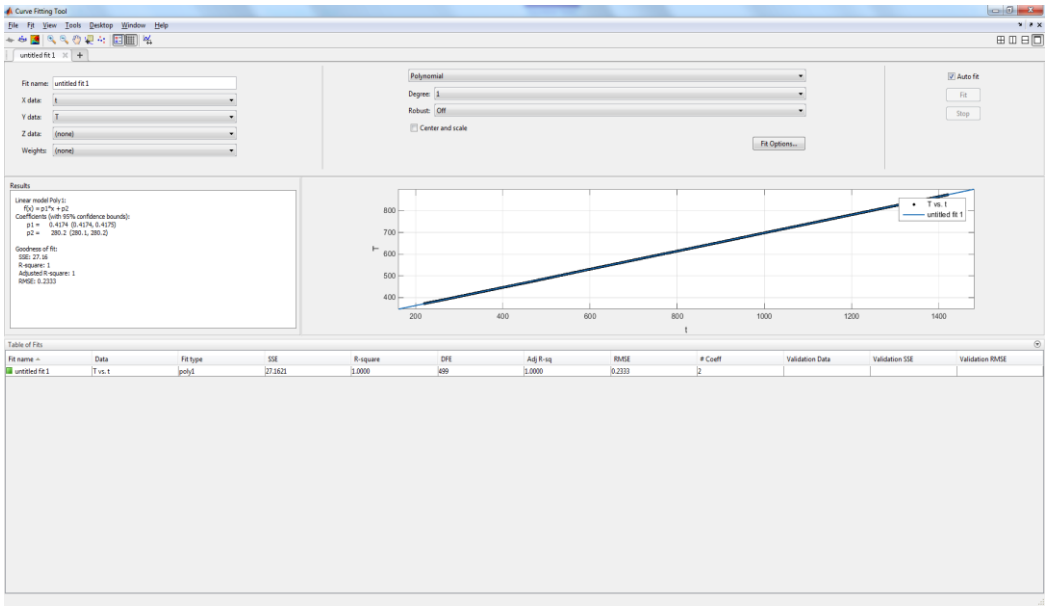

Figure A.5. The relationship of CII 25 K/min between T and t

$$T = 0.4174t + 280.2 \qquad R^2 = 1 \qquad \text{Equation (31)}$$

So, when 25 K/min heating rate $\frac{d_T}{d_t} = 0.4174$

$$\ln\left(\frac{d_T}{d_t}\right) = -0.87 \qquad \text{Equation (32)}$$

$$T = 0.4174t + 280.2 \qquad R^2 = 1 \qquad \text{Equation (33)}$$

So, when 25 K/min heating rate $\frac{d_T}{d_t} = 0.4174$

$$\ln\left(\frac{d_T}{d_t}\right) = -0.87 \qquad \text{Equation (34)}$$

So, we had the following conclusions:

When 5 K/min heating rate $\ln\left(\frac{d_T}{d_t}\right) = -2.49$

When 15 K/min heating rate $\ln\left(\frac{d_T}{d_t}\right) = -1.39$

When 25 K/min heating rate $\ln\left(\frac{d_T}{d_t}\right) = -0.87$

Table A.2. $1000/T \sim \alpha$ for CII 5 K/min heating rate

| $\alpha$ | $\frac{1000}{T}$ |
|---|---|
| 0.1 | 1.85 |
| 0.15 | 1.79 |
| 0.2 | 1.75 |
| 0.25 | 1.72 |
| 0.3 | 1.7 |
| 0.35 | 1.67 |
| 0.4 | 1.65 |
| 0.45 | 1.63 |
| 0.5 | 1.62 |
| 0.55 | 1.6 |
| 0.6 | 1.58 |
| 0.65 | 1.54 |
| 0.7 | 1.42 |
| 0.75 | 1.19 |

Table A.3. $1000/T \sim \alpha$ for CII 15 K/min heating rate

| $\alpha$ | $\frac{1000}{T}$ |
|---|---|
| 0.1 | 1.82 |
| 0.15 | 1.76 |
| 0.2 | 1.72 |
| 0.25 | 1.69 |
| 0.3 | 1.66 |
| 0.35 | 1.64 |
| 0.4 | 1.62 |
| 0.45 | 1.6 |
| 0.5 | 1.58 |
| 0.55 | 1.565 |
| 0.6 | 1.545 |
| 0.65 | 1.52 |
| 0.7 | 1.43 |
| 0.75 | 1.28 |

Table A.4. $1000/T \sim \alpha$ for CII 25 K/min heating rate

| $\alpha$ | $\frac{1000}{T}$ |
|---|---|
| 0.1 | 1.79 |
| 0.15 | 1.73 |
| 0.2 | 1.69 |
| 0.25 | 1.66 |
| 0.3 | 1.64 |
| 0.35 | 1.615 |
| 0.4 | 1.6 |
| 0.45 | 1.58 |
| 0.5 | 1.56 |
| 0.55 | 1.54 |
| 0.6 | 1.53 |
| 0.65 | 1.5 |
| 0.7 | 1.42 |
| 0.75 | 1.28 |

Table A.5. First order Parameters for CII Kinetic Pyrolysis

| $\alpha$ | T | Ln(A) | R^2 | g | y | E/R |
|---|---|---|---|---|---|---|
| 0.15 | 526.3158 | 35.79 | 0.994 | 0.162519 | 35.13 | 19808 |
| 0.2 | 546.4481 | 35.42 | 0.958 | 0.223144 | 34.71 | 20339 |
| 0.25 | 558.6592 | 37.4 | 0.997 | 0.287682 | 36.69 | 21897 |
| 0.3 | 571.4286 | 39.26 | 0.995 | 0.356675 | 38.43 | 23367 |
| 0.35 | 581.3953 | 40.23 | 0.997 | 0.430783 | 39.48 | 24388 |
| 0.4 | 591.716 | 41.78 | 0.998 | 0.510826 | 40.6 | 25490 |
| 0.45 | 598.8024 | 36.8 | 0.997 | 0.597837 | 35.6 | 22816 |
| 0.5 | 606.0606 | 38.64 | 0.99 | 0.693147 | 37.4 | 24187 |
| 0.55 | 611.6208 | 39.49 | 1 | 0.798508 | 38.12 | 24842 |
| 0.6 | 617.284 | 39.53 | 0.998 | 0.916291 | 39.51 | 25913 |
| 0.65 | 619.9628 | 38.11 | 0.998 | 1.049822 | 36.79 | 24345 |
| 0.7 | 625 | 39.25 | 0.998 | 1.203973 | 38.99 | 25913 |
| 0.75 | 626.9592 | 37.45 | 1 | 1.386294 | 37.13 | 24842 |
| 0.8 | 630.1197 | 37.2 | 0.999 | 1.609438 | 35.66 | 24041 |
| 0.85 | 633.7136 | 36.3 | 0.999 | 1.89712 | 34.83 | 23657 |
| 0.9 | 640.2049 | 40.02 | 1 | 2.302585 | 38.34 | 26138 |

Table A.6. CII 5 K/min heating rate Kinetic Pyrolysis

| E1/RT | a | b1 | E1 | E2/E1 | b2 | ln (A) |
|---|---|---|---|---|---|---|
| 82.35274 | 40.9 | 0.4484 | 360358.2 | 1.019 | 0.4484 | 35.79 |
| 81.44501 | 40.4 | 0.4484 | 370018.5 | 1.019 | 0.4484 | 35.42 |
| 85.76724 | 42.3 | 0.4483 | 398362.5 | 1.019 | 0.4483 | 37.4 |
| 89.47976 | 44.1 | 0.4483 | 425105.6 | 1.019 | 0.4483 | 39.26 |
| 91.78853 | 45 | 0.4483 | 443680.2 | 1.019 | 0.4483 | 40.23 |
| 94.2628 | 46.5 | 0.4483 | 463728.4 | 1.019 | 0.4483 | 41.78 |
| 83.37575 | 41.4 | 0.4484 | 415081.5 | 1.019 | 0.4484 | 36.8 |
| 87.32724 | 43.2 | 0.4483 | 440023.5 | 1.019 | 0.4483 | 38.64 |
| 88.87674 | 44 | 0.4483 | 451939.6 | 1.019 | 0.4483 | 39.49 |
| 91.8579 | 45 | 0.4483 | 471423.8 | 1.019 | 0.4483 | 39.53 |
| 85.92666 | 42.5 | 0.4483 | 442897.9 | 1.019 | 0.4483 | 38.11 |
| 90.72385 | 44.6 | 0.4483 | 471423.8 | 1.019 | 0.4483 | 39.25 |
| 86.70239 | 42.75 | 0.4483 | 451939.6 | 1.019 | 0.4483 | 37.45 |
| 83.48592 | 41.4 | 0.4484 | 437367.3 | 1.019 | 0.4483 | 37.2 |
| 81.68653 | 40.4 | 0.4484 | 430381.4 | 1.019 | 0.4484 | 36.3 |
| 89.3382 | 44.1 | 0.4483 | 475517.1 | 1.019 | 0.4483 | 40.02 |

Table A.7. CII 15 K/min heating rate Kinetic Pyrolysis

| E1/RT | E2/RT | a | b1 | E1 | E2 | ln (A) |
|---|---|---|---|---|---|---|
| 79.75212 | 81.26741 | 39.5 | 0.4484 | 360358.2 | 367205 | 34.76 |
| 78.77468 | 80.2714 | 39.05 | 0.4484 | 370018.5 | 377048.8 | 34.43 |
| 83.37151 | 84.95557 | 41.37 | 0.4484 | 398362.5 | 405931.4 | 36.83 |
| 86.92319 | 88.57474 | 43.22 | 0.4483 | 425105.6 | 433182.6 | 38.75 |
| 89.12026 | 90.81355 | 44.14 | 0.4483 | 443680.2 | 452110.1 | 39.73 |
| 91.47396 | 93.21197 | 45.07 | 0.4483 | 463728.4 | 472539.2 | 40.7 |
| 80.87947 | 82.41618 | 40 | 0.4484 | 415081.5 | 422968 | 35.76 |
| 84.68096 | 86.2899 | 41.83 | 0.4483 | 440023.5 | 448383.9 | 37.6 |
| 86.43059 | 88.07277 | 42.75 | 0.4483 | 451939.6 | 460526.4 | 39.94 |
| 89.02278 | 90.71421 | 44.14 | 0.4483 | 471423.8 | 480380.9 | 40.03 |
| 83.10328 | 84.68224 | 41.37 | 0.4484 | 442897.9 | 451312.9 | 37.35 |
| 87.88873 | 89.55862 | 43.68 | 0.4483 | 471423.8 | 480380.9 | 39.69 |
| 83.71265 | 85.30319 | 41.37 | 0.4484 | 451939.6 | 460526.4 | 37.46 |
| 80.48737 | 82.01663 | 40 | 0.4484 | 437367.3 | 445677.3 | 36.17 |
| 79.20177 | 80.70661 | 39.51 | 0.4484 | 430381.4 | 438558.6 | 35.76 |
| 86.36407 | 88.00499 | 42.75 | 0.4483 | 475517.1 | 484552 | 39.04 |

Table A.8. CII 25 K/min heating rate Kinetic Pyrolysis

| E1/RT | E2/RT | a | b1 | E1 | E2 | ln (A) |
|---|---|---|---|---|---|---|
| 78.88525 | 80.38407 | 39.05 | 0.4484 | 360358.2 | 367205 | 34.3 |
| 78.32963 | 79.81789 | 39.05 | 0.4484 | 370018.5 | 377048.8 | 34.43 |
| 82.41322 | 83.97907 | 40.9 | 0.4484 | 398362.5 | 405931.4 | 36.36 |
| 85.90057 | 87.53268 | 42.75 | 0.4483 | 425105.6 | 433182.6 | 38.28 |
| 88.58661 | 90.26975 | 43.22 | 0.4483 | 443680.2 | 452110.1 | 38.8 |
| 90.91619 | 92.6436 | 45.07 | 0.4483 | 463728.4 | 472539.2 | 40.7 |
| 79.88096 | 81.3987 | 39.5 | 0.4484 | 415081.5 | 422968 | 35.26 |
| 83.62245 | 85.21128 | 41.4 | 0.4483 | 440023.5 | 448383.9 | 37.2 |
| 85.34341 | 86.96494 | 42.3 | 0.4483 | 451939.6 | 460526.4 | 38.15 |
| 88.45575 | 90.13641 | 43.7 | 0.4483 | 471423.8 | 480380.9 | 39.6 |
| 82.57057 | 84.13941 | 40.9 | 0.4484 | 442897.9 | 451312.9 | 36.88 |
| 87.32171 | 88.98082 | 43.2 | 0.4483 | 471423.8 | 480380.9 | 39.2 |
| 83.16906 | 84.74927 | 41.4 | 0.4484 | 451939.6 | 460526.4 | 37.5 |
| 79.96131 | 81.48058 | 39.5 | 0.4484 | 437367.3 | 445677.3 | 35.7 |
| 78.16646 | 79.65162 | 39.05 | 0.4484 | 430381.4 | 438558.6 | 35.3 |
| 85.79212 | 87.42217 | 42.3 | 0.4483 | 475517.1 | 484552 | 38.59 |

For example, when $\alpha = 0.1$, heating rate 5 K/min, slope= $27000K$

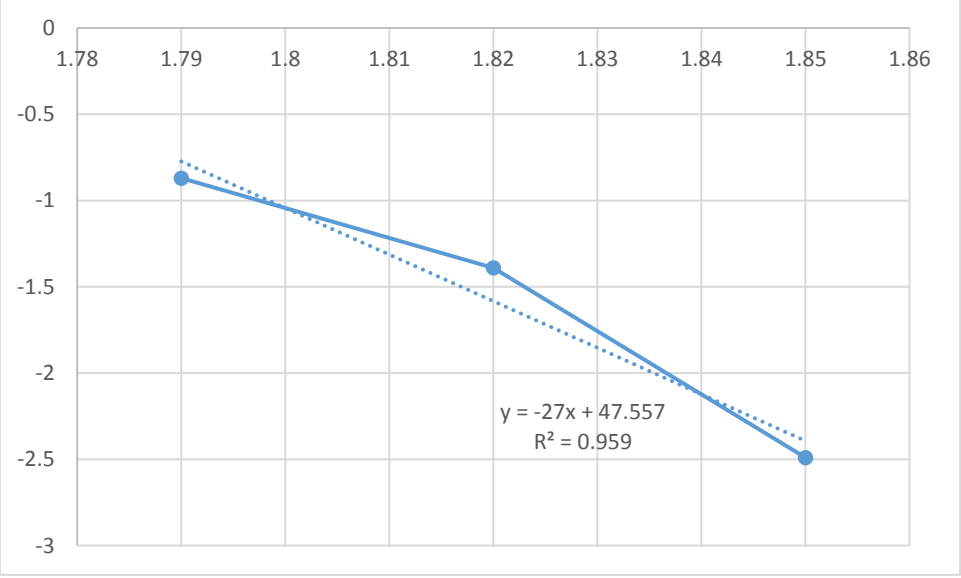


Figure A.6. The slope of CII 5 K/min (α =0.1)

The temperature was $T = \frac{1000}{1.85} = 540.54K$

As the first estimation: $b = 0.457$

Used equation: $E = 8.314 \times 27000/0.457$=491199.13J/mol

Calculating the value of $E/RT$:

$$\frac{E}{RT} = \frac{491199}{8.314}/540.54 = 109.3 \qquad \text{Equation (35)}$$

From Table 1 for $\frac{E}{RT} = 109.3$, b=0.4483

Reiterating yields:

E=500731.7J/mol

E/RT=111.42

b=0.4483

$E' = 500731.7J/mol$

Example calculation for pre-exponential factor (A):

$\beta' = 5 \quad \alpha = 0.1$

From Table 1:

E=500731.7J/mol

a=53.6

Using equation:

$$A = -5 \times 8.314 \times \ln(1 - 0.1) \times \frac{10^{53.6}}{500731.7} \qquad \text{Equation (36)}$$

$$= 1.79 \times 10^{48.3} = 10^{48.87} \qquad \ln(A) = 48.87$$

# APPENDIX B: THERMAL CONDUCTIVITY DATA

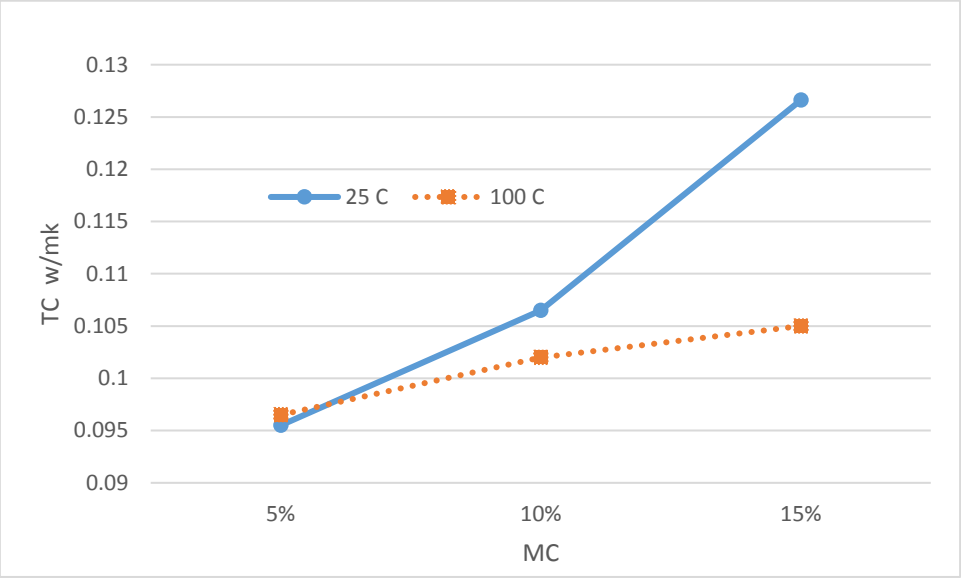


Figure B.1. SPF (Material B) thermal conductivity vs.MC

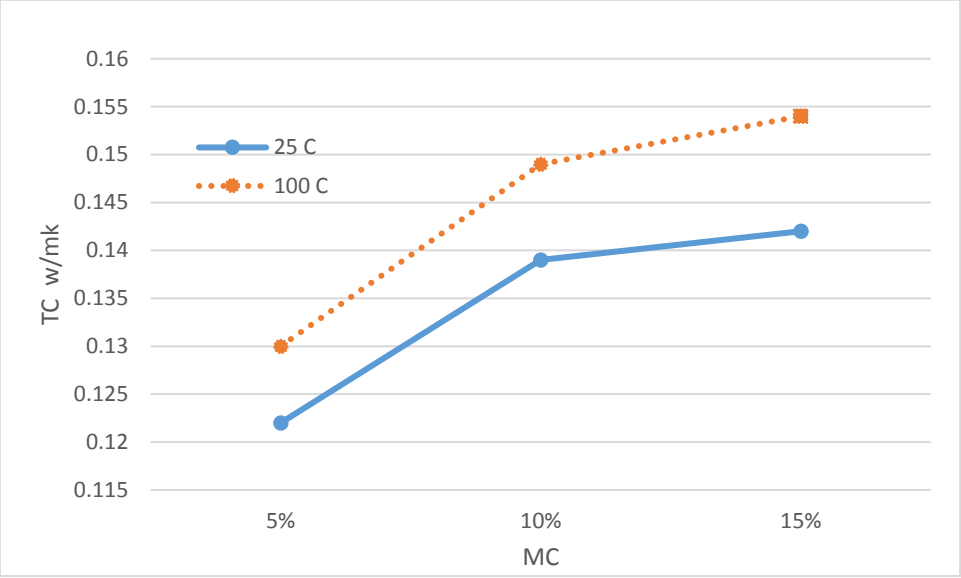


Figure B.2. OSB-Siding (Material D) thermal conductivity vs.MC

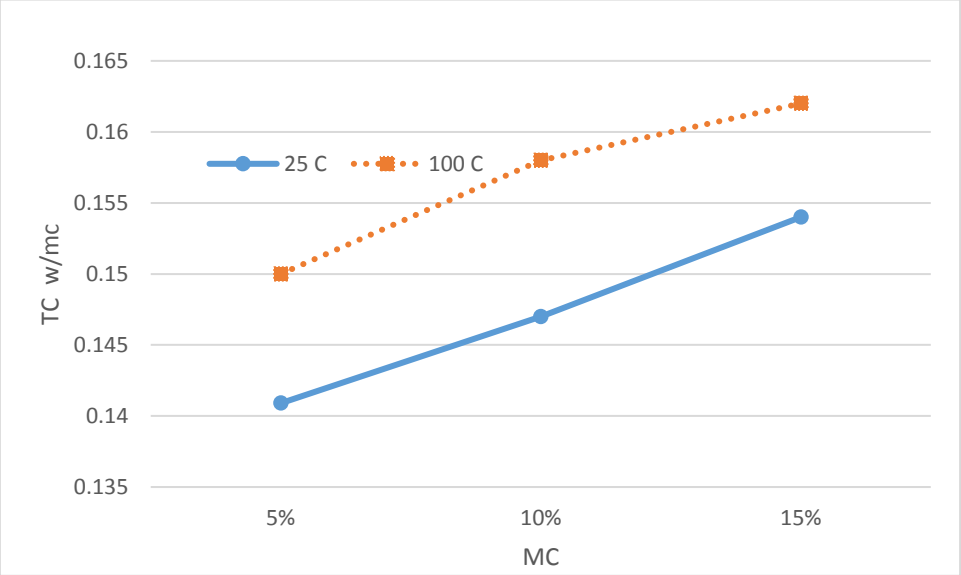


Figure B.3. OSB-H (Material E) thermal conductivity vs.MC

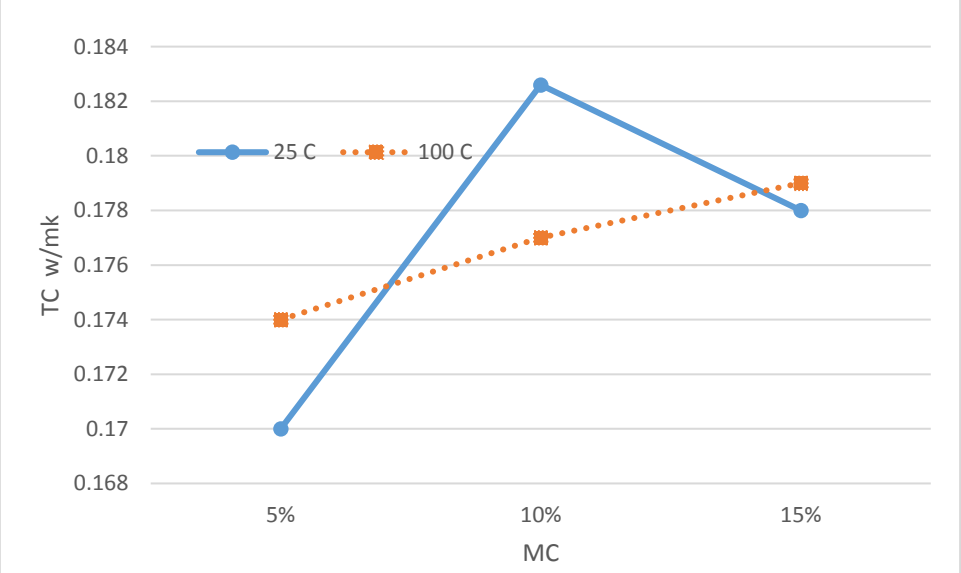


Figure B.4. CDX (Material F) thermal conductivity vs. MC

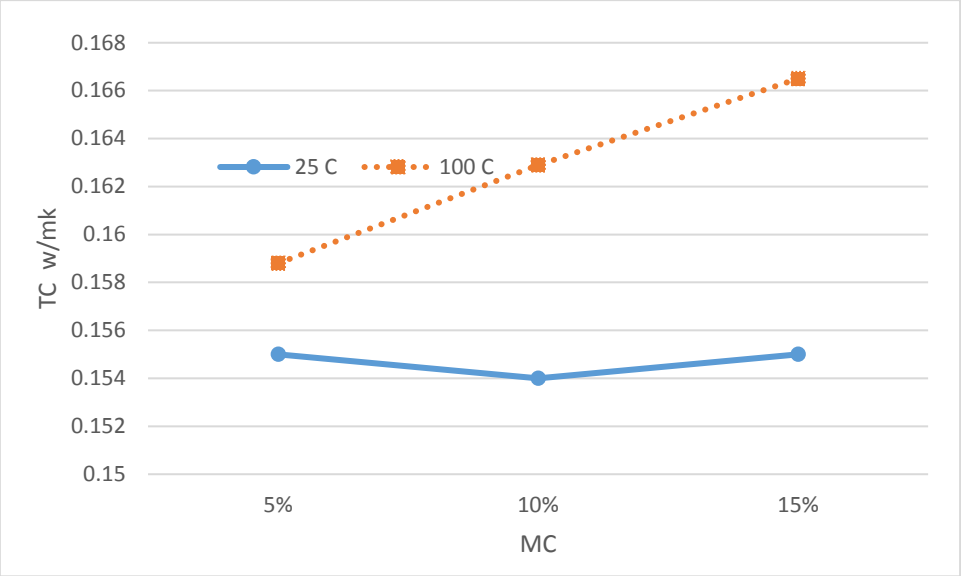


Figure B.5. HB (Material G) thermal conductivity vs. MC

# APPENDIX C: TII (Time to ignition) DATA

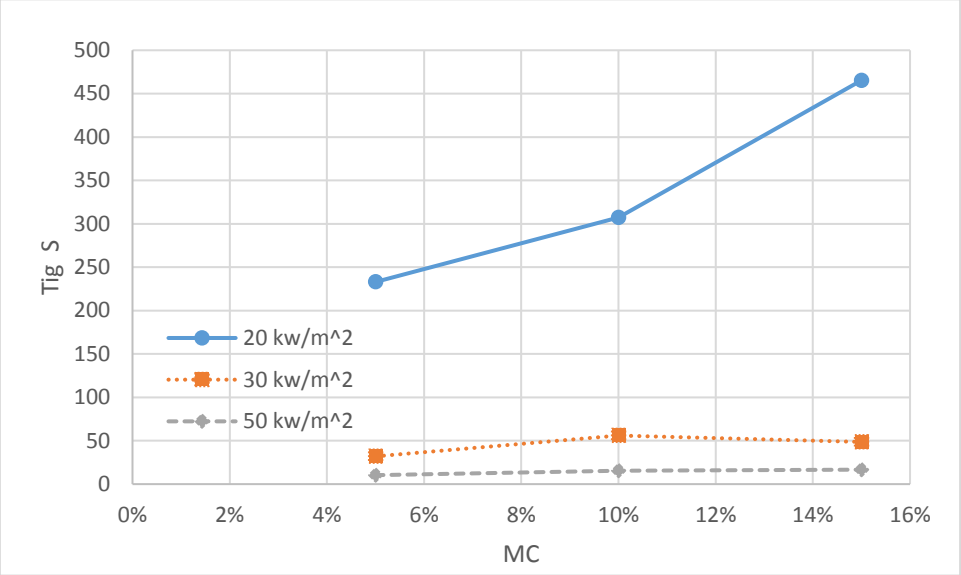


Figure C.1. SPF (Material B) ignition time vs.MC

The ignition time of SPF increased as the MC level increased, heat flux decreased.

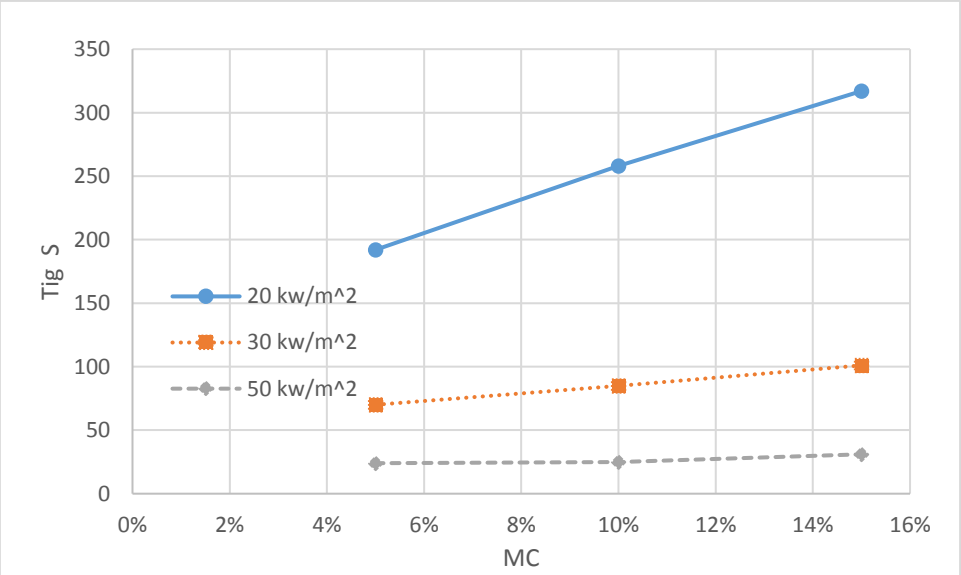


Figure C.2. OSB-PF (Material C) ignition time vs.MC

The ignition time of OSB-PF increased in a linear relationship as the MC level

increased, heat flux decreased.

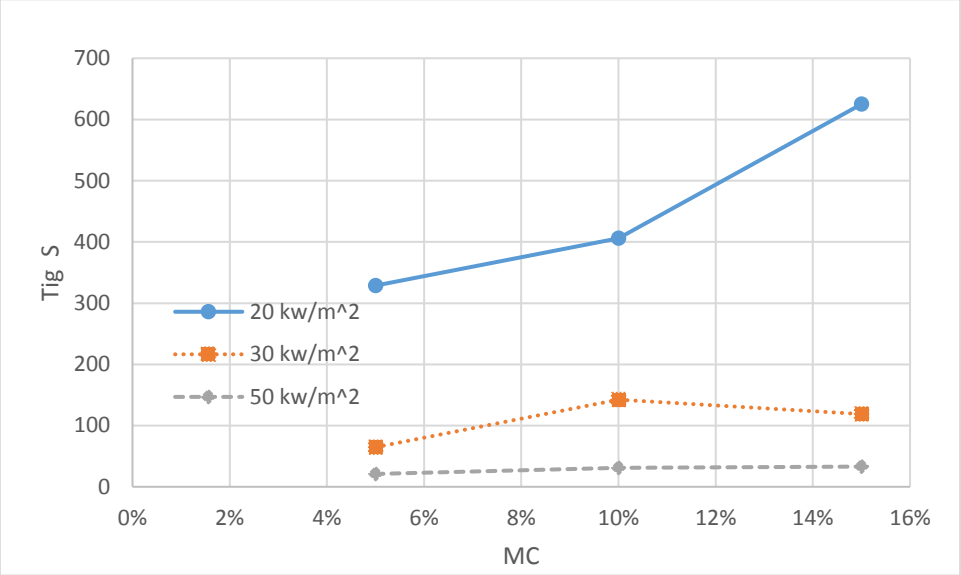


Figure C.3. OSB-Siding (Material D) ignition time vs.MC

The ignition time of OSB-Siding increased as the MC level increased (except 30 kw/m^2), heat flux decreased.

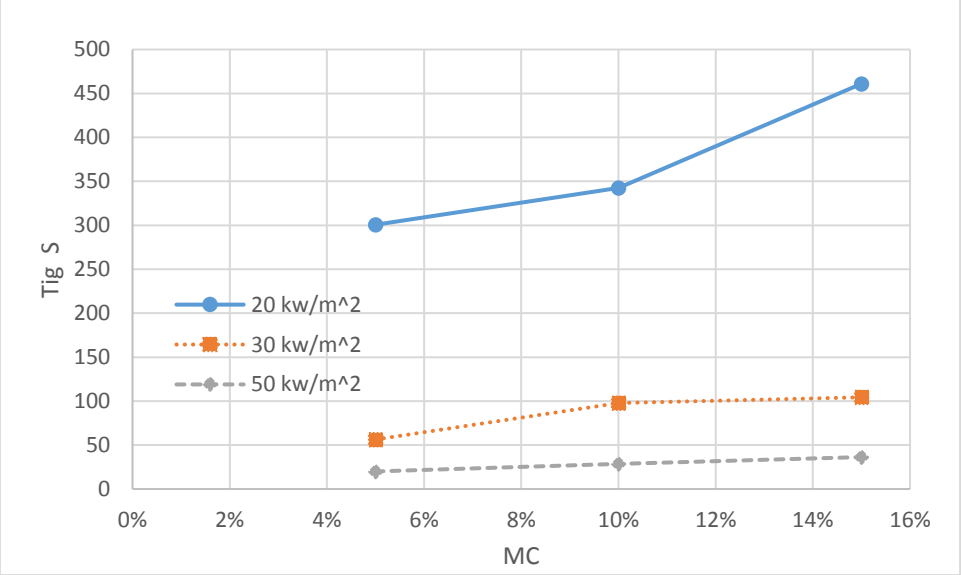


Figure C.4. OSB-H (Material E) ignition time vs.MC

The ignition time of OSB-H increased as the MC level increased, heat flux

decreased.

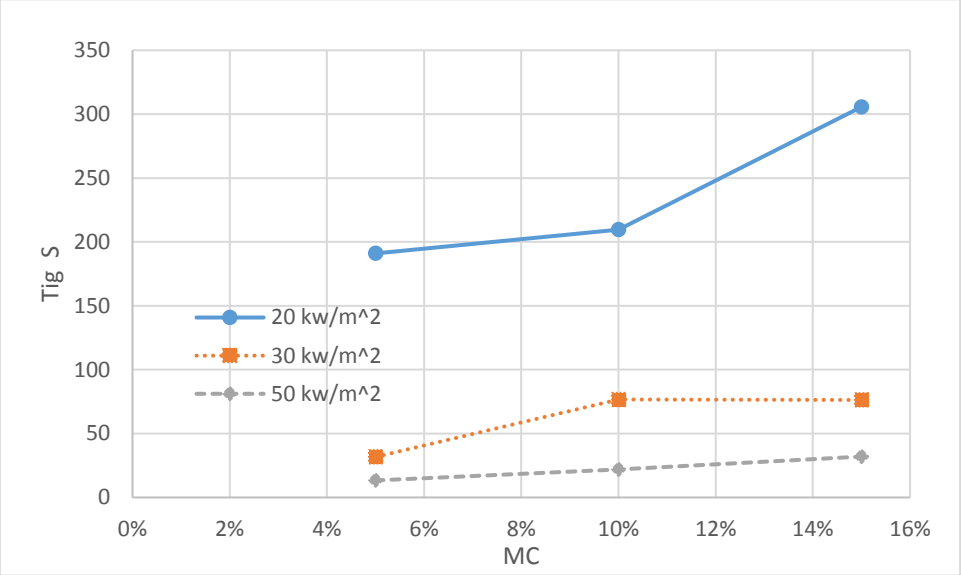


Figure C.5. CDX (Material F) ignition time vs.MC

The ignition time of CDX increased as the MC level increased, heat flux decreased.

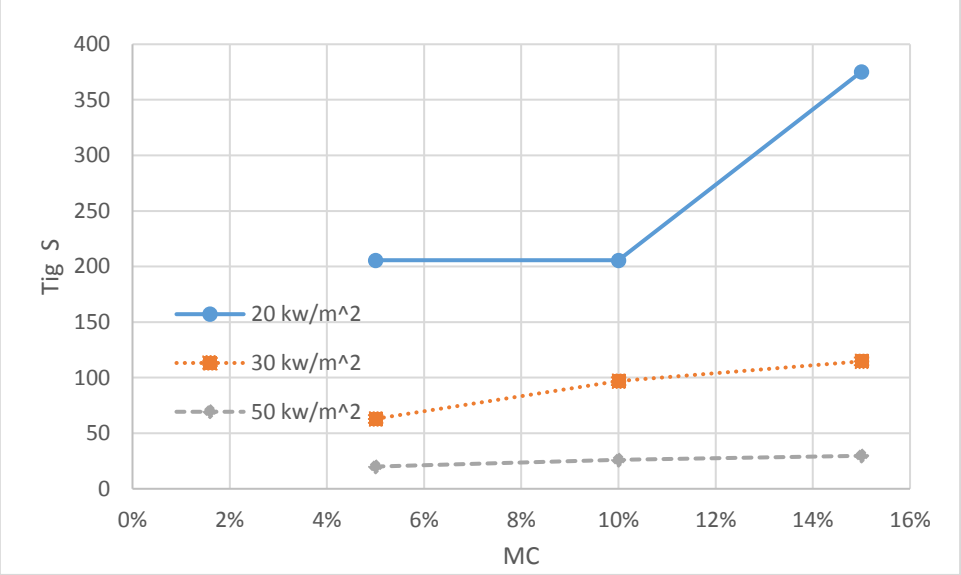


Figure C.6. HB (Material G) ignition time vs.MC

The ignition time of HB increased as the MC level increased, heat flux decreased.

# APPENDIX D: 180S HRR DATA

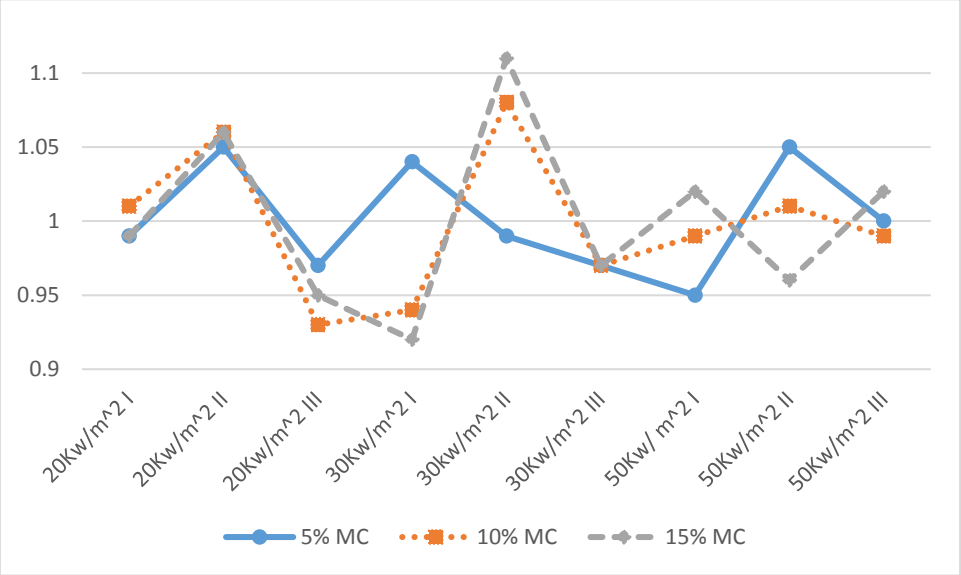


Figure D.1. SYP (Material A) ratio of ave HRR 180s vs.MC

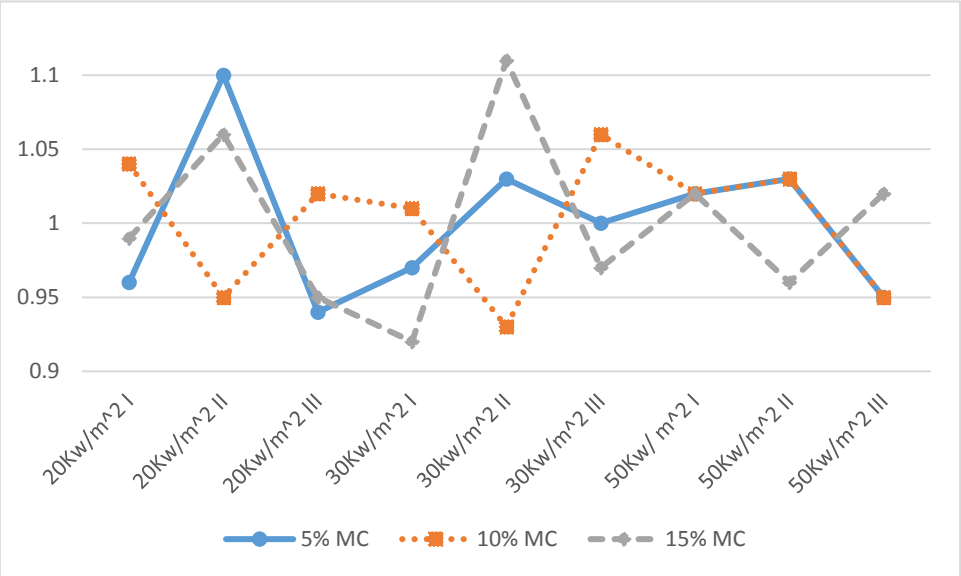


Figure D.2. SPF (Material B) ratio of ave HRR 180s vs.MC

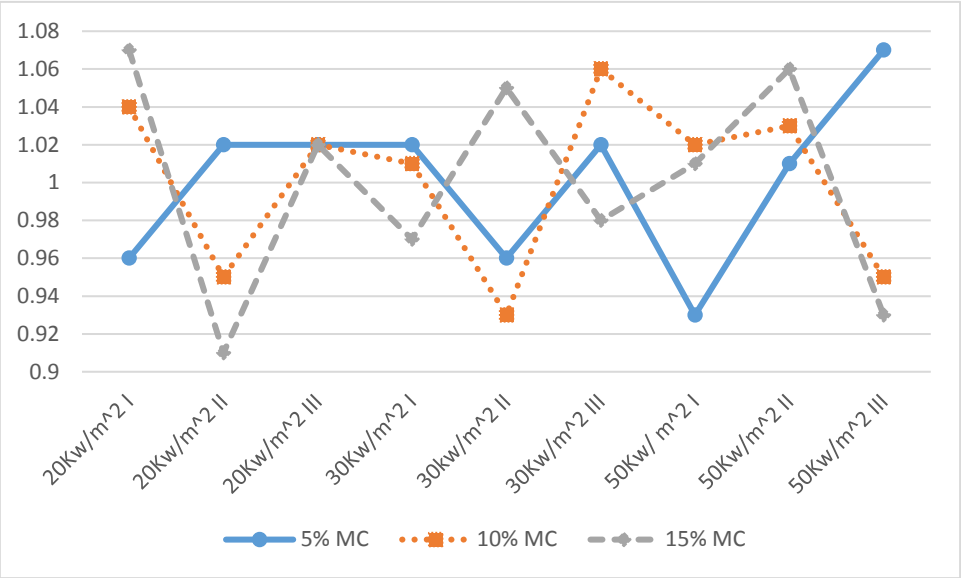


Figure D.3. OSB-PF (Material C) ratio of ave HRR 180s vs.MC

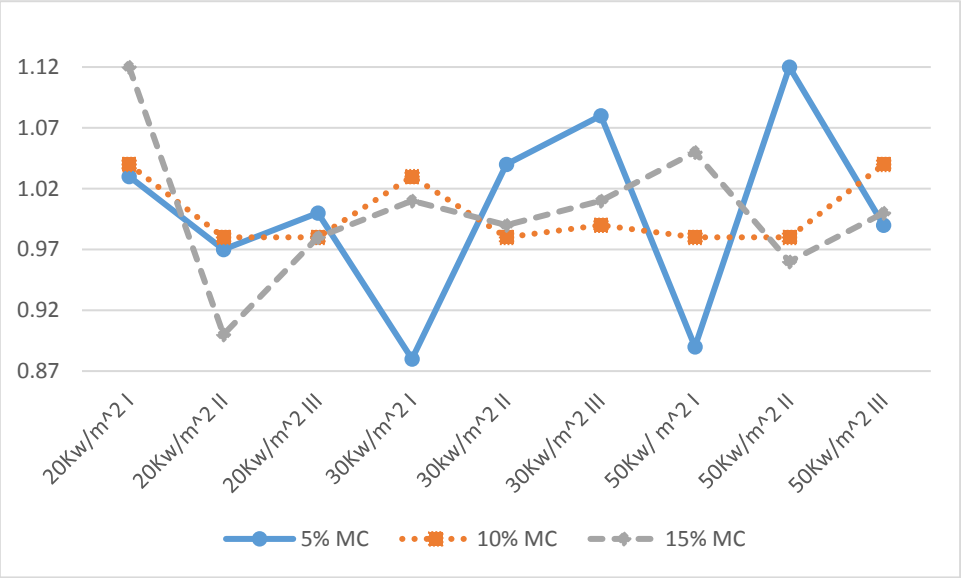


Figure D.4. OSB-Siding (Material D) ratio of ave HRR 180s vs.MC

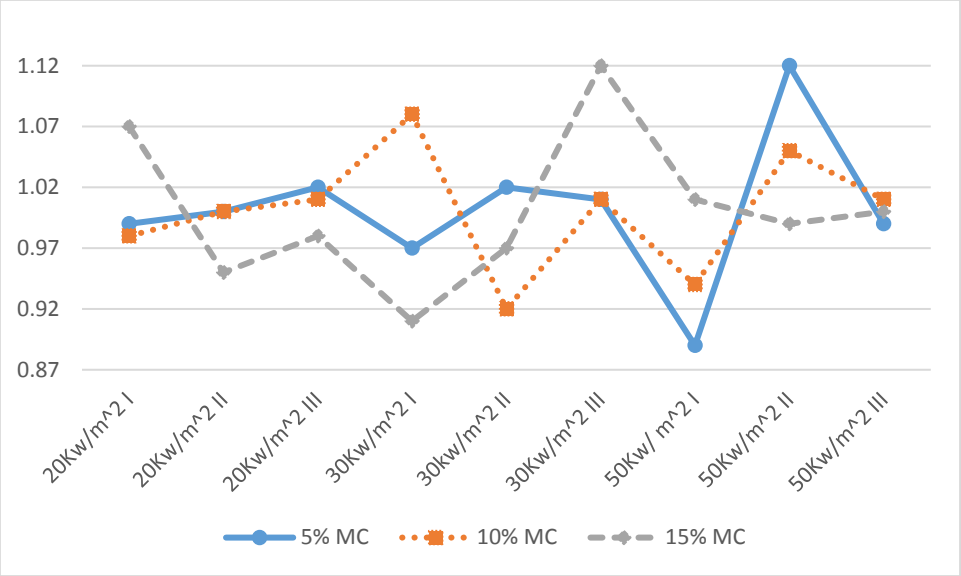


Figure D.5. OSB-H (Material E) ratio of ave HRR 180s vs.MC

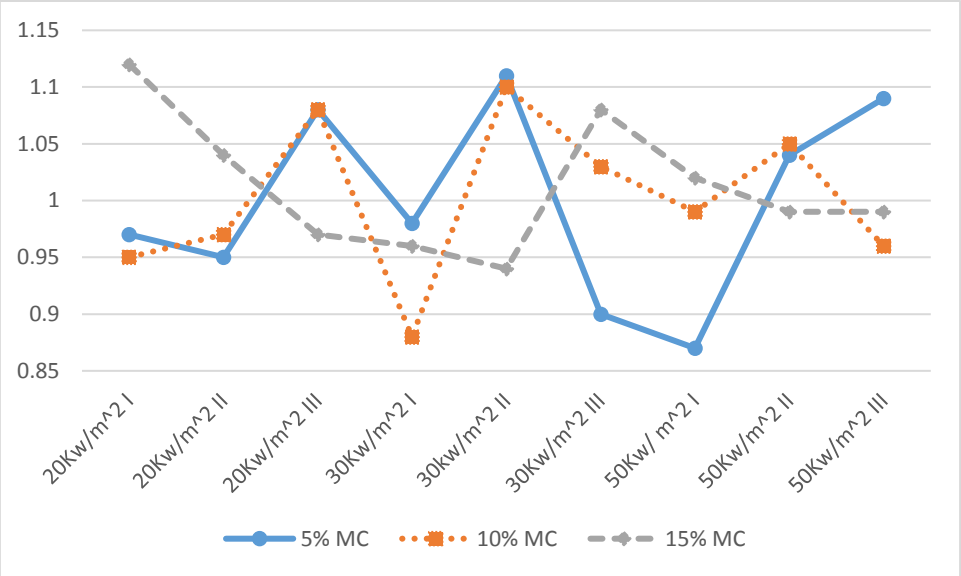


Figure D.6. CDX (Material F) ratio of ave HRR 180s vs.MC

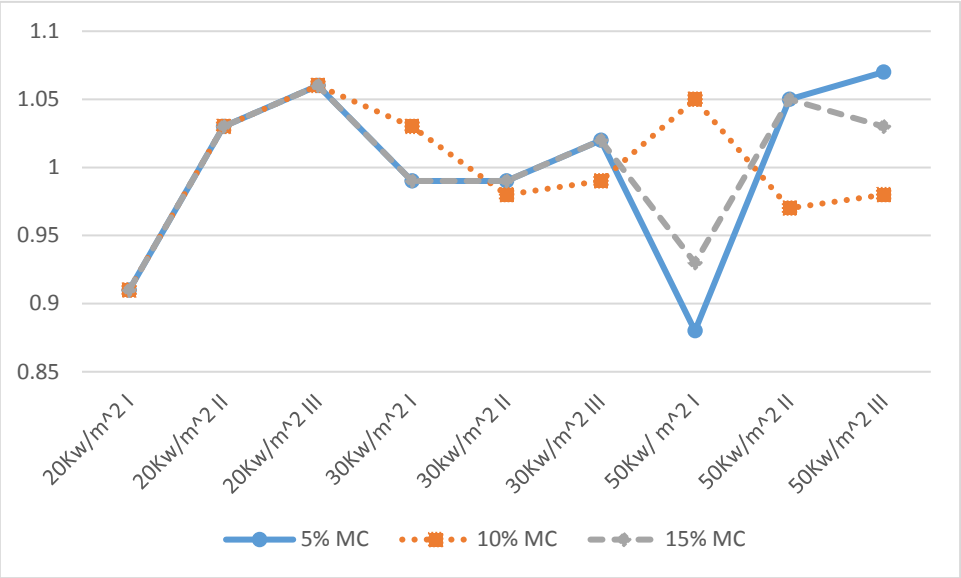


Figure D.7. HB (Material G) ratio of ave HRR 180s vs.MC

# APPENDIX E: PHRR DATA

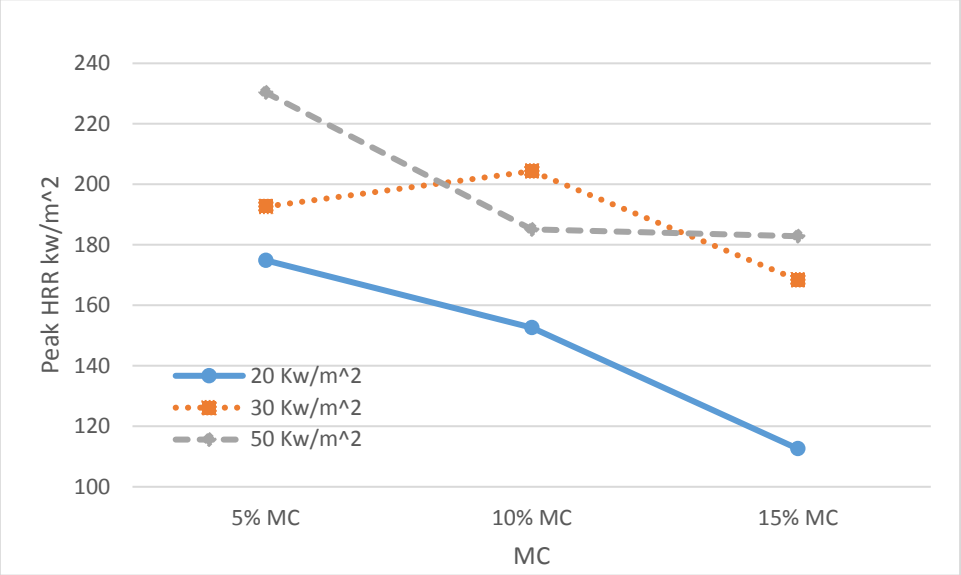


Figure E.1. SPF (Material B) PHRR vs.MC

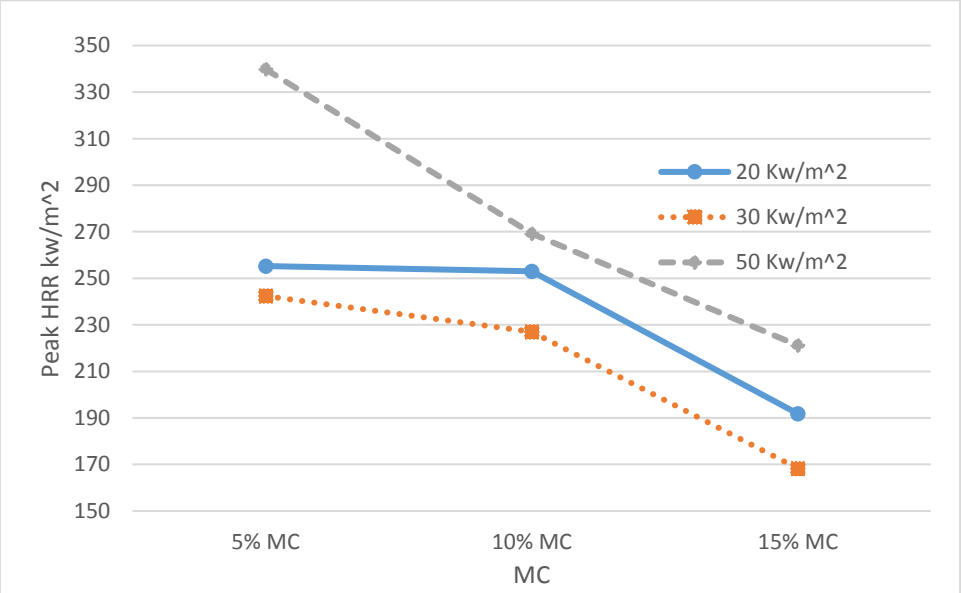


Figure E.2. OSB-Siding (Material D) PHRR vs.MC

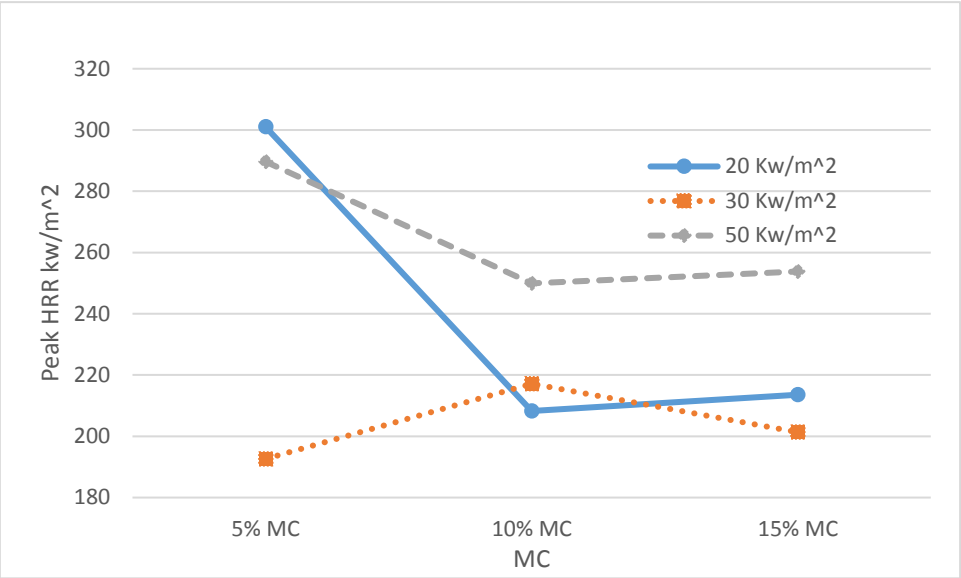


Figure E.3. OSB-H (Material E) PHRR vs.MC

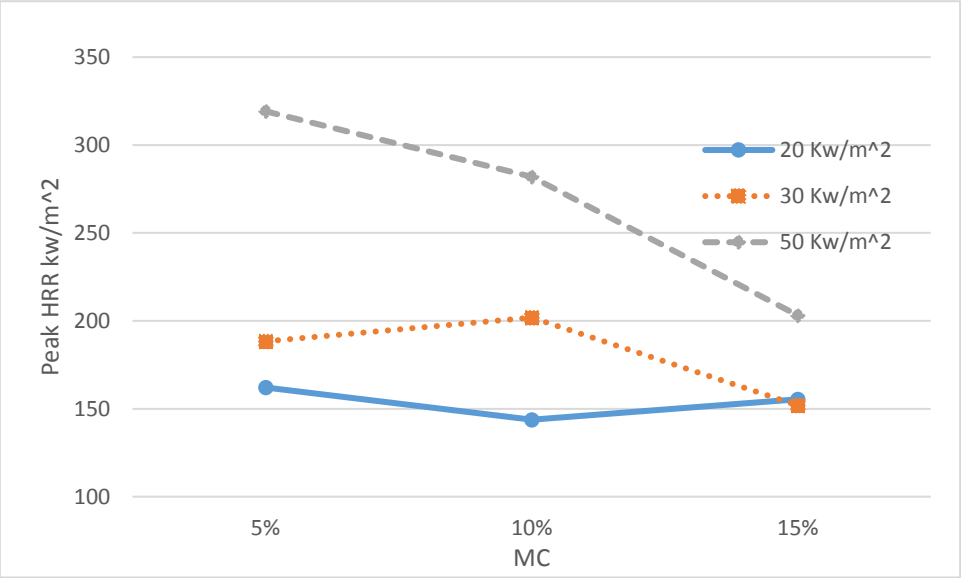


Figure E.4. CDX (Material F) PHRR vs.MC

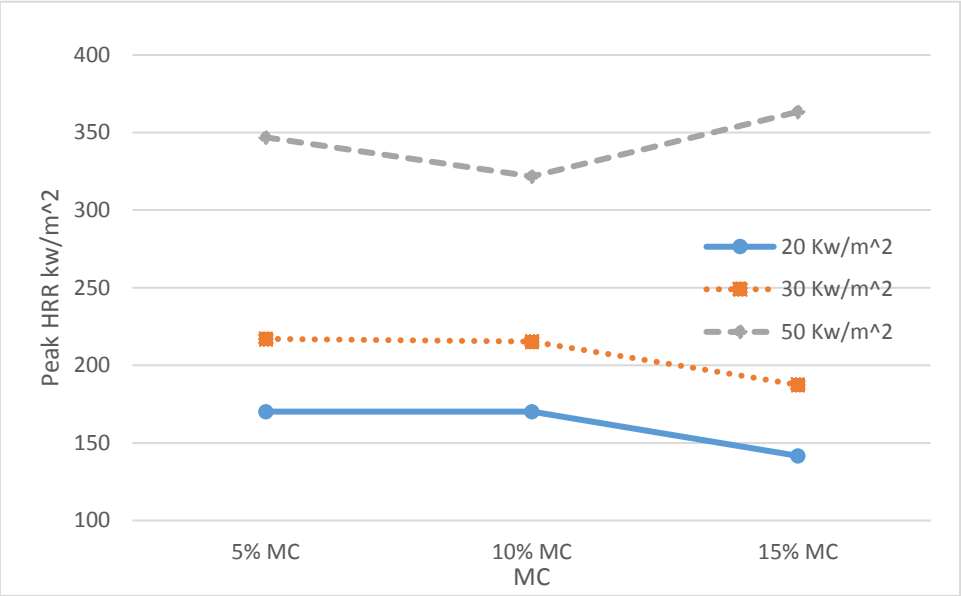


Figure E.5. HB (Material G) PHRR vs.MC

# APPENDIX F: Effective Heat of Combustion (EHC) DATA

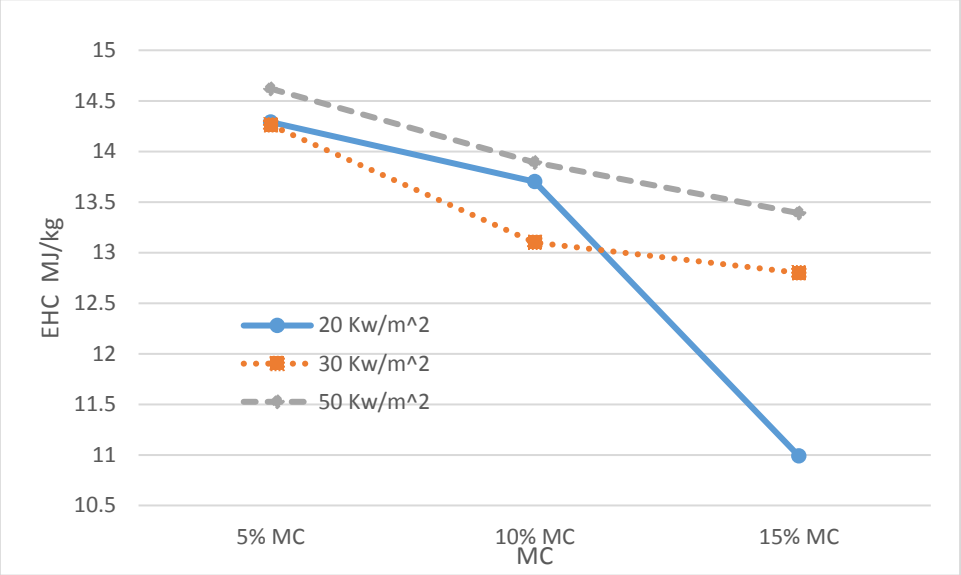


Figure F.1. SPF (Material B) EHC vs.MC

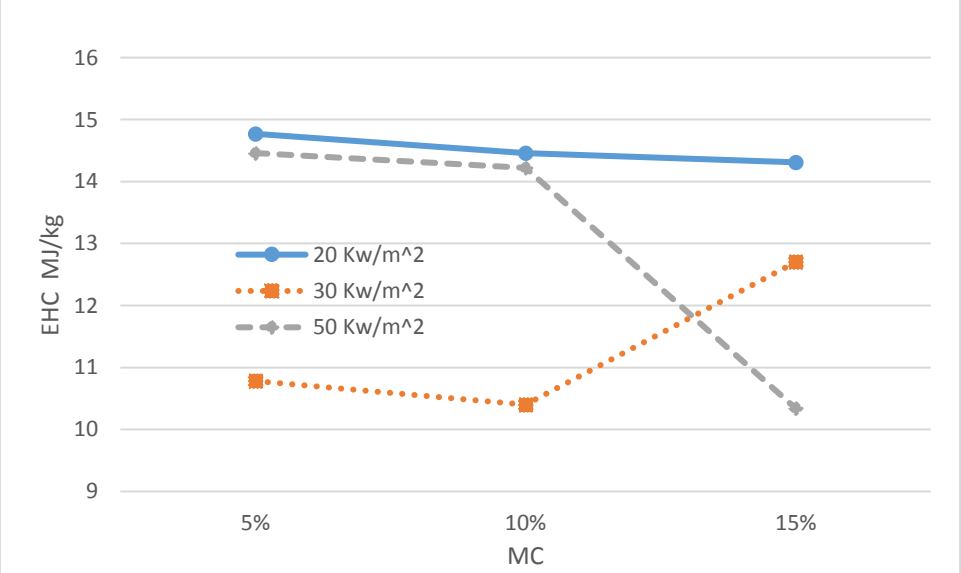


Figure F.2. OSB-Siding (Material D) EHC vs.MC

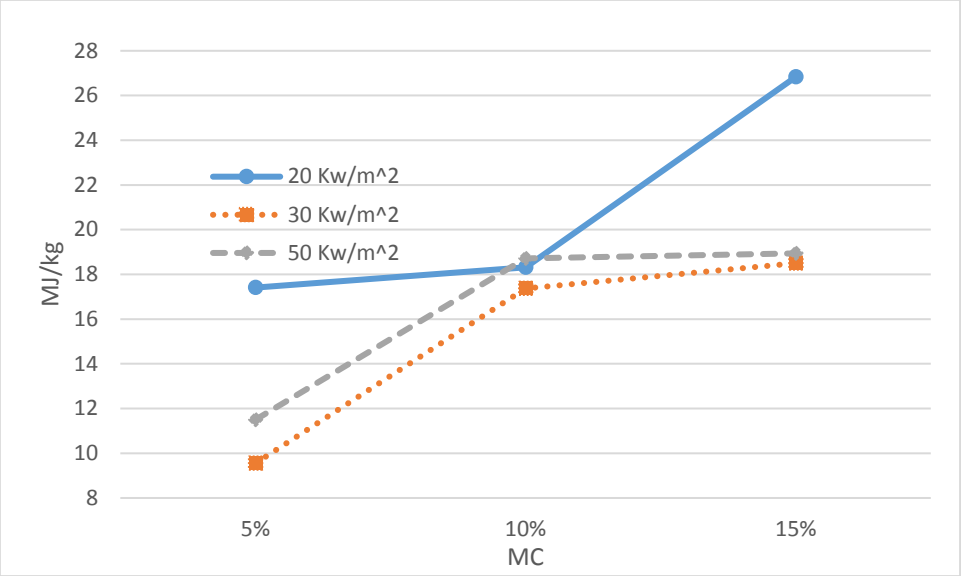


Figure F.3. OSB-H (Material E) EHC vs.MC

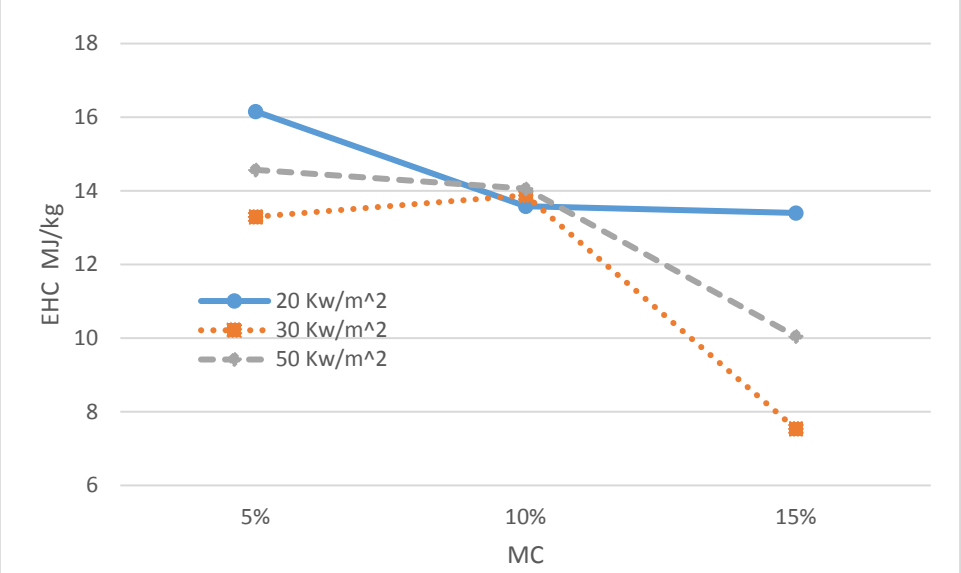


Figure F.4. CDX (Material F) EHC vs.MC

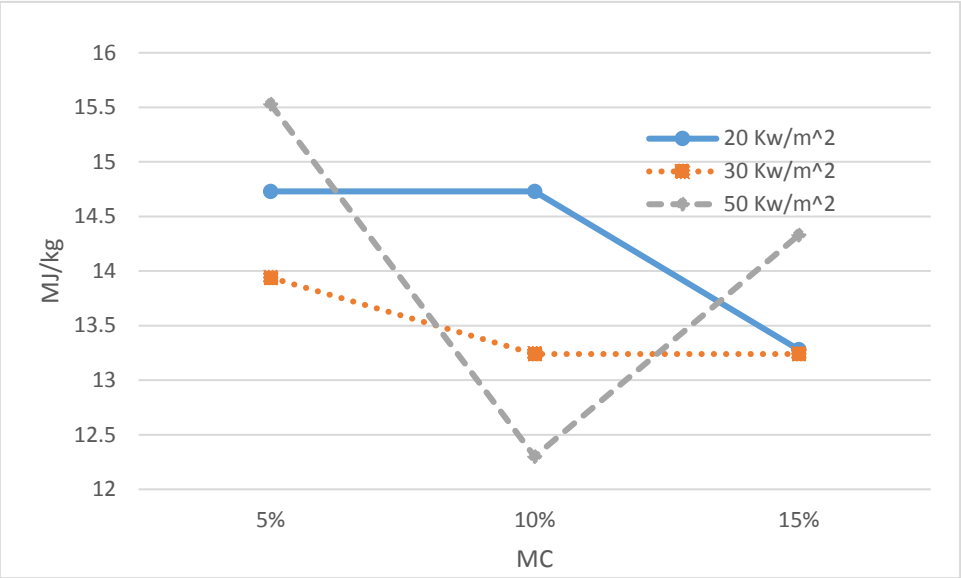


Figure F.5. HB (Material G) EHC vs.MC

# APPENDIX G: ML (Mass loss) DATA

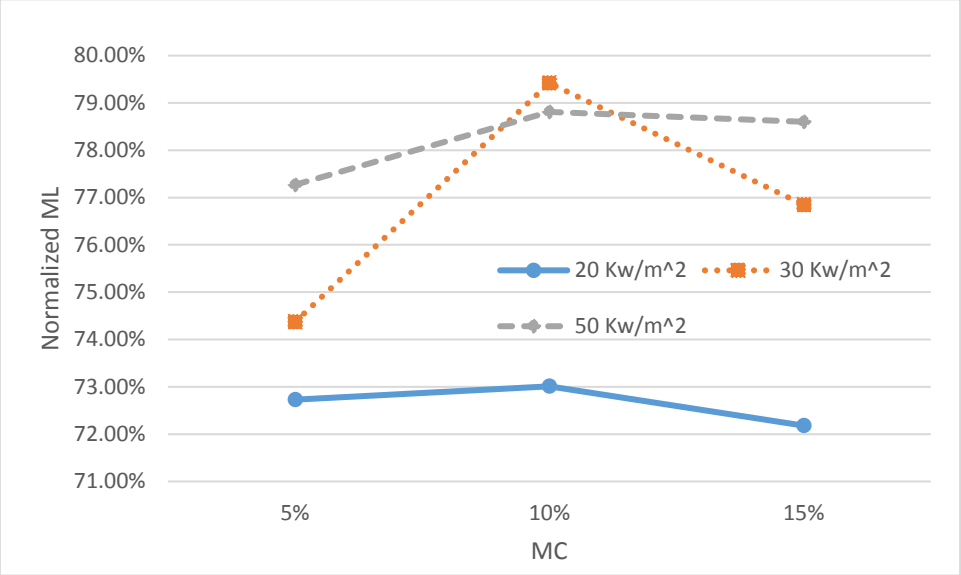


Figure G.1. SPF (Material B) Normalized ML vs.MC

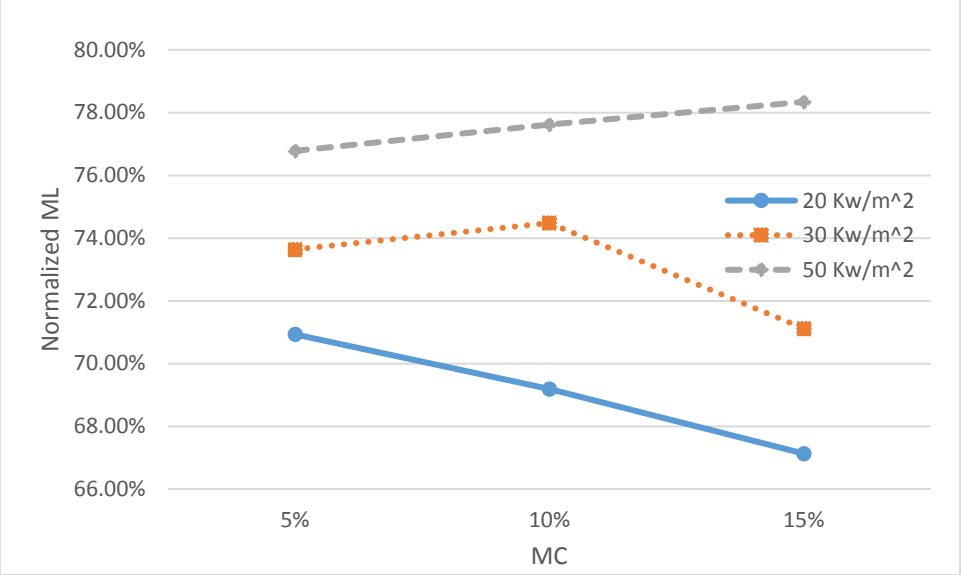


Figure G.2. OSB-Siding (Material D) Normalized ML vs.MC

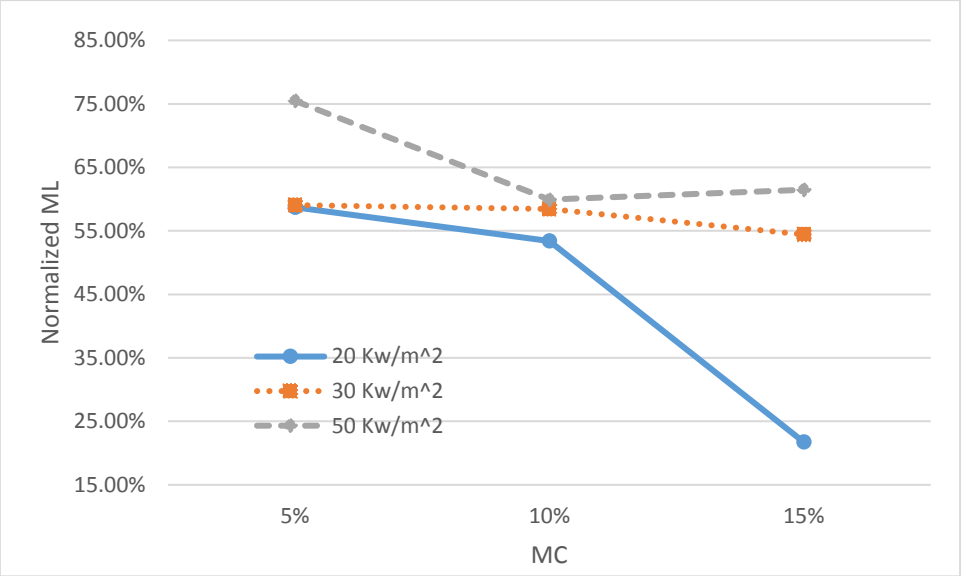


Figure G.3. OSB (Material E) Normalized ML vs.MC

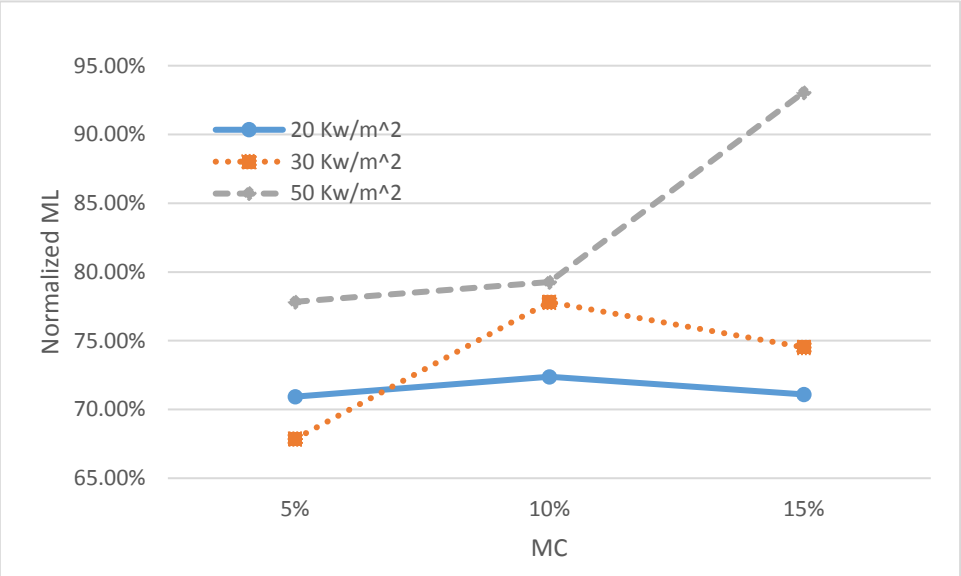


Figure G.4. CDX (Material F) Normalized ML vs.MC

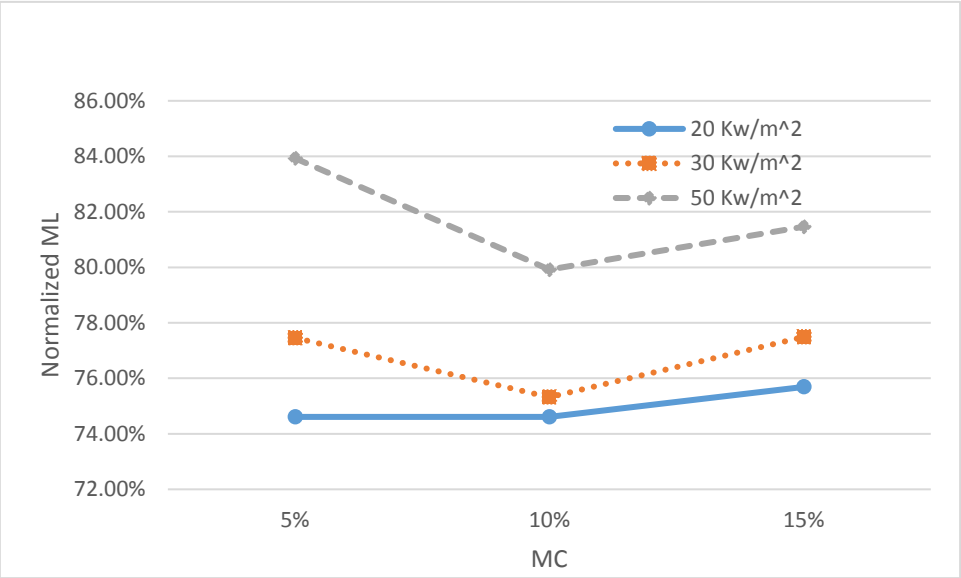


Figure G.5. HB (Material G) Normalized ML vs.MC

# APPENDIX H: MLR (Mass loss rate) DATA

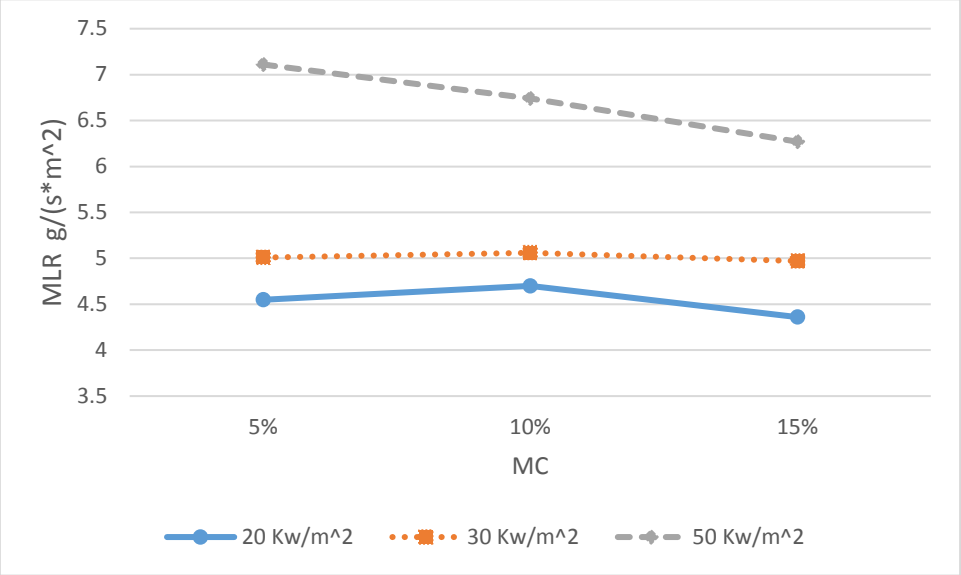


Figure H.1. SPF (Material B) MLR vs.MC

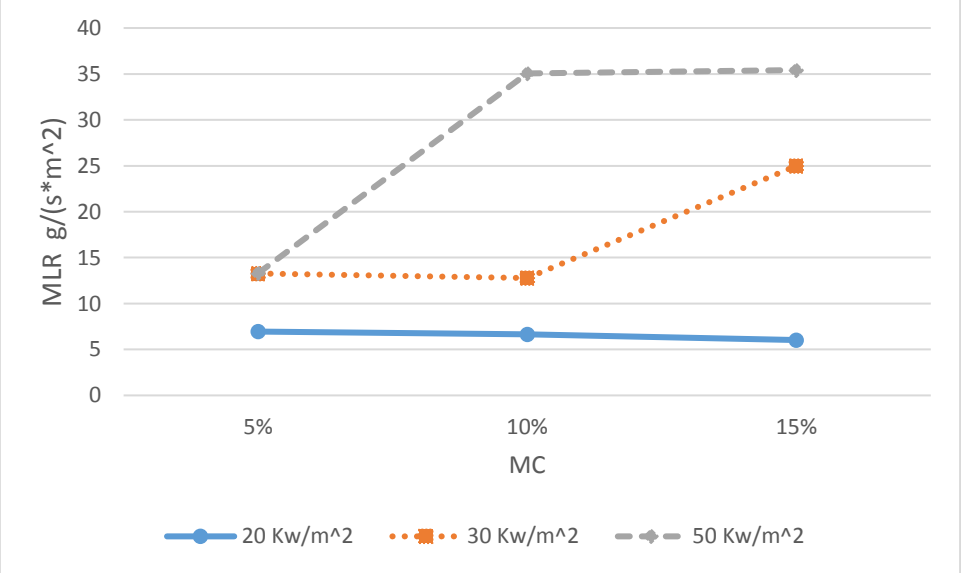


Figure H.2. OSB-Siding (Material D) MLR vs.MC

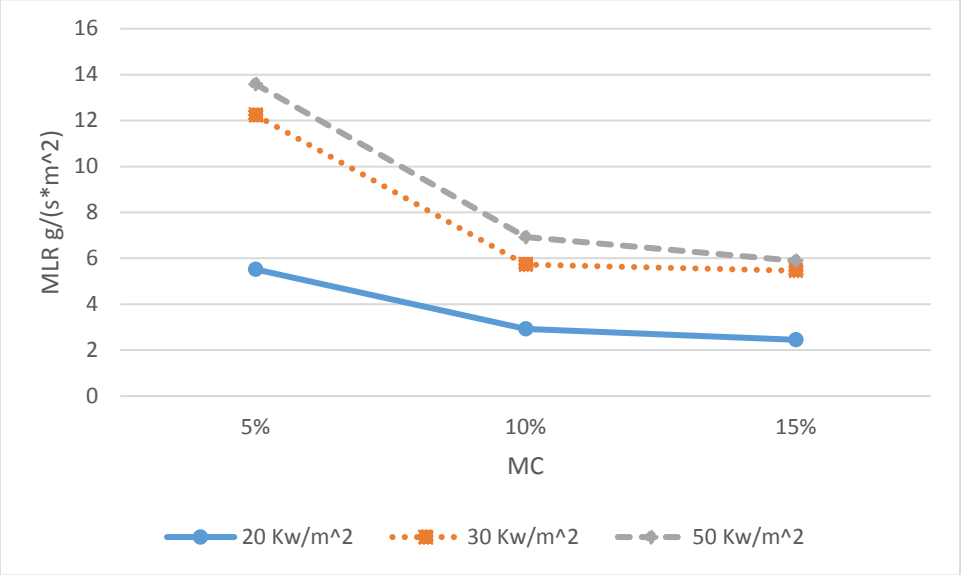


Figure H.3. OSB-H (Material E) MLR vs.MC

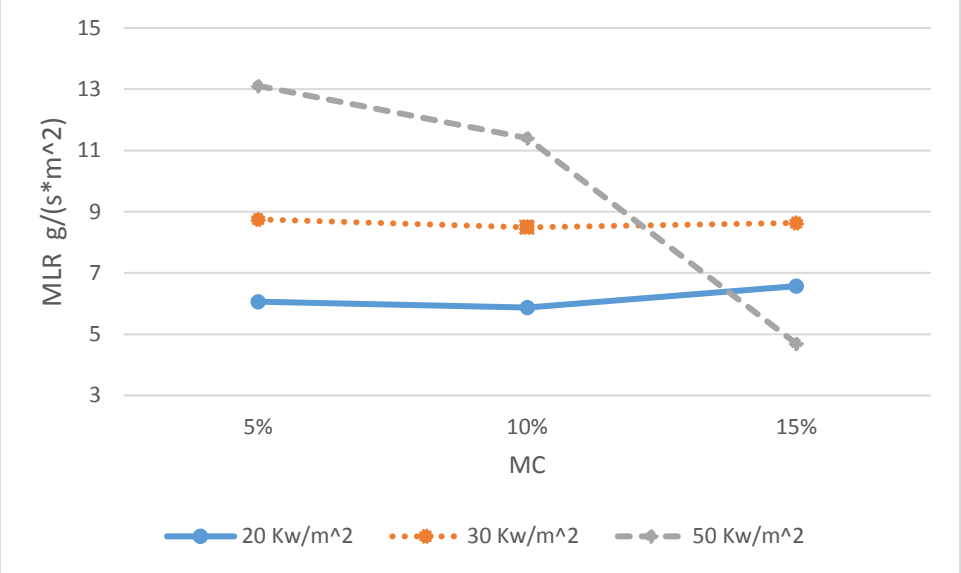


Figure H.4. CDX (Material F) MLR vs.MC

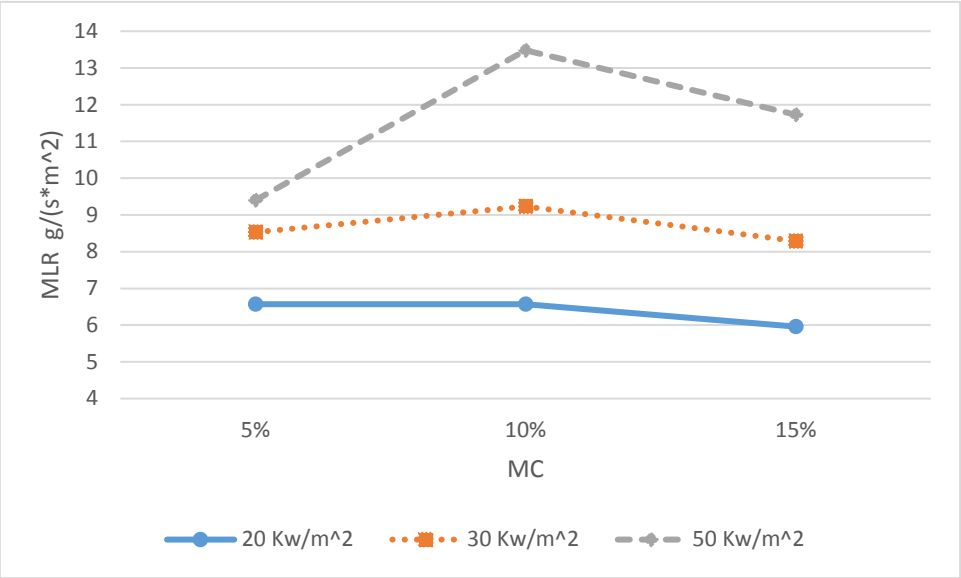


Figure H.5. HB (Material G) MLR vs.MC

# APPENDIX I: FLAMEOUT TIME DATA

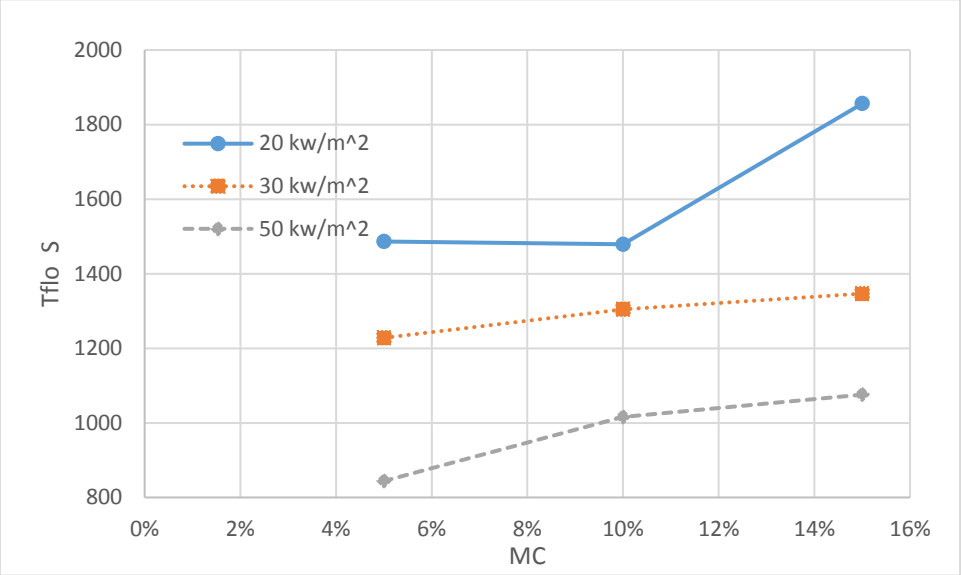


Figure I.1. SPF (Material B) flameout time vs.MC

The flameout time of SPF increased as the MC level increased (except 20 kw/m^2), heat flux decreased.

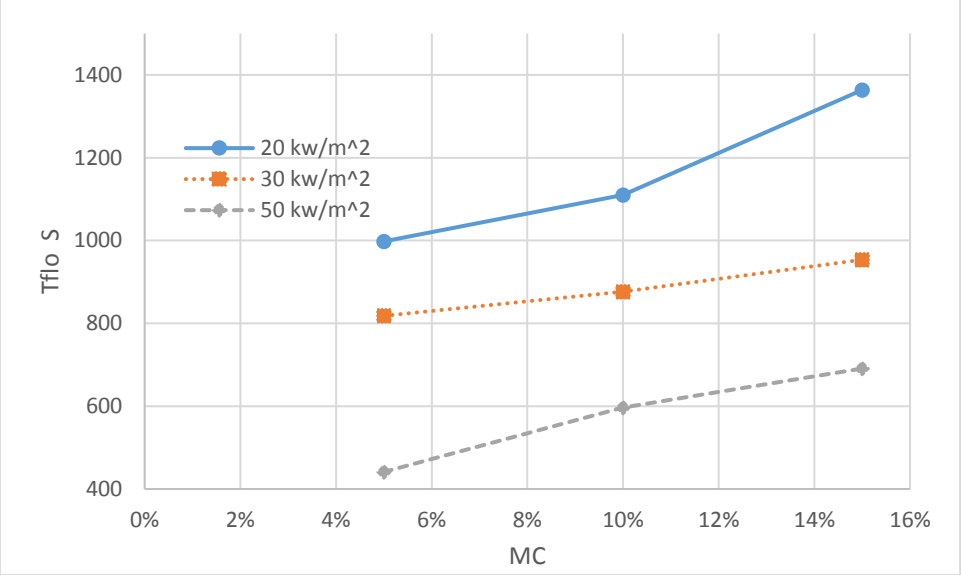


Figure I.2. OSB-Siding (Material D) flameout time vs.MC

The flameout time of OSB-Siding increased as the MC level increased, heat flux

decreased.

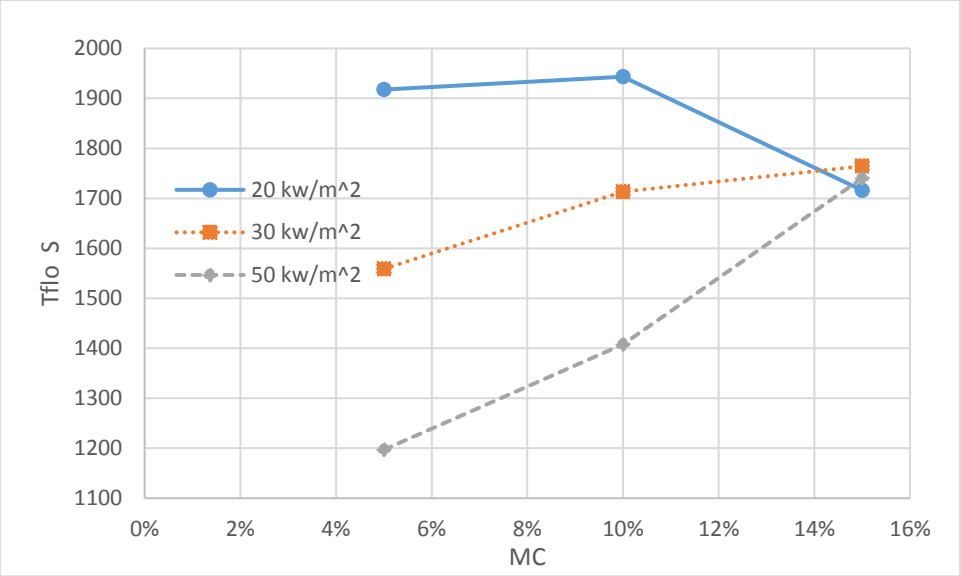


Figure I.3. OSB-H (Material E) flameout time vs.MC

The flameout time of OSB-H in different heat flux got closer as the MC increased.

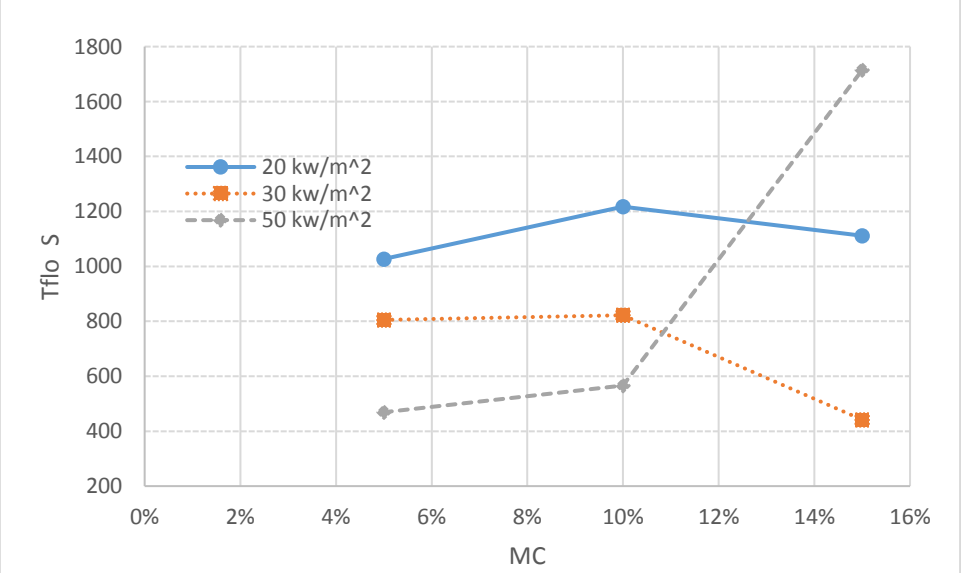


Figure I.4. CDX (Material F) flameout time vs.MC

The flameout time of CDX showed a complex relationship as the MC level and heat flux changed.

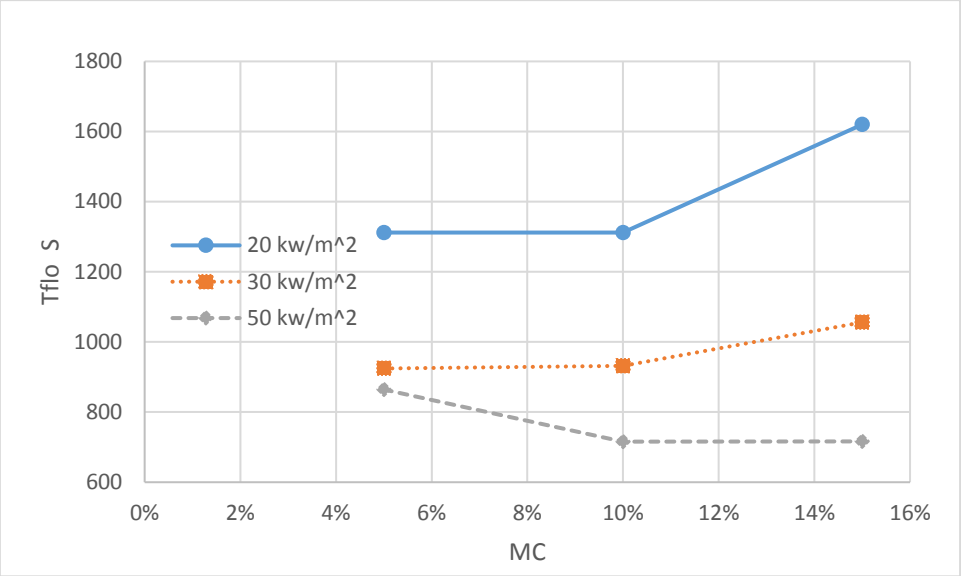


Figure I.5. HB (Material G) flameout time vs.MC

The flameout time of HB showed a complex relationship as the MC level and heat flux changed.